

Hypergraph motifs and their extensions beyond binary

Geon Lee* · Seokbum Yoon* · Jihoon Ko · Hyunju Kim · Kijung Shin†

Received: date / Accepted: date

Abstract Hypergraphs naturally represent group interactions, which are omnipresent in many domains: collaborations of researchers, co-purchases of items, and joint interactions of proteins, to name a few. In this work, we propose tools for answering the following questions in a systematic manner: **(Q1)** what are the structural design principles of real-world hypergraphs? **(Q2)** how can we compare local structures of hypergraphs of different sizes? **(Q3)** how can we identify domains from which hypergraphs are?

We first define *hypergraph motifs* (h-motifs), which describe the overlapping patterns of three connected hyperedges. Then, we define the significance of each h-motif in a hypergraph as its occurrences relative to those in properly randomized hypergraphs. Lastly, we define the *characteristic profile* (CP) as the vector of the normalized significance of every h-motif. Regarding Q1, we find that h-motifs' occurrences in 11 real-world hypergraphs from 5 domains are clearly distinguished from those of randomized hypergraphs. In addition, we

demonstrate that CPs capture local structural patterns unique to each domain, and thus comparing CPs of hypergraphs addresses Q2 and Q3. The concept of CP is naturally extended to represent the connectivity pattern of each node or hyperedge as a vector, which proves useful in node classification and hyperedge prediction.

Our algorithmic contribution is to propose MoCHy, a family of parallel algorithms for counting h-motifs' occurrences in a hypergraph. We theoretically analyze their speed and accuracy and show empirically that the advanced approximate version MoCHy-A⁺ is up to 25× more accurate and 32× faster than the basic approximate and exact versions, respectively.

Furthermore, we explore *ternary hypergraph motifs* that extends h-motifs by taking into account not only the presence but also the cardinality of intersections among hyperedges. This extension proves beneficial for all previously mentioned applications.

Keywords Hypergraph · Hypergraph motif · Ternary hypergraph motif · Counting algorithm

This work was supported by National Research Foundation of Korea (NRF) grant funded by the Korea government (MSIT) (No. NRF-2020R1C1C1008296) and Institute of Information & Communications Technology Planning & Evaluation (IITP) grant funded by the Korea government (MSIT) (No. 2019-0-00075, Artificial Intelligence Graduate School Program (KAIST)).

* Equal Contribution. † Corresponding Author.

G. Lee · S. Yoon · J. Ko · H. Kim
Kim Jaechul Graduate School of AI, KAIST, Seoul, South Korea, 02455
E-mail: {geonlee0325,jing9044,jihoonko,hyunju.kim}@kaist.ac.kr

K. Shin
Kim Jaechul Graduate School of AI and School of Electrical Engineering, KAIST, Seoul, South Korea, 02455
E-mail: kijungs@kaist.ac.kr

1 Introduction

Complex systems consisting of pairwise interactions between individuals or objects are naturally expressed in the form of graphs. Nodes and edges, which compose a graph, represent individuals (or objects) and their pairwise interactions, respectively. Thanks to their powerful expressiveness, graphs have been used in a wide variety of fields, including social network analysis, web, bioinformatics, and epidemiology. Global structural patterns of real-world graphs, such as power-law degree distribution [12, 34] and six degrees of separation [49, 107], have been extensively investigated.

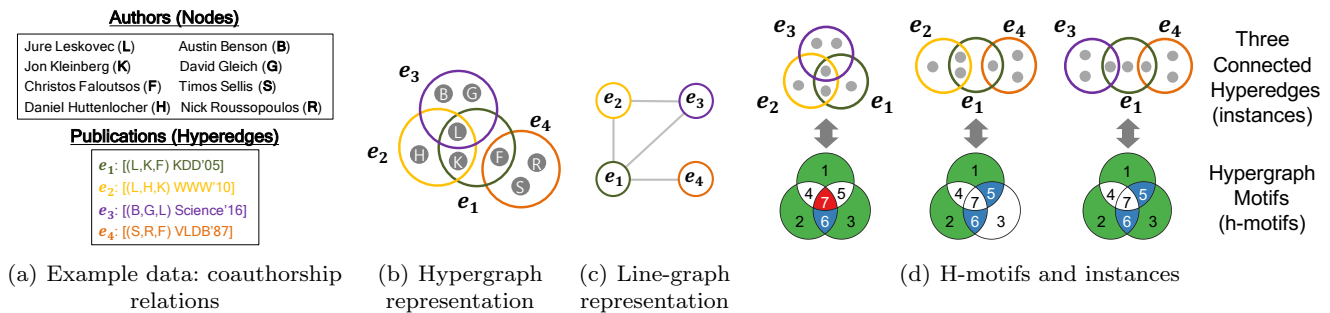


Fig. 1: (a) Example: co-authorship relations. (b) Hypergraph: the hypergraph representation of (a). (c) Line Graph: the line-graph representation of (b). (d) Hypergraph Motifs: example h-motifs and their instances in (b).

In addition to global patterns, real-world graphs exhibit patterns in their local structures, which differentiate graphs in the same domain from random graphs or those in other domains. Local structures are revealed by counting the occurrences of different network motifs [78, 79], which describe the patterns of pairwise interactions between a fixed number of connected nodes (typically 3, 4, or 5 nodes). As a fundamental building block, network motifs have played a key role in many analytical and predictive tasks, including community detection [15, 71, 103, 111], classification [25, 65, 78], and anomaly detection [13, 96].

Despite the prevalence of graphs, interactions in several complex systems are groupwise rather than pairwise: collaborations of researchers, co-purchases of items, joint interactions of proteins, tags attached to the same web post, to name a few. These group interactions cannot be represented by edges in a graph. Suppose three or more researchers coauthor a publication. This co-authorship cannot be represented as a single edge, and creating edges between all pairs of the researchers cannot be distinguished from multiple papers coauthored by subsets of the researchers.

This inherent limitation of graphs is addressed by hypergraphs, which consist of nodes and hyperedges. Each hyperedge is a subset of any number of nodes, and it represents a group interaction among the nodes. For example, the coauthorship relations in Figure 1(a) are naturally represented as the hypergraph in Figure 1(b). In the hypergraph, seminar work [66] coauthored by Jure Leskovec (L), Jon Kleinberg (K), and Christos Faloutsos (F) is expressed as the hyperedge $e_1 = \{L, K, F\}$, and it is distinguished from three papers coauthored by each pair, which, if they exist, can be represented as three hyperedges $\{K, L\}$, $\{F, L\}$, and $\{F, K\}$.

The successful investigation and discovery of local structural patterns in real-world graphs motivate us to explore local structural patterns in real-world hyper-

graphs. However, network motifs, which proved to be useful for graphs, are not trivially extended to hypergraphs. Due to the flexibility in the size of hyperedges, it is possible to form 2^n distinct hyperedges with a given set of n nodes. As a result, the potential number of hypergraphs is 2^{2^n} , which is extraordinarily large even for a small number of nodes. This implies that there can be numerous possible interactions among hyperedges, highlighting the complexity of hypergraph structures.

In this work, taking these challenges into consideration, we define 26 *hypergraph motifs* (h-motifs) so that they describe overlapping patterns of three connected hyperedges (rather than nodes). As seen in Figure 1(d), h-motifs describe the overlapping pattern of hyperedges e_1 , e_2 , and e_3 by the emptiness of seven subsets: $e_1 \setminus e_2 \setminus e_3$, $e_2 \setminus e_3 \setminus e_1$, $e_3 \setminus e_1 \setminus e_2$, $e_1 \cap e_2 \setminus e_3$, $e_2 \cap e_3 \setminus e_1$, $e_3 \cap e_1 \setminus e_2$, and $e_1 \cap e_2 \cap e_3$. As a result, every overlapping pattern is described by a unique h-motif, independently of the sizes of hyperedges. While this work focuses on overlapping patterns of three hyperedges, h-motifs are easily extended to four or more hyperedges.

We count the number of each h-motif's instances in 11 real-world hypergraphs from 5 different domains. Then, we measure the significance of each h-motif in each hypergraph by comparing the count of its instances in the hypergraph against the counts in properly randomized hypergraphs. Lastly, we compute the *characteristic profile* (CP) of each hypergraph, defined as the vector of the normalized significance of every h-motif. Comparing the counts and CPs of different hypergraphs leads to the following observations:

- Structural design principles of real-world hypergraphs that are captured by frequencies of different h-motifs are clearly distinguished from those of randomized hypergraphs.
- Hypergraphs from the same domains have similar CPs, while hypergraphs from different domains have distinct CPs (see Figure 2). In other words, CPs

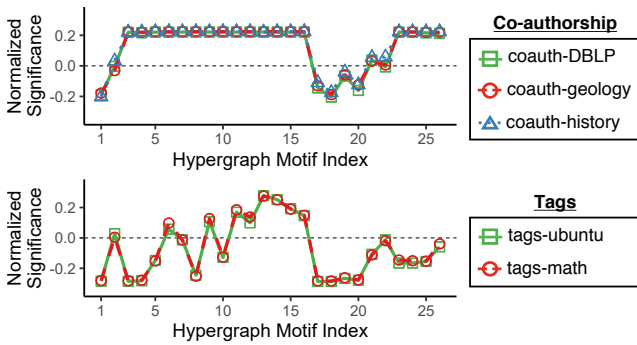


Fig. 2: Distributions of h-motifs’ instances precisely characterize local structural patterns of real-world hypergraphs. Note that the hypergraphs from the same domains have similar distributions, while the hypergraphs from different domains do not. See Section 6.3 for details.

successfully capture local structure patterns unique to each domain.

Similarly, h-motifs can also be employed to summarize the connectivity pattern of each node or hyperedge. Specifically, for each node, we can calculate its *node profile* (NP), a 26-element vector with each element indicating the frequency of each motif’s instances within the node’s ego-network. Likewise, the *hyperedge profile* (HP) of a hyperedge is a 26-element vector with each element representing the count of each motif’s instances that involve the hyperedge. We demonstrate empirically that NPs and HPs effectively capture local connectivity patterns, serving as valuable features for node classification and hyperedge prediction tasks.

Our algorithmic contribution is to design MoCHy (**M**otif **C**ounting in **H**ypergraphs), a family of parallel algorithms for counting h-motifs’ instances, which is the computational bottleneck of the aforementioned process. Note that since multi-way overlaps are taken into consideration, counting the instances of h-motifs is more challenging than counting the instances of network motifs, which are defined solely based on pairwise interactions. We provide one exact version, named MoCHy-E, and two approximate versions, named MoCHy-A and MoCHy-A⁺. Empirically, MoCHy-A⁺ is up to 25× more accurate than MoCHy-A, and it is up to 32× faster than MoCHy-E, with little sacrifice of accuracy. These empirical results are consistent with our theoretical analyses.

Additionally, we investigate *ternary hypergraph motifs* (3h-motifs) as a promising extension of h-motifs. While h-motifs focus only on the emptiness of seven subsets derived from intersections among hyperedges, 3h-motifs further differentiate patterns based on the

cardinality of these subsets. In particular, 3h-motifs consider whether the cardinality of each non-empty subset surpasses a specific threshold or not, resulting in 431 distinct patterns. We demonstrate that employing 3h-motifs instead of h-motifs leads to performance improvements in all the previously mentioned applications, i.e., hypergraph (domain) classification, node classification, and hyperedge prediction.

In summary, our contributions are summarized as follows:

- **Novel Concepts:** We introduce h-motifs, which capture the local structures of hypergraphs, independently of the sizes of hyperedges or hypergraphs. We extend this concept to 3h-motifs, allowing for a more detailed distinction of local structures.
- **Fast and Provable Algorithms:** We develop MoCHy, a family of parallel algorithms for counting h-motifs’ instances. We show theoretically and empirically that the advanced version significantly outperforms the basic ones, providing a better trade-off between speed and accuracy.
- **Discoveries in 11 Real-world Hypergraphs:** We show that h-motifs and 3h-motifs reveal local structural patterns that are shared by hypergraphs from the same domains but distinguished from those of random hypergraphs and hypergraphs from other domains (see Figure 2).
- **Machine Learning Applications:** We empirically demonstrate that h-motifs allow for the extraction of effective features in three machine-learning tasks, and employing 3h-motifs enables the extraction of even stronger features.

Reproducibility: The code and datasets used in this work are available at <https://github.com/jing9044/MoCHy-with-3h-motif>.

This paper is an extension of our previous work [62], which first introduced the concept of h-motifs and related counting algorithms. In this extended version, we investigate various extensions of h-motifs, including 3h-motifs (Section 5 and Appendices G and H). Furthermore, we develop an advanced on-the-fly algorithm for improved space efficiency (Section 4.4) and establish accuracy guarantees for the approximate counting algorithms in the form of sample concentration bounds (Theorems 4 and 7). We also evaluate the effectiveness of h-motifs for machine learning applications on three tasks using 7 to 11 datasets (Section 6.5 and Appendices J and K). We especially demonstrate the superior performance of 3h-motifs over their variants and h-motifs in these tasks (Sections 6.4 and 6.5, and Appendix L). Finally, we measure and compare the importance of different h-motifs in characterizing hypergraph

Table 1: Frequently-used symbols.

Notation	Definition
$G = (V, E)$	hypergraph with nodes V and hyperedges E
$E = \{e_1, \dots, e_{ E }\}$	set of hyperedges
E_v	set of hyperedges that contains a node v
\wedge	set of hyperwedges in G
\wedge_{ij}	hyperwedge consisting of e_i and e_j
$\bar{G} = (E, \wedge, \omega)$	line graph representation of G
$\omega(\wedge_{ij})$	the number of nodes shared between e_i and e_j
N_{e_i}	set of neighbors of e_i in \bar{G}
$h(\{e_i, e_j, e_k\})$	h-motif corresponding to an instance $\{e_i, e_j, e_k\}$
$M[t]$	count of h-motif t 's instances

structures and their correlation with global structural properties (Section 6.3 and Appendix E).

In Section 2, we introduce h-motifs and related concepts. In Section 3, we describe how we use these concepts to characterize hypergraphs, hyperedges, and nodes. In Section 4, we present exact and approximate algorithms for counting instances of h-motifs, and we analyze their theoretical properties. In Section 5, we extend h-motifs to 3h-motifs. In Section 6, we provide experimental results. After discussing related work in Section 7, we offer conclusions and future research directions in Section 8.

2 Proposed Concepts

In this section, we introduce preliminary concepts, and based on them, we define the proposed concept, i.e., hypergraph motifs. Refer to Table 1 for the notations frequently used in the paper.

2.1 Preliminaries and Notations

We introduce some preliminary concepts and notations.

Hypergraph: Consider a *hypergraph* $G = (V, E)$, where V and $E := \{e_1, e_2, \dots, e_{|E|}\}$ are sets of nodes and hyperedges, respectively.¹ Each hyperedge $e_i \in E$ is a non-empty subset of V , and we use $|e_i|$ to denote the number of nodes in it. For each node $v \in V$, we use $E_v := \{e_i \in E : v \in e_i\}$ to denote the set of hyperedges that include v . We say two hyperedges e_i and e_j are *adjacent* if they share any member, i.e., if $e_i \cap e_j \neq \emptyset$. Then, for each hyperedge e_i , we denote the set of hyperedges adjacent to e_i by $N_{e_i} := \{e_j \in E : e_i \cap e_j \neq \emptyset\}$ and the number of such hyperedges by $|N_{e_i}|$. Similarly, we say three hyperedges e_i, e_j , and e_k are *connected* if

¹ Note that, in this work, E is not a multi-set. That is, we assume that every hyperedge is unique.

there exists at least one hyperedge among them that is adjacent to the other two.

Hyperwedges: We define a *hyperwedge* as an unordered pair of adjacent hyperedges. We denote the set of hyperwedges in G by $\wedge := \{\{e_i, e_j\} \in \binom{E}{2} : e_i \cap e_j \neq \emptyset\}$. We use $\wedge_{ij} \in \wedge$ to denote the hyperwedge consisting of e_i and e_j . In the example hypergraph in Figure 1(b), there are four hyperwedges: \wedge_{12} , \wedge_{13} , \wedge_{23} , and \wedge_{14} .

Line Graph: We define the *line graph* (a.k.a., projected graph) of a hypergraph $G = (V, E)$ as $\bar{G} = (E, \wedge, \omega)$, where \wedge is the set of hyperwedges and $\omega(\wedge_{ij}) := |e_i \cap e_j|$. That is, in the line graph \bar{G} , hyperedges in G act as nodes, and two of them are adjacent if and only if they share any member. To be more precise, \bar{G} is a weighted variant of a line graph, where each edge is assigned a weight equal to the size of overlap of the corresponding hyperwedge in G . Note that for each hyperedge $e_i \in E$, N_{e_i} is the set of neighbors of e_i in \bar{G} , and $|N_{e_i}|$ is its degree in \bar{G} . Figure 1(c) shows the line graph of the example hypergraph in Figure 1(b).

Incidence Graph: We define the *incidence graph* (a.k.a., star expansion) of a hypergraph $G = (V, E)$ as $G' = (V', E')$ where $V' := V \cup E$ and $E' := \{(v, e) \in V \times E : v \in e\}$. That is, in the bipartite graph G' , V and E are the two subsets of nodes, and there exists an edge between $v \in V$ and $e \in E$ if and only if $v \in e$.

2.2 Hypergraph Motifs (H-Motifs)

We introduce hypergraph motifs, which are basic building blocks of hypergraphs. Then, we discuss their properties and generalization.

Definition and Representation: Hypergraph motifs (or h-motifs in short) are designed for describing the overlapping patterns of three connected hyperedges. Specifically, given a set $\{e_i, e_j, e_k\}$ of three connected hyperedges, h-motifs describe its overlapping pattern by the emptiness of the following seven sets: (1) $e_i \setminus e_j \setminus e_k$, (2) $e_j \setminus e_k \setminus e_i$, (3) $e_k \setminus e_i \setminus e_j$, (4) $e_i \cap e_j \setminus e_k$, (5) $e_j \cap e_k \setminus e_i$, (6) $e_k \cap e_i \setminus e_j$, and (7) $e_i \cap e_j \cap e_k$. Formally, a h-motif is defined as a binary vector of size 7 whose elements represent the emptiness of the above sets, respectively, and as seen in Figure 1(d), h-motifs are naturally represented in the Venn diagram. Equivalently, when we leave at most one node in each of the above subsets, h-motifs can be defined based on the isomorphism between sub-hypergraphs consisting of three connected hyperedges. While there can be 2^7 h-motifs, 26 h-motifs remain once we exclude symmetric ones, those that cannot be obtained from distinct hyperedges (see Figure 4), and those that cannot be obtained from connected hyperedges. The 26 cases, which we call *h-*

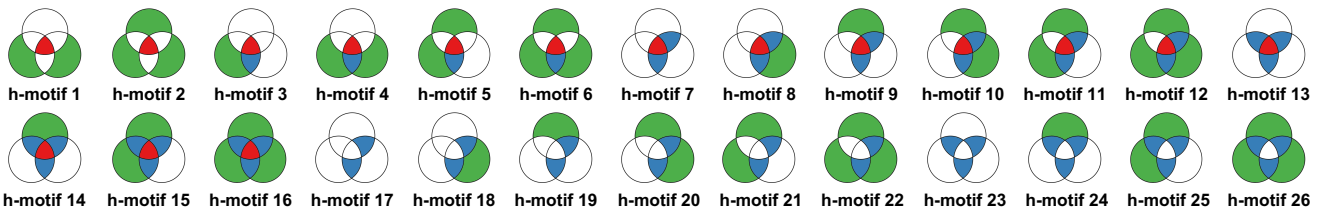


Fig. 3: The 26 h-motifs studied in this work. In each Venn diagram, uncolored regions are empty without containing any nodes, while colored regions include at least one node. H-motifs 17 - 22 are open, while the others are closed.



Fig. 4: The patterns that cannot be obtained from three distinct hyperedges. For example, any three hyperedges corresponding to the leftmost pattern are necessarily identical. However, according to our definition of hypergraphs in Section 2.1, every hyperedge is unique. Thus, there should be no instance of the pattern.

motif 1 through *h-motif 26*, are visualized in the Venn diagram in Figure 3.

Instances of H-motifs : Consider a hypergraph $G = (V, E)$. A set of three connected hyperedges is an *instance* of h-motif t if their overlapping pattern corresponds to h-motif t . The count of each h-motif's instances is used to characterize the local structure of G , as discussed in the following sections.

Open and Closed H-motifs : A h-motif is *closed* if all three hyperedges in its instances are adjacent to (i.e., overlapped with) each other. If its instances contain two non-adjacent (i.e., disjoint) hyperedges, a h-motif is *open*. In Figure 3, h-motifs 17 - 22 are open; the others are closed.

Properties of H-motifs: From the definition of h-motifs, the following desirable properties are immediate:

- **Exhaustivity**: h-motifs capture overlapping patterns of *all possible* three connected hyperedges.
- **Unicity**: overlapping pattern of any three connected hyperedges is captured by *at most one* h-motif.
- **Size Independence**: h-motifs capture overlapping patterns *independently of the sizes of hyperedges*. Note that there can be infinitely many combinations of sizes of three connected hyperedges.

Note that the exhaustiveness and the uniqueness imply that overlapping pattern of any three connected hyperedges is captured by *exactly one* h-motif.

Why Multi-way Overlaps?: Multi-way overlaps (e.g., the emptiness of $e_1 \cap e_2 \cap e_3$ and $e_1 \setminus e_2 \setminus e_3$) play a key role in capturing the local structural patterns of real-world hypergraphs. Taking only the pairwise overlaps

(e.g., the emptiness of $e_1 \cap e_2$, $e_1 \setminus e_2$, and $e_2 \setminus e_1$) into account limits the number of possible overlapping patterns of three distinct hyperedges to just eight,² significantly limiting their expressiveness and thus usefulness. Specifically, 12 (out of 26) h-motifs have the same pairwise overlaps, while their occurrences and significances vary substantially in real-world hypergraphs. For example, in Figure 1, $\{e_1, e_2, e_4\}$ and $\{e_1, e_3, e_4\}$ have the same pairwise overlaps, while their overlapping patterns are distinguished by h-motifs.

3 Characterization using H-motifs

In this section, we outline the process of using h-motifs to summarize local structural patterns within a hypergraph, as well as those around individual nodes and hyperedges, for the purpose of characterizing them.

3.1 Hypergraph Characterization

What are the structural design principles of real-world hypergraphs distinguished from those of random hypergraphs? Below, we introduce the characteristic profile (CP), which is a tool for answering the above question using h-motifs.

Randomized Hypergraphs: While one might try to characterize the local structure of a hypergraph by absolute counts of each h-motif's instances in it, some h-motifs may naturally have many instances. Thus, for more accurate characterization, we need random hypergraphs to be compared against real-world hypergraphs. In the network motif literature, configuration models have been widely employed for this purpose [78,79]. These models generate random graphs while preserving the degree distribution of the original graph. Using the configuration model does not introduce an excessive level of randomness, maintaining a meaningful and controlled comparison with the original graph.

² Note that using the conventional network motifs in s limits this number to two.

In line with prior research, we used a configuration model extended to hypergraphs to obtain random hypergraphs. Specifically, we employ the Chung-Lu model [7], which is a configuration model designed to generate random bipartite graphs while preserving in expectation the degree distributions of the original graph [7] (for a precise theoretical description, please refer to Eq.(20) in Appendix F). We first apply this model to the incidence graph G' of the input hypergraph G to obtain randomized bipartite graphs, and then we transform them into random hypergraphs. The empirical distributions of node degrees and hyperedge sizes in the random hypergraphs closely resemble those in G , as shown in Figure 17 in Appendix F, where we also provide pseudocode of the process (Algorithm 6) and its theoretical properties.

Significance of H-motifs: We measure the significance of each h-motif in a hypergraph by comparing the count of its instances against the count of them in randomized hypergraphs. Specifically, the *significance* of a h-motif t in a hypergraph G is defined as

$$\Delta_t := \frac{M[t] - M_{rand}[t]}{M[t] + M_{rand}[t] + \epsilon}, \quad (1)$$

where $M[t]$ is the number of instances of h-motif t in G , and $M_{rand}[t]$ is the average number of instances of h-motif t in randomized hypergraphs. We fixed ϵ to 1 throughout this paper. This way of measuring significance was proposed for network motifs [78] as an alternative of normalized Z scores, which can be dominated by few network motifs with small variances. Specifically, when the variance of the occurrences of a specific network motif in randomized graphs is very small, the Z-score becomes significantly large, and thus the Z-score of the particular network motif may dominate all others, regardless of its absolute occurrences.

Characteristic Profile (CP): By normalizing and concatenating the significances of all h-motifs in a hypergraph, we obtain the characteristic profile (CP), which summarizes the local structural pattern of the hypergraph. Specifically, the *characteristic profile* of a hypergraph G is a vector of size 26, where each t -th element is

$$CP_t := \frac{\Delta_t}{\sqrt{\sum_{t=1}^{26} \Delta_t^2}}. \quad (2)$$

Note that, for each t , CP_t is between -1 and 1 . The CP is used in Section 6.3 to compare the local structural patterns of real-world hypergraphs from diverse domains.

3.2 Hyperedge Characterization

Each individual hyperedge can also be characterized by the h-motif instances that contain it.

Hyperedge Profile (HP): Specifically, given a hypergraph $G = (V, E)$, the *hyperedge profile* (HP) of a hyperedge $e \in E$ is a 26-element vector, where each t -th element is the number of h-motif t 's instances that include e . It should be noticed that, for HPs, we use absolute counts of h-motif instances rather than their normalized significances. Normalized significances are introduced for CPs to enable direct comparison of hypergraphs at different scales, specifically with varying numbers of nodes and hyperedges. Since comparisons between individual hyperedges, such as for the purpose of hyperedge prediction within a hypergraph, may be free from such issues, we simply use the absolute counts of h-motif instances when defining HPs.³ In Section 6.5, we demonstrate the effectiveness of HPs as input features in hyperedge prediction tasks.

3.3 Node Characterization

Similarly, we characterize each node by the h-motif instances in its ego network. Below, we introduce three types of ego-networks in hypergraphs, and based on these, we elaborate on the node characterization method.

Hypergraph Ego-networks: Comrie and Kleinberg [30] defined three distinct types of ego-networks. For each node $v \in V$ in a hypergraph $G = (V, E)$, we denote the neighborhood of v (including v itself) by $V_v := \bigcup_{e_i \in E_v} e_i$, where $E_v := \{e_i \in E : v \in e_i\}$. The *star ego-network* of v is a subhypergraph of G with V_v as its node set and E_v (i.e., the hyperedges that contain v) as its hyperedge set. The *radial ego-network* of v is a subhypergraph of G with V_v as its node set and $R_v := \{e_i \in E : e_i \subseteq V_v\}$ (i.e., the hyperedges that are subsets of the neighborhood of v) as its hyperedge set. Lastly, the *contracted ego-network* of v has V_v as its node set and $C_v := \bigcup_{e_i \in E} \{e_i \cap V_v\} \setminus \emptyset$ as its hyperedge set, and mathematically, the contracted ego-network of

³ Recall that the CPs are specifically designed to capture structural similarity between hypergraphs of potentially varying scales, typically using a simple metric such as cosine similarity. Regarding HPs and NPs (defined in Section 3.3), our primary objectives of using them are to distinguish missing hyperedges from other candidates (for HPs) and to distinguish nodes from different domains (for NPs). For these purposes, the scale information can be useful, and thus, we employ absolute counts for both HPs and NPs to retain and leverage this scale information. It is also important to note that, in our experiments, NPs and HPs are used with classifiers (e.g., hypergraph neural networks) powerful enough to capture (dis)similarity even across differing scales.

v is the subhypergraph of G induced by V_v . Note that $E_v \subseteq R_v \subseteq C_v$. Compared to E_v , R_v additionally includes hyperedges that consist only of the neighbors of v but not include v . Compared to R_v , C_v additionally includes the non-empty intersection of each hyperedge and the neighborhood of v .

Node Profile (NP): Given a hypergraph $G = (V, E)$, the *node profile* (NP) of a node $v \in V$ is a 26-element where each t -th element is the number of h-motif t 's instances within an ego-network of v . Note that, as for HPs, we use the absolute counts of h-motifs, instead of their normalized significances, for NPs. Depending on the types of ego-networks, we define *star node profiles* (SNPs), *radial node profiles* (RNPs), and *contracted node profiles* (CNPs). In Appendix K, we provide an empirical comparison of these three types of NPs in the context of a node classification task. The results show that using RNPs consistently yields better performance than SNPs or CNPs, indicating that additional complete hyperedges (i.e., $R_v \setminus E_v$) are helpful, while partial ones extracted from hyperedges (i.e., $C_v \setminus R_v$) are not.

4 Proposed Algorithms

Given a hypergraph, how can we count the instances of each h-motif? Once we count them in the original and randomized hypergraphs, the significance of each h-motif and the CP are obtained immediately by Eq. (1) and Eq. (2).

In this section, we present **MoCHy** (**Motif Counting in Hypergraphs**), which is a family of parallel algorithms for counting the instances of each h-motif in the input hypergraph. We first describe line-graph construction, which is a preprocessing step of every version of MoCHy. Then, we present MoCHy-E, which is for exact counting. After that, we present two different versions of MoCHy-A, which are sampling-based algorithms for approximate counting. Lastly, we discuss parallel and on-the-fly implementations.

Throughout this section, we use $h(\{e_i, e_j, e_k\})$ to denote the h-motif that describes the connectivity pattern of an h-motif instance $\{e_i, e_j, e_k\}$. We also use $M[t]$ to denote the count of instances of h-motif t .

Remarks: The problem of counting h-motifs' occurrences bears some similarity to the classic problem of counting network motifs' occurrences. However, differently from network motifs, which are defined solely based on pairwise interactions, h-motifs are defined based on triple-wise interactions (e.g., $e_i \cap e_j \cap e_k$). One might hypothesize that our problem can easily be reduced to the problem of counting the occurrences of network motifs,

Algorithm 1: Line Graph Construction

(Preprocess)

Input : input hypergraph: $G = (V, E)$

Output: line graph: $\bar{G} = (E, \wedge, \omega)$

1 $\wedge \leftarrow \emptyset$

2 $\omega \leftarrow$ map whose default value is 0

3 **for each hyperedge** $e_i \in E$ (*in parallel*) **do**

4 **for each node** $v \in e_i$ **do**

5 **for each hyperedge** $e_j \in E_v$ where $j > i$ **do**

6 $\wedge \leftarrow \wedge \cup \{\wedge_{ij}\}$

7 $\omega(\wedge_{ij}) = \omega(\wedge_{ij}) + 1$

8 **return** $\bar{G} = (E, \wedge, \omega)$

and thus existing solutions (e.g., [20, 87]) are applicable to our problem. In order to examine this possibility, we consider the following two attempts:

- (a) Represent pairwise relations between hyperedges using the line graph, where each edge $\{e_i, e_j\}$ indicates $e_i \cap e_j \neq \emptyset$.
- (b) Represent pairwise relations between hyperedges using the directed line graph where each directed edge $e_i \rightarrow e_j$ indicates $e_i \cap e_j \neq \emptyset$ and at the same time $e_i \not\subseteq e_j$.

The number of possible connectivity patterns (i.e., network motifs) among three distinct connected hyperedges is just two (i.e., closed and open triangles) and eight in (a) and (b), respectively. In both cases, instances of multiple h-motifs are not distinguished by network motifs, and the occurrences of h-motifs can not be inferred from those of network motifs.

In addition, another computational challenge stems from the fact that triple-wise and even pair-wise relations between hyperedges need to be computed from the input hypergraph, while pairwise relations between edges are given in graphs. This challenge necessitates the precomputation of partial relations, described in the next subsection.

4.1 Line Graph Construction (Algorithm 1)

As a preprocessing step, every version of MoCHy builds the line graph $\bar{G} = (E, \wedge, \omega)$ (see Section 2.1) of the input hypergraph $G = (V, E)$, as described in Algorithm 1. To find the neighbors of each hyperedge e_i (line 3), the algorithm visits each hyperedge e_j that contains v and satisfies $j > i$ (line 5) for each node $v \in e_i$ (line 4). Then for each such e_j , it adds $\wedge_{ij} = \{e_i, e_j\}$ to \wedge and increments $\omega(\wedge_{ij})$ (lines 6 and 7). The time complexity of this preprocessing step is given in Lemma 1.

Algorithm 2: MoChy-E: Exact H-motif Counting

Input : (1) input hypergraph: $G = (V, E)$
(2) line graph: $\bar{G} = (E, \wedge, \omega)$

Output: exact count of each h-motif t 's instances $M[t]$

- 1 $M \leftarrow$ map whose default value is 0
- 2 **for each** hyperedge $e_i \in E$ (**in parallel**) **do**
- 3 **for each** unordered hyperedge pair $\{e_j, e_k\} \in \binom{N_{e_i}}{2}$ **do**
- 4 **if** $e_j \cap e_k = \emptyset$ or $i < \min(j, k)$ **then**
- 5 $M[h(\{e_i, e_j, e_k\})] += 1$
- 6 **return** M

Lemma 1 (Complexity of Line Graph Construction) *The expected time complexity of Algorithm 1 is $O(\sum_{\wedge_{ij} \in \wedge} |e_i \cap e_j|)$.*

Proof. If all sets and maps are implemented using hash tables, the expected time complexity of lines 6 and 7 is $O(1)$ in expectation with uniform hash functions, and they are executed $|e_i \cap e_j|$ times for each $\wedge_{ij} \in \wedge$. \square

Since $|\wedge| < \sum_{e_i \in E} |N_{e_i}|$ and $|e_i \cap e_j| \leq |e_i|$, Eq. (3) holds.

$$\sum_{\wedge_{ij} \in \wedge} |e_i \cap e_j| < \sum_{e_i \in E} (|e_i| \cdot |N_{e_i}|). \quad (3)$$

4.2 Exact H-motif Counting (Algorithm 2)

We present MoChy-E (MoChy **E**xact), which counts the instances of each h-motif exactly. The procedures of MoChy-E are described in Algorithm 2. For each hyperedge $e_i \in E$ (line 2), each unordered pair $\{e_j, e_k\}$ of its neighbors, where $\{e_i, e_j, e_k\}$ is an h-motif instance, is considered (line 3). If $e_j \cap e_k = \emptyset$ (i.e., if the corresponding h-motif is open), $\{e_i, e_j, e_k\}$ is considered only once. However, if $e_j \cap e_k \neq \emptyset$ (i.e., if the corresponding h-motif is closed), $\{e_i, e_j, e_k\}$ is considered two more times (i.e., when e_j is chosen in line 2 and when e_k is chosen in line 2). Based on these observations, given an h-motif instance $\{e_i, e_j, e_k\}$, the corresponding count $M[h(\{e_i, e_j, e_k\})]$ is incremented (line 5) only if $e_j \cap e_k = \emptyset$ or $i < \min(j, k)$ (line 4). This guarantees that each instance is counted exactly once. The time complexity of MoChy-E is given in Theorem 1, which uses Lemma 2.

Lemma 2 (Complexity of Computing $h(\{e_i, e_j, e_k\})$) *Given the input hypergraph $G = (V, E)$ and its line graph $\bar{G} = (E, \wedge, \omega)$, for each h-motif instance $\{e_i, e_j, e_k\}$, the expected time for computing $h(\{e_i, e_j, e_k\})$ is $O(\min(|e_i|, |e_j|, |e_k|))$.*

Proof. Assume $|e_i| = \min(|e_i|, |e_j|, |e_k|)$, without loss of generality, and all sets and maps are implemented using hash tables. As defined in Section 2.2, $h(\{e_i, e_j, e_k\})$ is computed in $O(1)$ time from the emptiness of the following sets: (1) $e_i \setminus e_j \setminus e_k$, (2) $e_j \setminus e_k \setminus e_i$, (3) $e_k \setminus e_i \setminus e_j$, (4) $e_i \cap e_j \setminus e_k$, (5) $e_j \cap e_k \setminus e_i$, (6) $e_k \cap e_i \setminus e_j$, and (7) $e_i \cap e_j \cap e_k$. We check their emptiness from their cardinalities. We obtain e_i , e_j , and e_k , which are stored in G , and their cardinalities in $O(1)$ time. Similarly, we obtain $|e_i \cap e_j|$, $|e_j \cap e_k|$, and $|e_k \cap e_i|$, which are stored in \bar{G} , in $O(1)$ time in expectation with uniform hash functions. Then, we compute $|e_i \cap e_j \cap e_k|$ in $O(|e_i|)$ time in expectation by checking for each node in e_i whether it is also in both e_j and e_k . From these cardinalities, we obtain the cardinalities of the six other sets in $O(1)$ time as follows:

$$\begin{aligned} (1) & |e_i \setminus e_j \setminus e_k| = |e_i| - |e_i \cap e_j| - |e_k \cap e_i| + |e_i \cap e_j \cap e_k|, \\ (2) & |e_j \setminus e_k \setminus e_i| = |e_j| - |e_i \cap e_j| - |e_j \cap e_k| + |e_i \cap e_j \cap e_k|, \\ (3) & |e_k \setminus e_i \setminus e_j| = |e_k| - |e_k \cap e_i| - |e_j \cap e_k| + |e_i \cap e_j \cap e_k|, \\ (4) & |e_i \cap e_j \setminus e_k| = |e_i \cap e_j| - |e_i \cap e_j \cap e_k|, \\ (5) & |e_j \cap e_k \setminus e_i| = |e_j \cap e_k| - |e_i \cap e_j \cap e_k|, \\ (6) & |e_k \cap e_i \setminus e_j| = |e_k \cap e_i| - |e_i \cap e_j \cap e_k|. \end{aligned}$$

Hence, the expected time complexity of computing $h(\{e_i, e_j, e_k\})$ is $O(|e_i|) = O(\min(|e_i|, |e_j|, |e_k|))$. \square

Theorem 1 (Complexity of MoChy-E) *The expected time complexity of Algorithm 2 is $O(\sum_{e_i \in E} (|N_{e_i}|^2 \cdot |e_i|))$.*

Proof. Assume all sets and maps are implemented using hash tables. The total number of triples $\{e_i, e_j, e_k\}$ considered in line 3 is $O(\sum_{e_i \in E} |N_{e_i}|^2)$. By Lemma 2, for such a triple $\{e_i, e_j, e_k\}$, the expected time for computing $h(\{e_i, e_j, e_k\})$ is $O(|e_i|)$. Thus, the total expected time complexity of Algorithm 2 is $O(\sum_{e_i \in E} (|e_i| \cdot |N_{e_i}|^2))$, which dominates that of the preprocessing step (see Lemma 1 and Eq. (3)). \square

Extension of MoChy-E to H-motif Enumeration:

Since MoChy-E visits all h-motif instances to count them, it is extended to the problem of enumerating every h-motif instance (with its corresponding h-motif), as described in Algorithm 3. The time complexity remains the same.

4.3 Approximate H-motif Counting

We present two different versions of MoChy-A (MoChy **A**pproximate), which approximately count the instances of each h-motif. Both versions yield unbiased estimates of the counts by exploring the input hypergraph partially through hyperedge and hyperwedge sampling, respectively.

Algorithm 3: MoCHy-ENUM for H-motif Enumeration

Input : (1) input hypergraph: $G = (V, E)$
(2) line graph: $\tilde{G} = (E, \wedge, \omega)$

Output: h-motif instances and their corresponding h-motifs

- 1 **for each** hyperedge $e_i \in E$ (*in parallel*) **do**
- 2 **for each** unordered hyperedge pair $\{e_j, e_k\} \in \binom{N_{e_i}}{2}$ **do**
- 3 **if** $e_j \cap e_k = \emptyset$ or $i < \min(j, k)$ **then**
- 4 write($e_i, e_j, e_k, h(\{e_i, e_j, e_k\})$)

Algorithm 4: MoCHy-A: Approximate H-motif Counting Based on Hyperedge Sampling

Input : (1) input hypergraph: $G = (V, E)$
(2) line graph: $\tilde{G} = (E, \wedge, \omega)$
(3) number of samples: s

Output: estimated count of each h-motif t 's instances: $\bar{M}[t]$

- 1 $\bar{M}[t] \leftarrow$ map whose default value is 0
- 2 **for** $n \leftarrow 1 \dots s$ (*in parallel*) **do**
- 3 $e_i \leftarrow$ sample a uniformly random hyperedge
- 4 **for each** hyperedge $e_j \in N_{e_i}$ **do**
- 5 **for each** hyperedge
- 6 $e_k \in (N_{e_i} \cup N_{e_j} \setminus \{e_i, e_j\})$ **do**
- 7 **if** $e_k \not\subseteq N_{e_i}$ or $j < k$ **then**
- 8 $\bar{M}[h(\{e_i, e_j, e_k\})] += 1$
- 9 **for each** h-motif t **do**
- 10 $\bar{M}[t] \leftarrow \bar{M}[t] \cdot \frac{|E|}{3s}$
- 11 **return** \bar{M}

MoCHy-A: Hyperedge Sampling (Algorithm 4):

MoCHy-A (Algorithm 4) is based on hyperedge sampling. It repeatedly samples s hyperedges from the hyperedge set E uniformly at random with replacement (line 3). For each sampled hyperedge e_i , the algorithm searches for all h-motif instances that contain e_i (lines 4-7), and to this end, the 1-hop and 2-hop neighbors of e_i in the line graph \tilde{G} are explored. After that, for each such instance $\{e_i, e_j, e_k\}$ of h-motif t , the corresponding count $\bar{M}[t]$ is incremented (line 7). Lastly, each estimate $\bar{M}[t]$ is rescaled by multiplying it with $\frac{|E|}{3s}$ (lines 8-9), which is the reciprocal of the expected number of times that each of the h-motif t 's instances is counted.⁴ This rescaling makes each estimate $\bar{M}[t]$ unbiased, as formalized in Theorem 2.

⁴ Each hyperedge is expected to be sampled $\frac{s}{|E|}$ times, and each h-motif instance is counted whenever any of its 3 hyperedges is sampled.

Theorem 2 (Bias and Variance of MoCHy-A) For every h-motif t , Algorithm 4 provides an unbiased estimate $\bar{M}[t]$ of the count $M[t]$ of its instances, i.e.,

$$\mathbb{E}[\bar{M}[t]] = M[t]. \quad (4)$$

The variance of the estimate is

$$\text{Var}[\bar{M}[t]] = \frac{1}{3s} \cdot M[t] \cdot (|E| - 3) + \frac{1}{9s} \sum_{l=0}^2 p_l[t] \cdot (l|E| - 9), \quad (5)$$

where $p_l[t]$ is the number of pairs of h-motif t 's instances that share l hyperedges.

Proof. See Appendix A. \square

The time complexity of MoCHy-A is given in Theorem 3.

Theorem 3 (Complexity of MoCHy-A) The expected time complexity of Algorithm 4 is $O(\frac{s}{|E|} \sum_{e_i \in E} (|e_i| \cdot |N_{e_i}|^2))$.

Proof. Assume all sets and maps are implemented using hash tables. For a sample hyperedge e_i , computing $N_{e_i} \cup N_{e_j}$ for every $e_j \in N_{e_i}$ takes $O(\sum_{e_j \in N_{e_i}} (|N_{e_i}| + |N_{e_j}|))$ time in expectation with uniform hash functions if we compute $N_{e_i} \cup N_{e_j}$ by checking whether each hyperedge $e \in N_{e_j}$ is also in N_{e_i} . By Lemma 2, computing $h(\{e_i, e_j, e_k\})$ for all considered h-motif instances takes $O(\min(|e_i|, |e_j|) \cdot \sum_{e_j \in N_{e_i}} |N_{e_i}| + |N_{e_j}|)$ time in expectation. Thus, the expected time complexity for processing a sample e_i is

$$\begin{aligned} &O(\min(|e_i|, |e_j|) \cdot \sum_{e_j \in N_{e_i}} (|N_{e_i}| + |N_{e_j}|)) \\ &= O(|e_i| \cdot |N_{e_i}|^2 + \sum_{e_j \in N_{e_i}} (|e_j| \cdot |N_{e_j}|)), \end{aligned}$$

which can be written as

$$\begin{aligned} &O(\sum_{e_i \in E} (\mathbb{1}(e_i \text{ is sampled}) \cdot |e_i| \cdot |N_{e_i}|^2) \\ &+ \sum_{e_j \in E} (\mathbb{1}(e_j \text{ is adjacent to the sample}) \cdot |e_j| \cdot |N_{e_j}|)). \end{aligned}$$

From this, linearity of expectation, $\mathbb{E}[\mathbb{1}(e_i \text{ is sampled})] = \frac{1}{|E|}$, and $\mathbb{E}[\mathbb{1}(e_j \text{ is adjacent to the sample})] = \frac{|N_{e_j}|}{|E|}$, the expected time complexity per sample hyperedge becomes $O(\frac{1}{|E|} \sum_{e_i \in E} (|e_i| \cdot |N_{e_i}|^2))$. Hence, the expected total time complexity for processing s samples is $O(\frac{s}{|E|} \sum_{e_i \in E} (|e_i| \cdot |N_{e_i}|^2))$. \square

We also obtain concentration inequalities of MoCHy-A (Theorem 4) using Hoeffding's inequality (Lemma 3), and the inequalities particularly depend on the number of samples and the number of instances of each h-motif.

Algorithm 5: MoCHy-A⁺: Approximate H-motif Counting Based on Hyperwedge Sampling

Input : (1) input hypergraph: $G = (V, E)$
 (2) line graph: $\bar{G} = (E, \wedge, \omega)$
 (3) number of samples: r

Output: estimated count of each h-motif t 's instances: $\hat{M}[t]$

```

1  $\hat{M} \leftarrow$  map whose default value is 0
2 for  $n \leftarrow 1 \dots r$  (in parallel) do
3    $\wedge_{ij} \leftarrow$  a uniformly random hyperwedge
4   for each hyperedge  $e_k \in (N_{e_i} \cup N_{e_j} \setminus \{e_i, e_j\})$ 
5     do
6        $\hat{M}[h(\{e_i, e_j, e_k\})] += 1$ 
7   for each h-motif  $t$  do
8     if  $17 \leq t \leq 22$  then ▷ open h-motifs
9        $\hat{M}[t] \leftarrow \hat{M}[t] \cdot \frac{|\wedge|}{2r}$ 
10    else ▷ closed h-motifs
11       $\hat{M}[t] \leftarrow \hat{M}[t] \cdot \frac{|\wedge|}{3r}$ 
12 return  $\hat{M}$ 

```

Lemma 3 (Hoeffding's Inequality [38]) Let X_1, X_2, \dots, X_n be independent random variables with $a_j \leq X_j \leq b_j$ for every $j \in \{1, 2, \dots, n\}$. Consider the sum of random variables $X = X_1 + \dots + X_n$, and let $\mu = \mathbb{E}[X]$. Then for any $\tau > 0$, we have

$$\Pr[|X - \mu| \geq \tau] \leq 2 \exp\left(-\frac{2\tau^2}{\sum_{j=1}^n (b_j - a_j)^2}\right).$$

Theorem 4 (Concentration Bound of MoCHy-A)

Let $d_{\max}[t] = \max_{e \in E[t]} |N_e|$ where $E[t] := \bigcup_{h(e_i, e_j, e_k)=t} \{e_i, e_j, e_k\}$. For any $\epsilon, \delta > 0$, if $M[t] > 0$ and the number of samples $s > \frac{1}{18\epsilon^2} \left(\frac{|E|d_{\max}[t]^2}{M[t]}\right)^2 \log\left(\frac{2}{\delta}\right)$, then $\Pr(|\bar{M}[t] - M[t]| \geq M[t] \cdot \epsilon) \leq \delta$ holds for each $t \in \{1, 2, \dots, 26\}$.

Proof. See Appendix B. □

MoCHy-A⁺: Hyperwedge Sampling (Algorithm 5):

MoCHy-A⁺ (Algorithm 5) provides a better trade-off between speed and accuracy than MoCHy-A. Differently from MoCHy-A, which samples hyperedges, MoCHy-A⁺ is based on hyperwedge sampling. It selects r hyperwedges uniformly at random with replacement (line 3), and for each sampled hyperwedge $\wedge_{ij} \in \wedge$, it searches for all h-motif instances that contain \wedge_{ij} (lines 4-5). To this end, the hyperedges that are adjacent to e_i or e_j in the line graph \bar{G} are considered (line 4). For each such instance $\{e_i, e_j, e_k\}$ of h-motif t , the corresponding estimate $\hat{M}[t]$ is incremented (line 5). Lastly, each estimate $\hat{M}[t]$ is rescaled so that it unbiasedly estimates $M[t]$, as

formalized in Theorem 5. To this end, it is multiplied by the reciprocal of the expected number of times that each instance of h-motif t is counted.⁵

Theorem 5 (Bias and Variance of MoCHy-A⁺)

For every h-motif t , Algorithm 5 provides an unbiased estimate $\hat{M}[t]$ of the count $M[t]$ of its instances, i.e.,

$$\mathbb{E}[\hat{M}[t]] = M[t]. \quad (6)$$

For every closed h-motif t , the variance of the estimate is

$$\text{Var}[\hat{M}[t]] = \frac{1}{3r} \cdot M[t] \cdot (|\wedge| - 3) + \frac{1}{9r} \sum_{n=0}^1 q_n[t] \cdot (n|\wedge| - 9), \quad (7)$$

where $q_n[t]$ is the number of pairs of h-motif t 's instances that share n hyperwedges. For every open h-motif t , the variance is

$$\text{Var}[\hat{M}[t]] = \frac{1}{2r} \cdot M[t] \cdot (|\wedge| - 2) + \frac{1}{4r} \sum_{n=0}^1 q_n[t] \cdot (n|\wedge| - 4). \quad (8)$$

Proof. See Appendix C. □

The time complexity of MoCHy-A⁺ is given in Theorem 6.

Theorem 6 (Complexity of MoCHy-A⁺) The expected time complexity of Algorithm 5 is $O\left(\frac{r}{|\wedge|} \sum_{e_i \in E} (|e_i| \cdot |N_{e_i}|^2)\right)$.

Proof. Assume all sets and maps are implemented using hash tables. For a sample hyperwedge \wedge_{ij} , computing $N_{e_i} \cup N_{e_j}$ takes $O(|N_{e_i}| + |N_{e_j}|)$ time in expectation with uniform hash functions if we compute $N_{e_i} \cup N_{e_j}$ by checking whether each hyperedge $e \in N_{e_j}$ is also in N_{e_i} . By Lemma 2, computing $h(\{e_i, e_j, e_k\})$ for all considered h-motif instances takes $O(\min(|e_i|, |e_j|) \cdot |N_{e_i}| + |N_{e_j}|)$ time in expectation. Thus, the expected time complexity for processing a sample \wedge_{ij} is $O(\min(|e_i|, |e_j|) \cdot (|N_{e_i}| + |N_{e_j}|)) = O(|e_i| \cdot |N_{e_i}| + |e_j| \cdot |N_{e_j}|)$, which can be written as

$$O\left(\sum_{e_i \in E} (\mathbb{1}(e_i \text{ is included in the sample}) \cdot |e_i| \cdot |N_{e_i}|) + \sum_{e_j \in E} (\mathbb{1}(e_j \text{ is included in the sample}) \cdot |e_j| \cdot |N_{e_j}|)\right).$$

⁵ Note that each instance of open and closed h-motifs contains 2 and 3 hyperwedges, respectively. Each instance of closed h-motifs is counted if one of the 3 hyperwedges in it is sampled, while that of open h-motifs is counted if one of the 2 hyperwedges in it is sampled. Thus, in expectation, each instance of open and closed h-motifs is counted $3r/|\wedge|$ and $2r/|\wedge|$ times, respectively.

From this, linearity of expectation, $\mathbb{E}[\mathbb{1}(e_i \text{ is included in the sample})] = \frac{|N_{e_i}|}{|\wedge|}$, and $\mathbb{E}[\mathbb{1}(e_j \text{ is included in the sample})] = \frac{|N_{e_j}|}{|\wedge|}$, the expected time complexity per sample hyperwedge is $O(\frac{1}{|\wedge|} \sum_{e_i \in E} (|e_i| \cdot |N_{e_i}|^2))$. Hence, the total time complexity for processing r samples is $O(\frac{r}{|\wedge|} \sum_{e_i \in E} (|e_i| \cdot |N_{e_i}|^2))$. \square

Additionally, we derive concentration inequalities for MoCHy-A⁺ (Theorem 7), following a similar approach to that of Theorem 4, but with different minimum sample sizes for guaranteeing the same bound.

Theorem 7 (Concentration Bound of MoCHy-A⁺)

Let $d_{\max}[t] = \max_{e \in E[t]} |N_e|$ where $E[t] := \bigcup_{h(e_i, e_j, e_k)=t} \{e_i, e_j, e_k\}$. For each $t \in \{1, \dots, 26\}$ such that $M[t] > 0$ and for any $\epsilon, \delta > 0$, a sufficient condition of being $\Pr(|\hat{M}[t] - M[t]| \geq M[t] \cdot \epsilon) \leq \delta$ is $r > \frac{1}{18\epsilon^2} \left(\frac{|A|d_{\max}[t]}{M[t]} \right)^2 \log(\frac{2}{\delta})$, if h-motif t is closed, and $r > \frac{1}{8\epsilon^2} \left(\frac{|A|d_{\max}[t]}{M[t]} \right)^2 \log(\frac{2}{\delta})$, if motif t is open.

Proof. See Appendix D. \square

Comparison of MoCHy-A and MoCHy-A⁺:

Empirically, MoCHy-A⁺ provides a better trade-off between speed and accuracy than MoCHy-A, as presented in Section 6.7. We provide an analysis that supports this observation. Assume that the numbers of samples in both algorithms are set so that $\alpha = \frac{s}{|E|} = \frac{r}{|\wedge|}$. For each h-motif t , since both estimates $\bar{M}[t]$ of MoCHy-A and $\hat{M}[t]$ of MoCHy-A⁺ are unbiased (see Eqs. (4) and (6)), we only need to compare their variances. By Eq. (5), $\text{Var}[\bar{M}[t]] = O(\frac{M[t]+p_1[t]+p_2[t]}{\alpha})$, and by Eq. (7) and Eq. (8), $\text{Var}[\hat{M}[t]] = O(\frac{\hat{M}[t]+q_1[t]}{\alpha})$. By definition, $q_1[t] \leq p_2[t]$, and thus $\frac{\hat{M}[t]+q_1[t]}{\alpha} \leq \frac{M[t]+p_1[t]+p_2[t]}{\alpha}$. Moreover, in real-world hypergraphs, $p_1[t]$ tends to be several orders of magnitude larger than the other terms (i.e., $p_2[t]$, $q_1[t]$, and $M[t]$), and thus $\bar{M}[t]$ of MoCHy-A tends to have larger variance (and thus larger estimation error) than $\hat{M}[t]$ of MoCHy-A⁺. Despite this fact, as shown in Theorems 3 and 6, MoCHy-A and MoCHy-A⁺ have the same time complexity, $O(\alpha \cdot \sum_{e_i \in E} (|e_i| \cdot |N_{e_i}|^2))$. Hence, MoCHy-A⁺ is expected to give a better trade-off between speed and accuracy than MoCHy-A, as confirmed empirically in Section 6.7.

Regarding the concentration lower bounds of the number of samples (Theorems 4 and 7), the ratio of the bound in MoCHy-A to that MoCHy-A⁺ is $\frac{|E| \cdot d_{\max}[t]}{|\wedge|}$ for each closed h-motif t , and $\frac{4|E| \cdot d_{\max}[t]}{9|\wedge|}$ for each open h-motif t . In real-world datasets (refer to Table 2 in Section 6.1), the maximum value (across all h-motifs)

of $\frac{|E| \cdot d_{\max}[t]}{|\wedge|}$ varies from 5 (in the *contact-primary*) to 500 (in the *coauth-history*). That is, MoCHy-A⁺ requires fewer samples than MoCHy-A for the same bound, thereby supporting the empirical superiority of MoCHy-A⁺ over MoCHy-A. However, it is important to note a limitation in this comparison of bounds. Our concentration bounds may not be optimal since they are based on worst-case scenarios, relying on the term $d_{\max}[t]$.

4.4 Parallel and On-the-fly Implementations

We discuss parallelization of MoCHy and then on-the-fly computation of line graphs.

Parallelization: All versions of MoCHy and line-graph construction are easily parallelized as highlighted in Algorithms 1-5. Specifically, we can parallelize line-graph construction and MoCHy-E by letting multiple threads process different hyperedges (in line 3 of Algorithm 1 and line 2 of Algorithm 2) independently in parallel. Similarly, we can parallelize MoCHy-A and MoCHy-A⁺ by letting multiple threads sample and process different hyperedges (in line 3 of Algorithm 4) and hyperwedges (in line 3 of Algorithm 5) independently in parallel. The estimated counts of the same h-motif obtained by different threads are summed up only once before they are returned as outputs. We present some empirical results in Section 6.7.

H-motif Counting without Line Graphs: If the input hypergraph G is large, computing its line graph \tilde{G} (Algorithm 1) is time and space-consuming. Specifically, building \tilde{G} takes $O(\sum_{\wedge_{ij} \in \wedge} |e_i \cap e_j|)$ time (see Lemma 1) and requires $O(|E| + |\wedge|)$ space, which often exceeds $O(\sum_{e_i \in E} |e_i|)$ space required for storing G . Thus, instead of precomputing \tilde{G} entirely, we can build it incrementally while memoizing partial results within a given memory budget. We apply this idea to MoCHy-A⁺, resulting in the following two versions of the algorithm:

- **On-the-fly MoCHy-A⁺ (Basic):** This is a straightforward application of the memoization idea to MoCHy-A⁺ (Algorithm 5). We compute the neighborhood of a hyperedge $e_i \in E$ in \tilde{G} (i.e., $\{(k, \omega(\wedge_{ik})) : k \in N_{e_i}\}$) only if (1) a hyperwedge with e_i (e.g., \wedge_{ij}) is sampled (in line 3) and (2) its neighborhood is not memoized. The computed neighborhood is memoized with priority based on the degree $|N_{e_i}|$ of e_i in \tilde{G} . That is, if the memoization budget is exceeded, we evict the memoized neighborhood of hyperedges in decreasing order of their degrees in \tilde{G} until the budget is met. This is because the neighborhood of high-degree hyperedges is frequently retrieved, despite a higher computational cost. According to our

preliminary studies, this memoization scheme based on degree demonstrates faster speeds compared to memoizing the neighborhood of random hyperedges or least recently used (LRU) hyperedges.

- **On-the-fly MoCHy-A⁺ (Adv.)**: This is an improved version that considers the order in which hyperwedges are processed. It first collects a list W of sampled hyperwedges and groups the hyperwedges consisting of the same hyperedge. Between the two hyperedges forming a hyperwedge, the one with the larger neighborhood is used to group the hyperwedge. The hyperwedges are processed group by group, and thus hyperwedges consisting of the same hyperedges are more likely to be processed consecutively, thereby increasing the chance of utilizing memoized neighborhoods before they are evicted. As a result, On-the-fly MoCHy-A⁺ (Adv.) is empirically faster than On-the-fly MoCHy-A⁺ (Basic), as shown in Section 6.7.

For details of On-the-fly MoCHy-A⁺ (Basic) and On-the-fly MoCHy-A⁺ (Adv.), refer to Algorithms 8 and 9, respectively, in Appendix I.

5 Extensions of H-motifs

In this section, we explore two distinct approaches to extending the concept of h-motifs. We especially define ternary hypergraph motifs, which demonstrate consistent advantages for a variety of real-world applications.

5.1 Extensions Beyond Binary

As defined in Section 2.2, h-motifs describe overlapping patterns of three hyperedges solely based on the emptiness of the seven subsets derived from their intersections. That is, for each subset, h-motifs classify it into binary states, non-empty or empty, which corresponds to being colored or uncolored in Figure 3. This coarse classification inevitably results in the loss of detailed information within the intersections. Below, we introduce ternary hypergraph motifs, which mitigate this information loss by assigning ternary states to each subset based on its cardinality.

Definition of 3H-motifs: Ternary hypergraph motifs (or 3h-motifs in short) are the extension of h-motifs, so as h-motifs are, they are designed for describing the overlapping pattern of three connected hyperedges. Given an instance (i.e., three connected hyperedges) $\{e_i, e_j, e_k\}$, 3h-motifs describe its overlapping pattern by the cardinality of the following seven sets: (1) $e_i \setminus e_j \setminus e_k$, (2) $e_j \setminus e_k \setminus e_i$, (3) $e_k \setminus e_i \setminus e_j$, (4) $e_i \cap e_j \setminus e_k$, (5)



Fig. 5: The six 3h-motifs subdivided from h-motif 1. In each Venn diagram, uncolored regions are empty without containing any nodes. Colored regions with a triangle contain more than 0 and at most θ nodes, while colored regions with a circle contain more than θ nodes. Throughout this paper, we set θ to 1.

$e_j \cap e_k \setminus e_i$, (6) $e_k \cap e_i \setminus e_j$, and (7) $e_i \cap e_j \cap e_k$. Differently from h-motifs, which consider two states for each subset (empty or non-empty), 3h-motifs takes into account three (denoted by the ‘3’ in 3h-motifs.) states for each subset. Specifically, for each of these seven sets, we classify it into three states based on its cardinality c as follows: (1) $c = 0$, (2) $0 < c \leq \theta$, (3) $c > \theta$, where $\theta \geq 1$. Throughout this paper, we set the value of θ to 1, and thus each of these seven sets is classified into one of three categories: empty, singleton, and multiple. Equivalently, if we leave $\min(\lceil c/\theta \rceil, 2)$ node in each of the above subsets with cardinality c , 3h-motifs can be defined based on the isomorphism between sub-hypergraphs formed by three connected hyperedges. Refer to Appendix L for a discussion on 3h-motifs with different values of θ and additional variants of 3h-motifs. Out of the 3^7 possible patterns, 431 3h-motifs remain if we exclude symmetric ones, those that cannot be obtained from distinct hyperedges, and those that cannot be derived from connected hyperedges. Visual representations of 3h-motifs 1-6, which are the six 3h-motifs subdivided from h-motif 1, are provided in Figure 5. For a complete list of all 431 3h-motifs, refer to Appendix L.

Characterization using 3H-motifs: 3H-motifs can naturally substitute h-motifs for characterizing hypergraphs, hyperedges, and nodes. By using 3h-motifs, characteristic profiles (CPs), hyperedge profiles (HPs), and node profiles (NPs) become 431-element vectors.

Counting 3H-motifs’ Instances: To count instances of 3h-motifs using the MoCHy, the only necessary change is to replace $h(\{e_i, e_j, e_k\})$ with $h_3(\{e_i, e_j, e_k\})$, which provides the corresponding 3h-motif for a given instance $\{e_i, e_j, e_k\}$. As formalized in Lemma 4, $h_3(\{e_i, e_j, e_k\})$ can be computed with the same time complexity as $h(\{e_i, e_j, e_k\})$, and thus replacing $h(\{e_i, e_j, e_k\})$ with $h_3(\{e_i, e_j, e_k\})$ does not change the time complexity of all versions of MoCHy.

Lemma 4 (Complexity of Computing $h_3(\{e_i, e_j, e_k\})$)
Given the input hypergraph $G = (V, E)$ and its line

graph $\bar{G} = (E, \wedge, \omega)$, for each 3h-motif instance $\{e_i, e_j, e_k\}$, the expected time complexity for computing $h_3(\{e_i, e_j, e_k\})$ is $O(\min(|e_i|, |e_j|, |e_k|))$.

Proof. Following the proof of Lemma 2, we can show that it takes $O(\min(|e_i|, |e_j|, |e_k|))$ time in expectation to obtain the cardinalities of all the following sets: (1) $e_i \setminus e_j \setminus e_k$, (2) $e_j \setminus e_k \setminus e_i$, (3) $e_k \setminus e_i \setminus e_j$, (4) $e_i \cap e_j \setminus e_k$, (5) $e_j \cap e_k \setminus e_i$, (6) $e_k \cap e_i \setminus e_j$, and (7) $e_i \cap e_j \cap e_k$. Based on the cardinality c of each of the seven sets, it takes $O(1)$ time to classify it into (1) $c = 0$, (2) $0 < c \leq \theta$, and (3) $c > \theta$. Classifying all seven sets, which takes $O(1)$ time, determines a specific 3h-motif. Thus, the expected time complexity of computing $h_3(\{e_i, e_j, e_k\})$ is $O(\min(|e_i|, |e_j|, |e_k|))$, which is same as that of computing $h(\{e_i, e_j, e_k\})$. \square

Extensions Beyond Ternary: The concept of 3h-motifs can be generalized to kh -motifs for any $k > 3$ by classifying each of the seven considered sets into k states. For instance, for $k = 4$, each set can be classified into four states based on its cardinality c as follows: (1) $c = 0$, (2) $0 < c \leq \theta_1$, (3) $\theta_1 < c \leq \theta_2$, (4) $c > \theta_2$, where $\theta_2 > \theta_1 \geq 1$. The number of kh -motifs increases rapidly with respect to k . Specifically, the number becomes 3,076 for $k = 4$, 14,190 for $k = 5$, and 49,750 for $k = 6$, as derived in Appendix H. In this study, we concentrate on h-motifs and 3h-motifs (i.e., $k = 2$ and $k = 3$), which are already capable of characterizing local structures in real-world hypergraphs, as evidenced by the empirical results in Section 6.

5.2 Extensions Beyond Three Hyperedges

The concept of h-motifs is easily generalized to four or more hyperedges. For example, a h-motif for four hyperedges can be defined as a binary vector of size 15 indicating the emptiness of each region in the Venn diagram for four sets. After excluding disconnected ones, symmetric ones, and those that cannot be obtained from distinct hyperedges, there remain 1,853 and 18,656,322 h-motifs for four and five hyperedges, respectively, as discussed in detail in Appendix G. This work focuses on the h-motifs for three hyperedges, which are already capable of characterizing local structures of real-world hypergraphs, as shown empirically in Section 6.

6 Experiments

In this section, we review the experiments that we design for answering the following questions:

Table 2: Statistics of 11 real hypergraphs from 5 domains.

Dataset	$ V $	$ E $	$ \bar{e} ^*$	$ \wedge $	$ \bar{N}_e ^{**}$	# H-motifs
coauth-DBLP	1,924,991	2,466,792	25	125M	3,016	26.3B \pm 18M
coauth-geology	1,256,385	1,203,895	25	37.6M	1,935	6B \pm 4.8M
coauth-history	1,014,734	895,439	25	1.7M	855	83.2M
contact-primary	242	12,704	5	2.2M	916	617M
contact-high	327	7,818	5	593K	439	69.7M
email-Enron	143	1,512	18	87.8K	590	9.6M
email-EU	998	25,027	25	8.3M	6,152	7B
tags-ubuntu	3,029	147,222	5	564M	40,836	4.3T \pm 1.5B
tags-math	1,629	170,476	5	913M	49,559	9.2T \pm 3.2B
threads-ubuntu	125,602	166,999	14	21.6M	5,968	11.4B
threads-math	176,445	595,749	21	647M	39,019	2.2T \pm 883M

* The maximum size of a hyperedge. ** The maximum degree in the line graph.

- **Q1. Comparison with Random:** Does counting instances of different h-motifs reveal structural design principles of real-world hypergraphs distinguished from those of random hypergraphs?
- **Q2. Comparison across Domains:** Do characteristic profiles capture local structural patterns of hypergraphs unique to each domain?
- **Q3. Comparison of Characterization Powers:** How well do h-motifs, 3h-motifs, and network motifs capture the structural properties of real-world hypergraphs?
- **Q4. Machine Learning Applications:** Can h-motifs and 3h-motifs offer useful input features for machine learning applications?
- **Q5. Further Discoveries:** What interesting discoveries can be uncovered by employing h-motifs in real-world hypergraphs?
- **Q6. Performance of Counting Algorithms:** How fast and accurate are the different versions of MoCHy?

6.1 Experimental Settings

Machines: We conducted all the experiments on a machine with an AMD Ryzen 9 3900X CPU and 128GB RAM.

Implementations: We implemented every version of MoCHy using C++ and OpenMP. For hash tables, we used the implementation named ‘unordered_map’ provided by the C++ Standard Template Library.

Datasets: We used the following eleven real-world hypergraphs from five different domains:

- **co-authorship** (coauth-DBLP, coauth-geology [97], and coauth-history [97]): A node represents an author. A hyperedge represents all authors of a publication.

Table 3: Real-world and random hypergraphs have distinct distributions of h-motif instances. We report the absolute counts of each h-motif’s instances in a real-world hypergraph from each domain and its corresponding random hypergraph. To compare the counts in both hypergraphs, we measure the relative count (RC) of each h-motif. We also rank the counts, and we report each h-motif’s rank difference (RD) in the real-world and corresponding random hypergraphs.

h-motif	coauth-DBLP				contact-primary				email-EU				tags-math				threads-math			
	count (rank)		RD	RC	count (rank)		RD	RC	count (rank)		RD	RC	count (rank)		RD	RC	count (rank)		RD	RC
	real	random			real	random			real	random			real	random			real	random		
1	9.6E07 (7)	1.3E09 (4)	3	-0.86	4.8E04 (16)	2.8E07 (5)	11	-1.00	7.5E06 (13)	1.7E08 (7)	6	-0.91	9.0E08 (13)	2.2E11 (6)	7	-0.99	6.4E08 (7)	2.4E11 (4)	3	-0.99
2	7.0E09 (2)	7.2E09 (2)	0	-0.01	1.1E08 (3)	8.6E07 (3)	0	0.12	6.3E08 (2)	8.2E08 (3)	1	-0.13	1.6E12 (2)	1.6E12 (2)	0	0.02	1.1E12 (2)	7.7E11 (2)	0	0.16
3	2.2E06 (17)	6.1E03 (14)	3	0.99	2.8E03 (21)	1.7E05 (16)	5	-0.97	1.6E06 (21)	7.8E05 (17)	4	0.34	3.0E06 (20)	1.1E09 (15)	5	-0.99	1.7E05 (20)	1.7E08 (14)	6	-1.00
4	9.6E06 (11)	1.1E05 (12)	1	0.98	8.4E02 (24)	9.2E05 (12)	12	-1.00	4.3E06 (16)	1.5E07 (12)	4	-0.55	1.5E08 (17)	1.6E10 (12)	5	-0.98	3.1E06 (13)	1.2E09 (11)	2	-0.99
5	1.5E08 (6)	1.2E05 (11)	5	1.00	4.6E06 (5)	1.6E06 (11)	6	0.49	7.5E07 (7)	1.1E07 (13)	6	0.74	7.4E09 (8)	2.5E10 (8)	0	-0.54	4.1E08 (8)	1.7E09 (10)	2	-0.61
6	9.9E08 (3)	1.8E06 (9)	6	1.00	1.3E07 (4)	8.2E06 (7)	3	0.24	3.9E08 (4)	1.9E08 (6)	2	0.34	6.8E11 (3)	3.3E11 (4)	1	0.35	1.4E10 (4)	1.1E10 (8)	4	0.11
7	1.9E05 (23)	0.0E00 (20)	3	1.00	1.6E04 (17)	2.0E02 (24)	7	0.98	7.5E04 (24)	1.2E02 (25)	1	1.00	8.3E05 (25)	9.1E05 (25)	0	-0.05	8.8E03 (24)	1.7E04 (24)	0	-0.32
8	3.9E05 (22)	0.0E00 (20)	2	1.00	4.6E03 (20)	2.6E03 (22)	2	0.27	4.2E06 (17)	2.5E04 (21)	4	0.99	2.0E06 (23)	3.4E07 (22)	1	-0.89	2.2E04 (23)	3.5E05 (21)	2	-0.88
9	2.4E06 (16)	0.0E00 (20)	4	1.00	1.7E05 (12)	4.6E03 (20)	8	0.95	1.8E06 (20)	1.1E04 (22)	2	0.99	1.4E08 (18)	5.4E07 (21)	3	0.45	5.1E05 (17)	4.5E05 (20)	3	0.06
10	7.6E06 (13)	7.5E00 (18)	5	1.00	5.7E04 (15)	5.5E04 (17)	2	0.03	2.8E07 (10)	1.7E06 (14)	4	0.88	7.1E08 (14)	1.9E09 (14)	0	-0.45	2.3E06 (15)	9.4E06 (17)	2	-0.61
11	8.6E06 (12)	0.9E00 (19)	7	1.00	4.1E05 (11)	2.4E04 (18)	7	0.89	9.0E06 (11)	1.9E05 (19)	8	0.96	3.5E09 (10)	7.4E08 (16)	6	0.65	2.8E06 (14)	3.1E06 (18)	4	-0.05
12	6.4E07 (8)	1.9E02 (16)	8	1.00	1.7E05 (13)	2.7E05 (14)	1	-0.24	8.2E07 (6)	2.4E07 (10)	4	0.55	6.9E10 (6)	2.4E10 (10)	4	0.49	8.2E07 (10)	6.2E07 (15)	5	0.14
13	1.6E04 (26)	0.0E00 (20)	6	1.00	5.5E03 (19)	1.6E00 (26)	7	1.00	2.7E04 (26)	0.4E00 (26)	0	1.00	1.1E06 (24)	1.7E04 (26)	2	0.97	1.5E02 (26)	8.6E00 (26)	0	0.89
14	1.4E05 (24)	0.0E00 (20)	4	1.00	6.0E03 (18)	7.1E01 (25)	7	0.98	7.2E05 (22)	3.7E02 (24)	2	1.00	2.8E07 (19)	1.8E06 (24)	5	0.88	3.9E03 (25)	9.3E02 (25)	0	0.61
15	6.5E05 (19)	0.0E00 (20)	1	1.00	1.7E03 (22)	8.6E02 (23)	1	0.34	3.6E06 (19)	5.0E04 (20)	1	0.97	2.9E08 (15)	5.7E07 (20)	5	0.67	2.7E04 (22)	2.0E04 (23)	1	0.16
16	2.0E06 (18)	0.0E00 (20)	2	1.00	1.4E02 (25)	3.2E03 (21)	4	-0.92	6.7E06 (14)	1.7E06 (15)	1	0.60	1.9E09 (11)	5.8E08 (18)	7	0.53	2.4E05 (18)	1.3E05 (22)	4	0.29
17	4.2E05 (21)	2.0E06 (8)	13	-0.65	1.0E03 (23)	6.3E05 (13)	10	-1.00	3.8E04 (25)	8.7E05 (16)	9	-0.92	5.1E05 (26)	5.0E08 (19)	7	-1.00	2.3E05 (19)	9.2E08 (12)	7	-1.00
18	2.6E06 (15)	6.4E07 (7)	8	-0.92	1.2E02 (26)	7.0E06 (8)	18	-1.00	6.0E06 (15)	4.0E07 (8)	7	-0.74	2.5E06 (22)	1.6E10 (13)	9	-1.00	8.3E05 (16)	1.3E10 (7)	9	-1.00
19	3.6E07 (9)	6.7E07 (6)	3	-0.30	2.0E06 (6)	1.2E07 (6)	0	-0.72	8.7E06 (12)	2.9E07 (9)	3	-0.54	9.4E08 (12)	2.4E10 (9)	3	-0.93	3.5E08 (9)	1.8E10 (6)	3	-0.96
20	3.4E08 (5)	2.2E09 (3)	2	-0.73	6.0E05 (10)	1.3E08 (2)	8	-0.99	2.2E08 (5)	1.2E09 (2)	3	-0.69	9.2E09 (7)	7.2E11 (3)	4	-0.97	1.9E09 (5)	2.4E11 (3)	2	-0.98
21	7.9E08 (4)	5.6E08 (5)	1	0.17	1.7E08 (2)	5.7E07 (4)	2	0.50	5.3E08 (3)	2.3E08 (4)	1	0.39	1.2E11 (5)	2.8E11 (5)	0	-0.40	2.8E10 (3)	8.6E10 (5)	2	-0.51
22	1.7E10 (1)	1.8E10 (1)	0	-0.03	3.1E08 (1)	5.8E08 (1)	0	-0.30	4.9E09 (1)	8.5E09 (1)	0	-0.27	6.6E12 (1)	7.6E12 (1)	0	-0.07	1.1E12 (1)	1.2E12 (1)	0	-0.02
23	2.4E04 (25)	1.5E01 (17)	8	1.00	1.2E05 (14)	5.4E03 (19)	5	0.91	8.8E04 (23)	4.0E03 (23)	0	0.91	2.6E06 (21)	7.9E06 (23)	2	-0.51	1.4E05 (21)	7.8E05 (19)	2	-0.70
24	4.4E05 (20)	1.4E03 (15)	5	0.99	7.7E05 (9)	1.8E05 (15)	6	0.63	4.2E06 (18)	5.4E05 (18)	0	0.77	2.2E08 (17)	7.2E08 (17)	1	-0.53	7.5E06 (12)	3.1E07 (16)	4	-0.61
25	3.8E06 (14)	4.6E04 (13)	1	0.98	1.7E06 (8)	1.8E06 (10)	2	-0.03	3.2E07 (9)	2.0E07 (11)	2	0.23	6.0E09 (9)	2.0E10 (11)	2	-0.54	8.0E07 (11)	4.2E08 (13)	2	-0.68
26	2.3E07 (10)	4.9E05 (10)	0	0.96	1.8E06 (7)	6.14E06 (9)	2	-0.54	7.5E07 (8)	2.1E08 (5)	3	-0.48	1.3E11 (4)	1.8E11 (7)	3	-0.14	1.2E09 (6)	1.9E09 (9)	3	-0.21

- **contact** (contact-primary [99] and contact-high [75]): A node represents a person. A hyperedge represents a group interaction among individuals.
- **email** (email-Enron [55] and email-EU [66, 111]): A node represents an e-mail account. A hyperedge consists of the sender and all receivers of an email.
- **tags** (tags-ubuntu and tags-math): A node represents a tag. A hyperedge represents all tags attached to a post.
- **threads** (threads-ubuntu and threads-math): A node represents a user. A hyperedge groups all users participating in a thread.

These hypergraphs are made public by the authors of [14], and in Table 2 we provide some statistics of the hypergraphs after removing duplicated hyperedges. We used MoChy-E for the *coauth-history* dataset, the *threads-ubuntu* dataset, and all datasets from the **contact** and **email** domains. For the other datasets, we used MoChy-A⁺ with $r = 2,000,000$, unless otherwise stated. We used a single thread unless otherwise stated. We computed CPs based on five hypergraphs randomized as described in Section 2.2. We computed CPs based on h-motifs (instead of 3h-motifs), unless otherwise stated.

6.2 Q1. Comparison with Random

We analyze the counts of different h-motifs’ instances in real and random hypergraphs. In Table 3, we report the (approximated) count of each h-motif t ’s instances in each real hypergraph with the corresponding count averaged over five random hypergraphs obtained as described in Section 2.2. For each h-motif t , we measure its relative count, which we define as $\frac{M[t] - M_{rand}[t]}{M[t] + M_{rand}[t]}$. We also rank h-motifs by the counts of their instances and examine the difference between the ranks in real and corresponding random hypergraphs. As seen in the table, the count distributions in real hypergraphs are clearly distinguished from those of random hypergraphs.

H-motifs in Random Hypergraphs: We notice that instances of h-motifs 17 and 18 appear much more frequently in random hypergraphs than in real hypergraphs from all domains. For example, instances of h-motif 17 appear only about 510 thousand times in the *tags-math* dataset, while they appear about 500 million times (about **980**× more often) in the corresponding randomized hypergraph. In the *threads-math* dataset, instances of h-motif 18 appear about 830 thousand times, while they appear about 13 billion times (about **15,660**× more often) in the corresponding randomized hypergraph. In-

stances of h-motifs 17 and 18 consist of a hyperedge and its two disjoint subsets (see Figure 3).

H-motifs in Co-authorship Hypergraphs: We observe that instances of h-motifs 10, 11, and 12 appear more frequently in all three hypergraphs from the *co-authorship* domain than in the corresponding random hypergraphs. Although there are only about 190 instances of h-motif 12 in the corresponding random hypergraphs, there are about 64 million such instances (about $337,000\times$ more instances) in the *coauth-DBLP* dataset. As seen in Figure 3, in instances of h-motifs 10, 11, and 12, a hyperedge is overlapped with the two other overlapped hyperedges in three different ways.

H-motifs in Contact Hypergraphs: Instances of h-motifs 9, 13, and 14 are noticeably more common in both *contact* datasets than in the corresponding random hypergraphs. As seen in Figure 3, in instances of h-motifs 9, 13, and 14, hyperedges are tightly connected and nodes are mainly located in the intersections of all or some hyperedges.

H-motifs in Email Hypergraphs: Both email datasets contain particularly many instances of h-motifs 8 and 10, compared to the corresponding random hypergraphs. As seen in Figure 3, instances of h-motifs 8 and 10 consist of three hyperedges one of which contains the most nodes.

H-motifs in Tags Hypergraphs: In addition to instances of h-motif 11, which are common in most real hypergraphs, instances of h-motif 16, where all seven regions are not empty (see Figure 3), are particularly frequent in both *tags* datasets than in corresponding random hypergraphs.

H-motifs in Threads Hypergraphs: Lastly, in both data sets from the *threads* domain, instances of h-motifs 12 and 24 are noticeably more frequent than expected from the corresponding random hypergraphs.

In Appendix E, we analyze how the significance of each h-motif is correlated with the global structural properties of hypergraphs.

6.3 Q2. Comparison across Domains

We compare the characteristic profiles (CPs) of the real-world hypergraphs. In Figure 6, we present the CPs (i.e., the significances of the 26 h-motifs) of each hypergraph. As seen in the figure, hypergraphs from the same domains have similar CPs. Specifically, all three hypergraphs from the *co-authorship* domain share extremely similar CPs, even when the absolute counts of h-motifs in them are several orders of magnitude different. Similarly, the CPs of both hypergraphs from the *tags* domain are extremely similar. However, the CPs

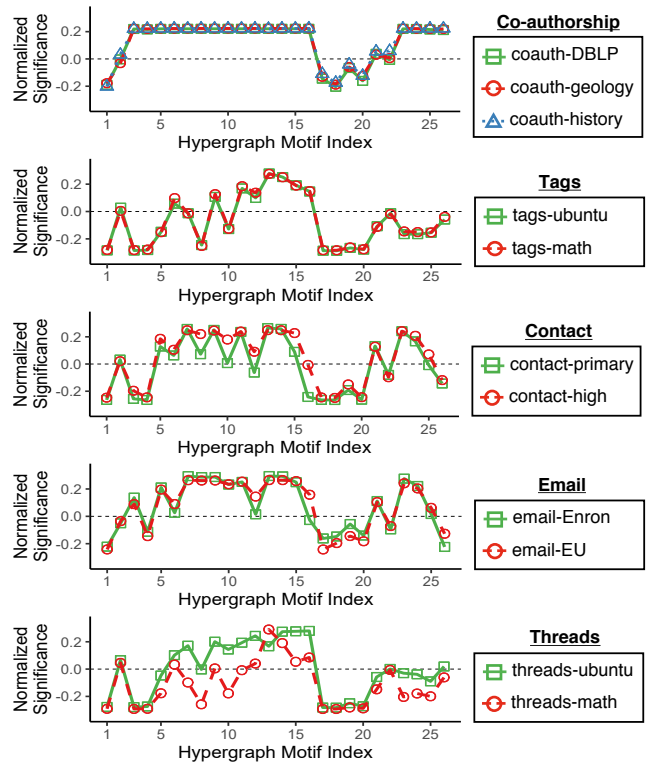


Fig. 6: Characteristic profiles (CPs) capture local structural patterns of real-world hypergraphs accurately. The CPs are similar within domains but different across domains. Note that the significance of h-motif 3 distinguishes the contact hypergraphs from the email hypergraphs.

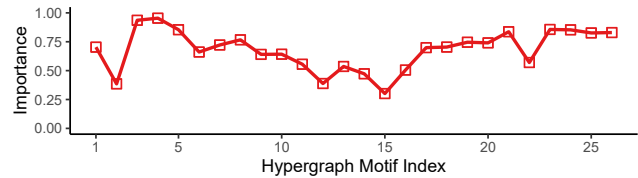


Fig. 7: Importance of h-motifs in differentiating hypergraph domains: All 26 h-motifs contribute to distinguishing hypergraph domains, with each h-motif having varying levels of importance.

of the three hypergraphs from the *co-authorship* domain are clearly distinguished by them of the hypergraphs from the *tags* domain. While the CPs of the hypergraphs from the *contact* domain and the CPs of those from the *email* domain are similar for the most part, they are distinguished by the significance of h-motif 3. These observations confirm that CPs accurately capture local structural patterns of real-world hypergraphs.

Importance of H-motifs: Since some h-motifs can be more useful than others, we measure the importance of

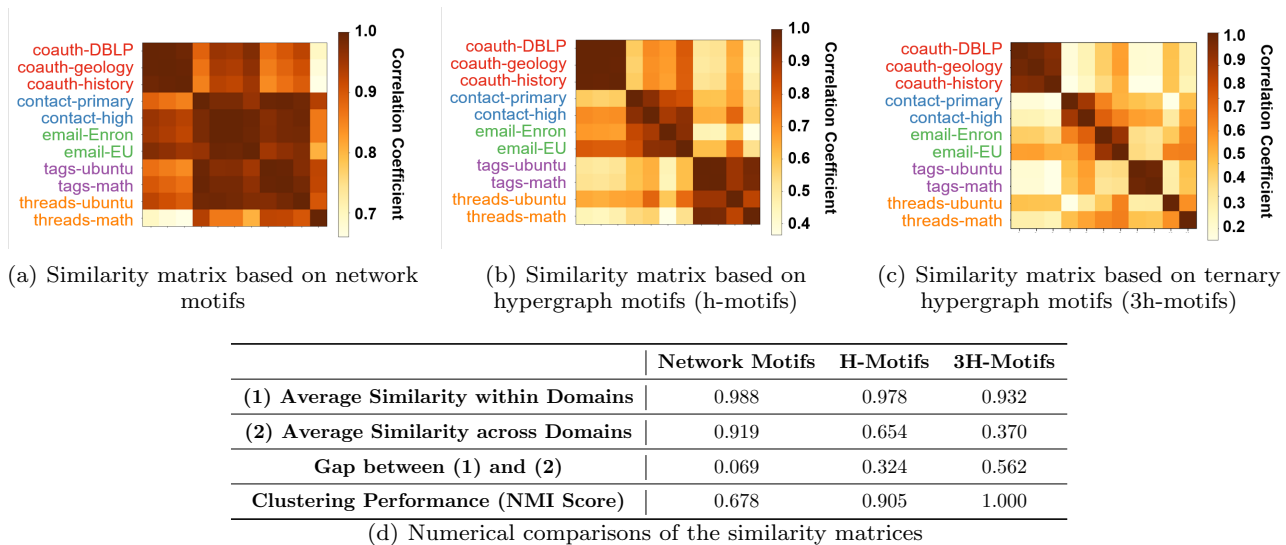


Fig. 8: Real-world hypergraphs from the same domain exhibit similar characteristic profiles (CPs), while those from different domains have distinct CPs. Notably, the CPs based on h-motifs and 3h-motifs capture local structural patterns more accurately than those based on network motifs, as supported numerically in the table.

each h-motif in distinguishing the domains of hypergraphs. We define the *importance* of a h-motif as its contribution to differentiating the domains of hypergraphs. The importance of each h-motif t is defined as:

$$importance[t] = 1 - \frac{dist_{within}[t]}{dist_{across}[t]},$$

where $dist_{within}[t]$ is the average CP distance between hypergraphs from the same domain, and $dist_{across}[t]$ is the average CP distance between hypergraphs from different domains. As seen in Figure 7, all 26 h-motifs have positive importances, indicating that all h-motifs do contribute to distinguishing the domains of hypergraphs. Note that each h-motif has different importance: some h-motifs are extremely important (e.g., h-motifs 3, 4, and 23), while some are less important (e.g., h-motifs 2, 12, and 15). It is important to note that these importance scores should be interpreted with caution, as they may be overfitted given the limited number of datasets (specifically, the similarities observed in 7 within-domain pairs and 48 cross-domain pairs).

6.4 Q3. Comparison of Characterization Powers

We compare the characterization power of h-motifs, 3h-motifs, and basic network motifs. Through this comparison, we demonstrate the effectiveness of h-motifs and 3h-motifs in capturing the structural properties of real-world hypergraphs.

CPs Based on Network Motifs: In addition to characteristic profiles (CPs) based on h-motifs and 3h-motifs, we additionally compute CPs based on network motifs. Specifically, we construct the incidence graph G' (defined in Section 2.1) of each hypergraph $G = (V, E)$. Then, we compute the CPs based on the network motifs consisting of 3 to 5 nodes, using [20].⁶ Using each of the three types of CPs, we compute the similarity matrices (specifically, correlation coefficient matrices) of the real-world hypergraphs and provide them in Figure 8.

Comparison of Pearson Correlations: As seen in Figures 8(a), 8(b) and 8(d), the domains of the real-world hypergraphs are distinguished more clearly by the CPs based on h-motifs than by the CPs based on network motifs. Numerically, when the CPs based on h-motifs are used, the average correlation coefficient is 0.978 within domains and 0.654 across domains, and the gap is 0.324. However, when the CPs based on network motifs are used, the average correlation coefficient is 0.988 within domains and 0.919 across domains, and the gap is just 0.069. As seen in Figures 8(c) and 8(d), the hypergraph domains are distinguished even more distinctly differentiated by the CPs based on 3h-motifs. Using 3h-motifs as a basis for the CPs results in significantly lower correlation coefficients between the contact and email domains, as well as between the tag and

⁶ Nine patterns can be obtained from incident graphs, which are bipartite graphs, and thus CPs based on network motifs are 9-element vectors.

thread domains, allowing for a better distinction between these domains. Numerically, when 3h-motifs are used, the average correlation coefficient is 0.932 within domains and 0.370 across domains, and the gap is 0.562. These results support that h-motifs and 3h-motifs play a key role in capturing local structural patterns of real-world hypergraphs.

Comparison of Clustering Performances: We further compare the characterization powers by evaluating clustering performance using each similarity matrix as the input for spectral clustering [86]. We set the target number of clusters to the number of hypergraph domains. As summarized in Figure 8(d), the NMI scores, where higher scores indicate better clustering performance, are 0.678, 0.905, and 1 when network motifs, h-motifs, and 3h-motifs, respectively, are used as a basis for the CPs. Notably, when 3h-motifs are used, the hypergraph domains are perfectly classified into distinct clusters. These results confirm again the effectiveness of h-motifs and 3h-motifs in characterizing real-world hypergraphs.

6.5 Q4. Machine Learning Applications

We demonstrate that h-motifs and 3h-motifs provide useful input features for two machine learning tasks.

Hyperedge Prediction: We first consider the task of predicting future hyperedges in the seven real-world hypergraphs where MoCHy-E completes within a reasonable duration. As in [112], we formulate this problem as a binary classification problem, aiming to classify real hyperedges and fake ones. To this end, we create fake hyperedges in both training and test sets by replacing some fraction of nodes in each real hyperedge with random nodes. Refer to Appendix J for detailed settings. Then, we train classifiers using each of the following sets of input hyperedge features:

- **HP26** ($\in \mathbb{R}^{26}$): HP based on h-motifs.
- **HP7** ($\in \mathbb{R}^7$): The seven features with the largest variance among those in HP based on h-motifs.
- **THP** ($\in \mathbb{R}^{431}$): HP based on 3h-motifs.
- **BASELINE** ($\in \mathbb{R}^7$): The mean, maximum, and minimum degree⁷ and the mean, maximum, and minimum number of neighbors⁸ of the nodes in each hyperedge and its size.

We employ XGBoost [26] as the classifier since it outperforms other classifiers, specifically logistic regression,

⁷ The degree of a node v is the number of hyperedges that v is in.

⁸ The neighbors of a node v is the nodes that appear in at least one hyperedge together with v .

Table 4: H-motifs and 3h-motifs give informative hyperedge features. The use of h-motifs and 3h-motifs for input features in HP26 and THP, respectively, consistently outperforms using the baseline features in BASELINE for predicting hyperedges in all datasets. Even when reducing the dimension of HM26 to that of BASELINE (i.e., using HP7), the accuracy of predictions using h-motif-based features remains superior. For each setting, the best result is in **bold** and the second best one is underlined. The standard deviations of all the results are smaller than 0.0001.

		HP26	HP7	THP	BASELINE
coauth-DBLP	ACC	<u>0.801</u>	0.744	0.836	0.646
	AUC	<u>0.886</u>	0.820	0.909	0.707
coauth-MAG-Geology	ACC	<u>0.782</u>	0.722	0.819	0.661
	AUC	<u>0.865</u>	0.798	0.892	0.741
coauth-MAG-History	ACC	<u>0.696</u>	0.683	0.716	0.608
	AUC	<u>0.811</u>	0.761	0.820	0.732
contact-primary-school	ACC	<u>0.772</u>	0.769	0.779	0.603
	AUC	<u>0.879</u>	0.868	0.886	0.647
contact-high-school	ACC	0.907	0.860	<u>0.904</u>	0.585
	AUC	0.968	0.949	<u>0.967</u>	0.641
email-Enron	ACC	<u>0.815</u>	0.725	0.827	0.633
	AUC	0.922	0.816	<u>0.921</u>	0.701
email-Eu	ACC	<u>0.911</u>	0.878	0.920	0.702
	AUC	<u>0.972</u>	0.954	0.977	0.781

Table 5: H-motifs and 3h-motifs provide valuable input features for node classification, with 3h-motifs showing particularly strong performance. The use of them for input features in NP26 and TNP yields better classification results than using the baseline features in BASELINE. For each metric, the best result is in **bold** and the second best one is underlined. The standard deviations of all the results are smaller than 0.0001.

	NP26	NP7	TNP	BASELINE
ACC	<u>0.682</u>	0.545	0.723	0.659
AVG AUC	<u>0.952</u>	0.901	0.967	0.950

random forest, decision tree, and multi-layer perception, on average, regardless of the feature sets used. Results with other classifiers can be found in Appendix J.

We report the accuracy (ACC) and the area under the ROC curve (AUC) in each setting in Table 4. Using HP26 and HP7, which are based on h-motifs, yields consistently better predictions than using BASELINE, which is a baseline feature set. In addition, using THP, which is based on 3h-motifs, leads to the best performance in almost all settings. These results suggest that h-motifs provide informative hyperedge features, and 3h-motifs provide even stronger hyperedge features for hyperedge prediction.

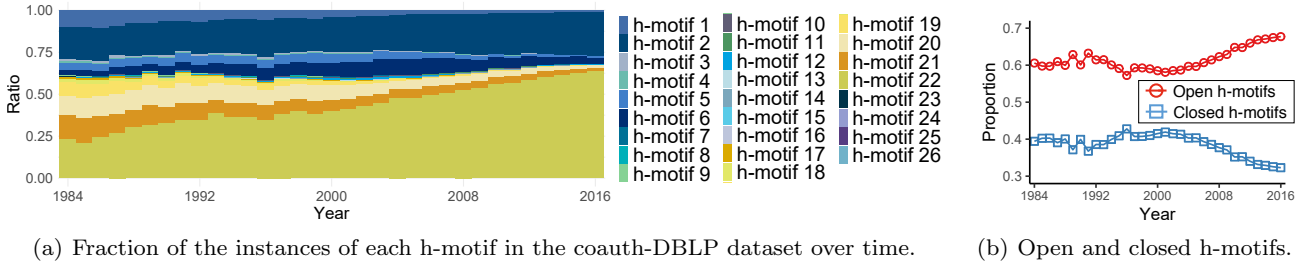


Fig. 9: Trends in the formation of collaborations are captured by h-motifs. (a) The fractions of the instances of h-motifs 2 and 22 have increased rapidly. (b) The fraction of the instances of open h-motifs has increased steadily since 2001.

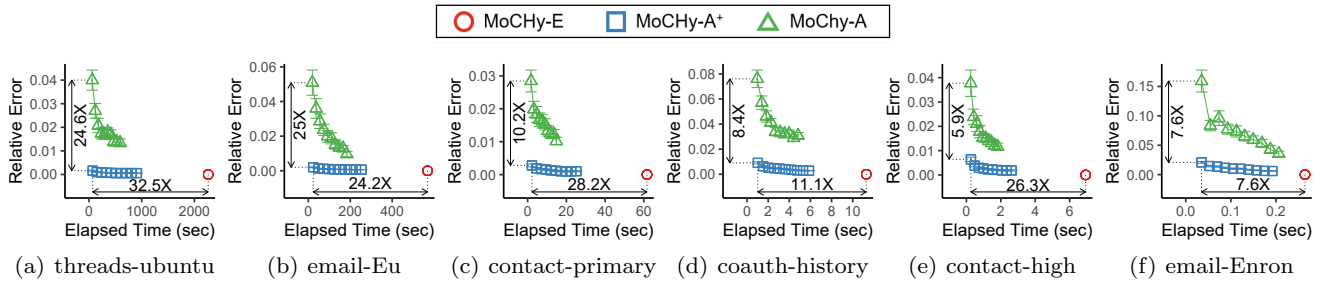


Fig. 10: MoChy-A⁺ gives the best trade-off between speed and accuracy. It yields up to 25× more accurate estimation than MoChy-A, and it is up to 32.5× faster than MoChy-E. The error bars indicate ± 1 standard error over 20 trials.

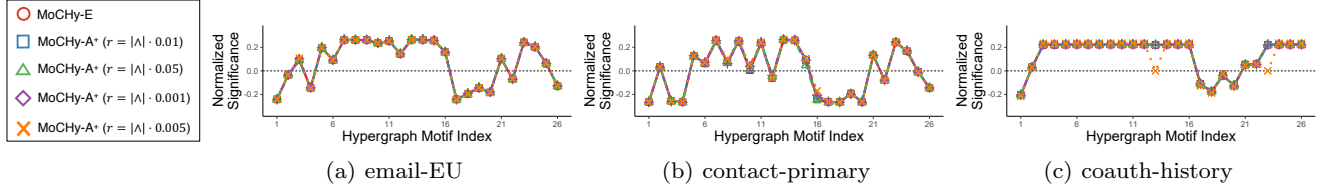


Fig. 11: Using MoChy-A⁺, characteristic profiles (CPs) can be estimated accurately from a small number of samples.

Node Classification: As another machine learning application, we consider the task of node classification, where the label of each node is the hypergraph it belongs to. Since we utilize all eleven real-world hypergraphs, each node can have one of eleven possible labels. We draw 100 nodes uniformly at random from each hypergraph, and we use 80% of them for training and the remaining 20% of them for testing. Refer to Appendix K for detailed experimental settings. We train four classifiers using each of the following sets of input node features:

- **NP26** ($\in \mathbb{R}^{26}$): NP based on h-motifs.
- **NP7** ($\in \mathbb{R}^7$): The seven features with the largest variance among those in NP based on h-motifs.
- **TNP** ($\in \mathbb{R}^{431}$): NP based on 3h-motifs.

- **BASELINE** ($\in \mathbb{R}^7$): The node count, hyperedge count, average hyperedge size, average overlapping size, density [40]⁹, overlapness [60]¹⁰, and the number of hyperedges that contain the ego-node in each ego-network.

For all feature sets, we use radial ego-networks as the ego-networks and XGBoost [26] as the classifier. This is because using radial ego-networks and XGBoost gives better classification results than using other types of ego-networks and other classifiers in most cases. Refer to Appendix K for full experimental results with other types of ego-networks and other classifiers.

⁹ The ratio between the hyperedge count and the node count.

¹⁰ The ratio between the sum of hyperedge sizes and the node count.

We report the accuracy (ACC) and the average area under the ROC curve (AVG AUC) in each setting in Table 5. Using TNP, which is based on 3h-motifs, yields the best classification result. Using NP26, which is based on h-motifs, outperforms using BASELINE, which is a baseline feature set. However, reducing the dimension of NP26 to that of BASELINE results in the worst performance. These results demonstrate that h-motifs and particularly 3h-motifs provide effective input features for node classification, highlighting the importance of local structural patterns in hypergraphs for this task.

6.6 Q5. Further Observations

We analyze the evolution of the co-authorship Hypergraphs by employing h-motifs. The dataset contains bibliographic information on computer science publications. Using the publications in each year from 1984 to 2016, we create 33 hypergraphs where each node corresponds to an author, and each hyperedge indicates the set of the authors of a publication. Then, we compute the fraction of the instances of each h-motif in each hypergraph to analyze patterns and trends in the formation of collaborations. As shown in Figure 9, over the 33 years, the fractions have changed with distinct trends. First, as seen in Figure 9(b), the fraction of the instances of open h-motifs has increased steadily since 2001, indicating that collaborations have become less clustered, i.e., the probability that two collaborations intersecting with a collaboration also intersect with each other has decreased. Notably, the fractions of the instances of h-motif 2 (closed) and h-motif 22 (open) have increased rapidly, accounting for most of the instances.

6.7 Q6. Performance of Counting Algorithms

We test the speed and accuracy of all versions of MoCHy under various settings. To this end, we measure elapsed time and relative error defined as

$$\frac{\sum_{t=1}^{26} |M[t] - \bar{M}[t]|}{\sum_{t=1}^{26} M[t]} \text{ and } \frac{\sum_{t=1}^{26} |M[t] - \hat{M}[t]|}{\sum_{t=1}^{26} M[t]},$$

for MoCHy-A and MoCHy-A⁺, respectively. Unless otherwise stated, we use a single thread without the on-the-fly computation scheme.

Speed and Accuracy: In Figure 10, we report the elapsed time and relative error of all versions of MoCHy on the 6 different datasets where MoCHy-E terminates within a reasonable time. The numbers of samples in MoCHy-A and MoCHy-A⁺ are set to $\{2.5 \times k : 1 \leq$

$k \leq 10\}$ percent of the counts of hyperedges and hyperwedges, respectively. MoCHy-A⁺ provides the best trade-off between speed and accuracy. For example, in the *threads-ubuntu* dataset, MoCHy-A⁺ provides $24.6\times$ lower relative error than MoCHy-A, consistently with our theoretical analysis (see the last paragraph of Section 4.3). Moreover, in the same dataset, MoCHy-A⁺ is $32.5\times$ faster than MoCHy-E with little sacrifice on accuracy.

Effects of the Sample Size on CPs: In Figure 11, we report the CPs obtained by MoCHy-A⁺ with different numbers of hyperwedge samples on 3 datasets. Even with a smaller number of samples, the CPs are estimated near perfectly.

Parallelization: We measure the running times of the proposed method with different numbers of threads on the *threads-ubuntu* and *coauth-DBLP* datasets. As seen in Figure 12, in both datasets, MoCHy achieves significant speedups with multiple threads. Specifically, with 8 threads, MoCHy-E and MoCHy-A⁺ ($r = 1M$) achieve speedups of 5.4 and 6.7, respectively in *threads-ubuntu* dataset. In the *coauth-DBLP* dataset, similar trends can be observed with speedups of 5.0 and 6.0 when using MoCHy-A⁺ for $r = 1M$ and $r = 8M$, respectively. MoCHy-E cannot be tested on the *coauth-DBLP* dataset since it does not complete within a reasonable duration.

Effects of On-the-fly Computation on Speed: We analyze the effects of the on-the-fly computation of line graphs (discussed in Section 4.4) on the speed of MoCHy-A⁺ under different memory budgets for memoization. To this end, we use the *coauth-DBLP* dataset, and we set the memory budgets so that up to $\{0\%, 0.1\%, 1\%, 10\%, 100\%\}$ of the edges in the line graph can be memoized. When the budget is 0%, we compute the neighbors of each hyperedge within the sampled hyperwedge every time, without precomputing or memoizing (a part of) the line graph. As shown in Figure 13, both On-the-fly MoCHy-A⁺ (Basic) and On-the-fly MoCHy-A⁺ (Adv.) faster than MoCHy-A⁺ without memoization, and their speed tends to improve as the memory budget increases. In addition, On-the-fly MoCHy-A⁺ (Adv.) is consistently faster than On-the-fly MoCHy-A⁺ (Basic) across different memory budgets. Specifically, it achieves up to $1.72\times$ reduced runtime, demonstrating the effectiveness of its carefully ordered processing schemes for sampled hyperwedges.

Comparison with Network-motif Counting: We assess the computational time needed for counting the instances of h-motifs, 3h-motifs, and network motifs on the *coauth-DBLP* dataset, which is our largest dataset. We employ MoCHy-A⁺ for both h-motifs and 3h-motifs, and for network motifs, we utilize Motivo [20], a re-

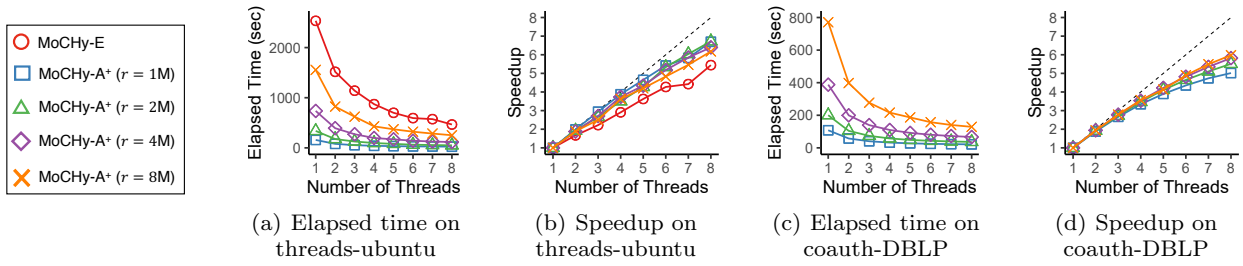


Fig. 12: Both MoCHy-E and MoCHy-A⁺ achieve significant speedups with multiple threads.

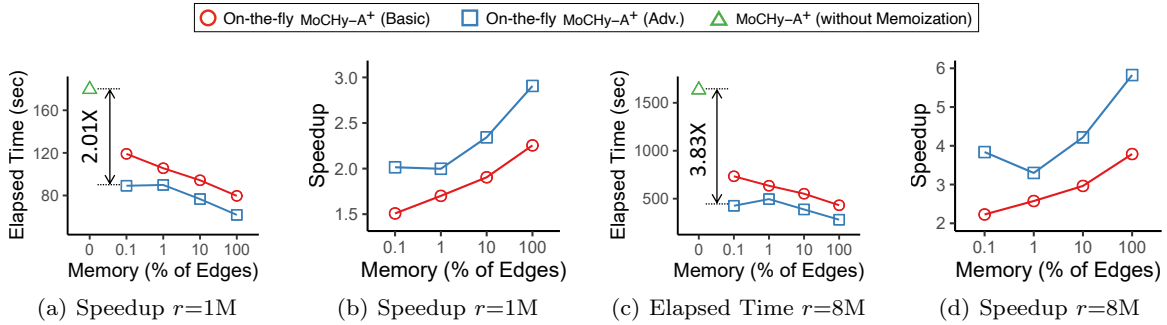


Fig. 13: On-the-fly MoCHy-A⁺ (Basic) and On-the-fly MoCHy-A⁺ (Adv.) achieve substantial speed improvements, compared to MoCHy-A⁺ without memoization, even when memoizing a small fraction of line graphs. Between the two methods, On-the-fly MoCHy-A⁺ (Adv.) is faster up to 1.72 \times than On-the-fly MoCHy-A⁺ (Basic), due to its carefully ordered processing scheme for sampled hyperwedges.

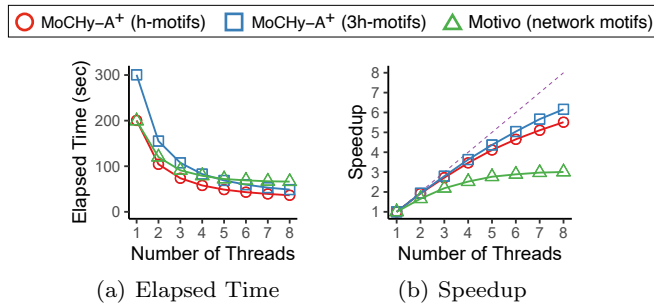


Fig. 14: MoCHy-A⁺ for counting the instances of h-motifs is consistently faster than Motivo [20], which counts the instances of network motifs of size up to 5, across different numbers of threads. When counting 3h-motifs, MoCHy-A⁺ is faster than Motivo with five or more threads. This is attributed to the fact that MoCHy-A⁺ exhibits better speedup as the number of threads increases compared to Motivo.

cently introduced algorithm, to count the instances of network motifs up to size 5. In all cases, we fix the sample size to 2 million. As shown in Figure 14(a), when counting instances of h-motifs, MoCHy-A⁺ is consistently faster than Motivo across different numbers of threads, and the gap increases as the number of threads

grows. When it comes to counting 3h-motifs, MoCHy-A⁺ is slower than Motivo with a single thread, but it becomes faster with five or more threads. This is attributed to MoCHy-A⁺ achieving significant speedups with more threads, compared to Motivo, as shown in Figure 14(b).

7 Related Work

We review prior work on network motifs, algorithms for counting them, and hypergraphs. While the definition of a network motif varies among studies, here we define it as a connected graph composed by a predefined number of nodes.

Network Motifs. Network motifs were proposed as a tool for understanding the underlying design principles and capturing the local structural patterns of graphs [39,94,79]. The occurrences of motifs in real-world graphs are significantly different from those in random graphs [79], and they vary also depending on the domains of graphs [78]. The concept of network motifs has been extended to various types of graphs, including dynamic [85] graphs, bipartite graphs [18], heterogeneous graphs [89], and simplicial complexes [14, 52,88]. The occurrences of network motifs have been

used in a wide range of graph applications: community detection [15, 103, 111, 71], ranking [119], graph embedding [90, 114], and graph neural networks [65], to name a few.

Algorithms for Network Motif Counting. We focus on algorithms for counting the occurrences of every network motif whose size is fixed or within a certain range [5, 6, 11, 20, 27, 37, 87], while many are for a specific motif (e.g., the clique of size 3) [4, 32, 41, 42, 47, 53, 57, 83, 92, 95, 96, 102, 104, 106]. Given a graph, they aim to count rapidly and accurately the instances of motifs with 4 or more nodes, despite the combinatorial explosion of the instances, using the following techniques:

- (1) **Combinatorics:** For exact counting, combinatorial relations between counts have been employed [5, 87, 85]. That is, prior studies deduce the counts of the instances of motifs from those of other smaller or equal-size motifs.
- (2) **MCMC:** Most approximate algorithms sample motif instances from which they estimate the counts. Based on MCMC sampling, the idea of performing a random walk over instances (i.e, connected subgraphs) until it reaches the stationarity to sample an instance from a fixed probability distribution (e.g., uniform) has been employed [17, 27, 37, 91, 105, 76].
- (3) **Color Coding:** Instead of MCMC, color coding [8] can be employed for sampling [19, 20, 21]. Specifically, prior studies color each node uniformly at random among k colors, count the number of k -trees with k colors rooted at each node, and use them to sample instances from a fixed probability distribution.

In our problem, which focuses on h-motifs with only 3 hyperedges, sampling instances with fixed probabilities is straightforward without (2) or (3), and the combinatorial relations on graphs in (1) are not applicable. In algorithmic aspects, we address the computational challenges discussed at the beginning of Section 4 by answering (a) what to precompute (Section 4.1), (b) how to leverage it (Sections 4.2 and 4.3), and (c) how to prioritize it (Sections 4.4 and 6.7), with formal analyses (Lemma 2; Theorems 1, 3, and 6).

Hypergraph Mining. Hypergraphs naturally represent group interactions occurring in a wide range of fields, including computer vision [43, 113], bioinformatics [45], circuit design [50, 82], social network analysis [68, 109], cryptocurrency [54], and recommender systems [23, 69]. There also has been considerable attention on machine learning on hypergraphs, including clustering [3, 9, 51, 59, 121], classification [48, 59, 100, 113], hyperedge prediction [14, 112, 117, 44], and anomaly detection [61]. Recent studies on real-world hypergraphs

revealed interesting patterns commonly observed across domains, including (a) global structural properties (e.g., giant connected components and small diameter) [33, 56, 22] and their temporal evolution (e.g., shrinking diameter) [56]; (b) structural properties of ego-networks (e.g., density and overlapness) [60] and their temporal evolution (e.g., decreasing rates of novel nodes) [30]; and (c) temporal patterns regarding arrivals of the same or overlapping hyperedges [16, 29, 24]. Notably, Benson et al. [14] studied how several local features, including edge density, average degree, and probabilities of simplicial closure events for 4 or less nodes¹¹, differ across domains. Our analysis using h-motifs is complementary to these approaches in that it (1) captures local patterns systematically without hand-crafted features, (2) captures static patterns without relying on temporal information, and (3) naturally uses hyperedges with any number of nodes without decomposing them into small ones.

Recently, there has been an extension of hypergraph motifs to temporal hypergraphs, which evolve over time [63, 64]. This extension introduces 96 temporal hypergraph motifs (TH-motifs) that capture not only the overlapping patterns but also the relative order among three connected hyperedges. This extension has been shown to improve the characterization power of h-motifs in hypergraph classification and hyperedge prediction tasks. Along with the concept of TH-motifs, a family of algorithms has been proposed for the exact and approximate counting of TH-motifs. The focuses of the algorithms are the dynamic update of the line graph over time and the prioritized sampling of time intervals for estimation. It is important to note that this conceptual and algorithmic extension requires temporal information as input, and is orthogonal to our extension to 3h-motifs, which only requires topological information.

8 Conclusions and Future Directions

In this section, we present conclusions and future research directions.

8.1 Conclusions

In this work, we introduce hypergraph motifs (h-motifs), and their extensions, ternary hypergraph motifs (3h-motifs). Using them, we investigate the local structures

¹¹ The emergence of the first hyperedge that includes a set of nodes each of whose pairs co-appear in previous hyperedges. The configuration of the pairwise co-appearances affects the probability.

of 11 real-world hypergraphs from 5 different domains. We summarize our contributions as follows:

- **Novel Concepts:** We define 26 h-motifs, which describe connectivity patterns of three connected hyperedges in a unique and exhaustive way, independently of the sizes of hyperedges (Figure 3). We extend this concept to 431 3h-motifs, enabling a more specific differentiation of local structures (Figure 5).
- **Fast and Provable Algorithms:** We propose 3 parallel algorithms for (approximately) counting every h-motif’s instances, and we theoretically and empirically analyze their speed and accuracy. Both approximate algorithms yield unbiased estimates (Theorems 2 and 5), and especially the advanced one is up to $32\times$ faster than the exact algorithm, with little sacrifice on accuracy (Figure 10).
- **Discoveries in 11 Real-world Hypergraphs:** We confirm the efficacy of h-motifs and 3h-motifs by showing that local structural patterns captured by them are similar within domains but different across domains (Figures 6 and 8).
- **Machine Learning Applications:** Our experiments have shown that h-motifs are effective in extracting features for hypergraphs, hyperedges, and nodes in tasks such as hypergraph clustering, hyperedge prediction, and node classification. Furthermore, using 3h-motifs has been demonstrated to improve the feature extraction capabilities, resulting in even better performances on these applications.

8.2 Future Research Directions

Future directions include exploring the practical applications of h-motifs and 3h-motifs, motivated by the numerous successful use cases of network motifs in practical applications. For example, network motifs have been used in the domain of biology, for identifying crucial interactions between proteins, DNA, and metabolites within biological networks [110, 74]. Another compelling example lies within mobile communication networks, where network motifs have been observed to significantly impact the efficiency of information delivery across users [118]. In addition, network motifs are proven to be powerful tools for enhancing the performance of other practical applications including anomaly detection [81, 116] and recommendation [36, 120, 101, 31]. Furthermore, they are recognized as a useful ingredient when designing graph-related algorithms, such as graph neural networks [93, 115] and graph clustering algorithms [111, 15]. These examples demonstrate the substantial potential of h-motifs in diverse applications,

and notably, most of them are less explored in hypergraphs than in graphs.

In Sections 6.4 and 6.5, we demonstrated the critical role of h-motifs and 3h-motifs in enhancing performance across hypergraph learning tasks, including node classification and hyperedge prediction. We believe that the considered hypergraph learning tasks can be readily applied to practical applications [28, 10]. For example, to achieve effective educational management and evaluation, it is important to classify the academic performance (e.g., poor, medium, and excellent) of students (nodes) based on the associations (hyperedges) among them [70]. It is also crucial to classify fake news (nodes) based on the patterns of news consumption by users (hyperedges) [46]. Accurately identifying labels for objects (nodes) in images (hyperedges) containing multiple entities is a crucial task in computer vision [108]. Refer to a survey [10] for a broader range of applications formulated as node classification on hypergraphs. In addition, hyperedge prediction can be employed for identifying novel sets (e.g., outfits) of items (e.g., fashion items) to be purchased together [72] (b) suggesting novel combinations of ingredients for recipes [117], (c) recommending new collaborations among researchers [73], and (d) discovering groups of genes collaborating for specific biological functions [80]. As we demonstrated in Sections 6.4 and 6.5, h-motifs and 3h-motifs serve as valuable tools for addressing such tasks, indicating their potential applicability in practical scenarios, which we leave for future work.

Other promising research directions include (a) extending h-motifs and 3h-motifs to complex and rich hypergraphs, such as labeled or heterogeneous hypergraphs, and (b) investigating alternative random hypergraph models for assessing the significance of h-motifs and 3h-motifs.

Reproducibility: The code and datasets used in this work are available at <https://github.com/jing9044/MoChy-with-3h-motif>.

References

1. *The On-Line Encyclopedia of Integer Sequences*. Sequence A000612.
2. *The On-Line Encyclopedia of Integer Sequences*. Sequence A323819.
3. S. Agarwal, J. Lim, L. Zelnik-Manor, P. Perona, D. Kriegman, and S. Belongie. Beyond pairwise clustering. In *CVPR*, 2005.
4. N. K. Ahmed, N. Duffield, T. L. Willke, and R. A. Rossi. On sampling from massive graph streams. *PVLDB*, 10(11):1430–1441, 2017.
5. N. K. Ahmed, J. Neville, R. A. Rossi, and N. Duffield. Efficient graphlet counting for large networks. In *ICDM*, 2015.

6. N. K. Ahmed, J. Neville, R. A. Rossi, N. G. Duffield, and T. L. Willke. Graphlet decomposition: Framework, algorithms, and applications. *KAIS*, 50(3):689–722, 2017.
7. S. G. Aksoy, T. G. Kolda, and A. Pinar. Measuring and modeling bipartite graphs with community structure. *Journal of Complex Networks*, 5(4):581–603, 2017.
8. N. Alon, R. Yuster, and U. Zwick. Color-coding. *JACM*, 42(4):844–856, 1995.
9. I. Amburg, N. Veldt, and A. R. Benson. Hypergraph clustering with categorical edge labels. In *WWW*, 2020.
10. A. Antelmi, G. Cordasco, M. Polato, V. Scarano, C. Spagnuolo, and D. Yang. A survey on hypergraph representation learning. *ACM Computing Surveys*, 56(1):1–38, 2023.
11. C. Aslay, M. A. U. Nasir, G. De Francisci Morales, and A. Gionis. Mining frequent patterns in evolving graphs. In *CIKM*, 2018.
12. A.-L. Barabási and R. Albert. Emergence of scaling in random networks. *Science*, 286(5439):509–512, 1999.
13. L. Becchetti, P. Boldi, C. Castillo, and A. Gionis. Efficient algorithms for large-scale local triangle counting. *TKDD*, 4(3):1–28, 2010.
14. A. R. Benson, R. Abebe, M. T. Schaub, A. Jadbabaie, and J. Kleinberg. Simplicial closure and higher-order link prediction. *PNAS*, 115(48):E11221–E11230, 2018.
15. A. R. Benson, D. F. Gleich, and J. Leskovec. Higher-order organization of complex networks. *Science*, 353(6295):163–166, 2016.
16. A. R. Benson, R. Kumar, and A. Tomkins. Sequences of sets. In *KDD*, 2018.
17. M. A. Bhuiyan, M. Rahman, M. Rahman, and M. Al Hasan. Guise: Uniform sampling of graphlets for large graph analysis. In *ICDM*, 2012.
18. S. P. Borgatti and M. G. Everett. Network analysis of 2-mode data. *Social networks*, 19(3):243–270, 1997.
19. M. Bressan, F. Chierichetti, R. Kumar, S. Leucci, and A. Panconesi. Counting graphlets: Space vs time. In *WSDM*, 2017.
20. M. Bressan, S. Leucci, and A. Panconesi. Motivo: fast motif counting via succinct color coding and adaptive sampling. *PVLDB*, 12(11):1651–1663, 2019.
21. M. Bressan, S. Leucci, and A. Panconesi. Faster motif counting via succinct color coding and adaptive sampling. *TKDD*, 15(6):1–27, 2021.
22. F. Bu, G. Lee, and K. Shin. Hypercore decomposition for non-fragile hyperedges: Concepts, algorithms, observations, and applications. *arXiv preprint arXiv:2301.08440*, 2023.
23. J. Bu, S. Tan, C. Chen, C. Wang, H. Wu, L. Zhang, and X. He. Music recommendation by unified hypergraph: combining social media information and music content. In *MM*, 2010.
24. G. Cencetti, F. Battiston, B. Lepri, and M. Karsai. Temporal properties of higher-order interactions in social networks. *Scientific reports*, 11(1):7028, 2021.
25. L. Chen, X. Qu, M. Cao, Y. Zhou, W. Li, B. Liang, W. Li, W. He, C. Feng, X. Jia, et al. Identification of breast cancer patients based on human signaling network motifs. *Scientific reports*, 3:3368, 2013.
26. T. Chen and C. Guestrin. Xgboost: A scalable tree boosting system. In *KDD*, 2016.
27. X. Chen, Y. Li, P. Wang, and J. C. Lui. A general framework for estimating graphlet statistics via random walk. *PVLDB*, 10(3):253–264, 2016.
28. M. Choe, S. Kim, J. Yoo, and K. Shin. Classification of edge-dependent labels of nodes in hypergraphs. In *KDD*, 2023.
29. H. Choo and K. Shin. On the persistence of higher-order interactions in real-world hypergraphs. In *SDM*, 2022.
30. C. Comrie and J. Kleinberg. Hypergraph ego-networks and their temporal evolution. In *ICDM*, 2021.
31. Z. Cui, Y. Cai, S. Wu, X. Ma, and L. Wang. Motif-aware sequential recommendation. In *SIGIR*, 2021.
32. L. De Stefani, A. Epasto, M. Riondato, and E. Ufal. Trièst: Counting local and global triangles in fully-dynamic streams with fixed memory size. In *KDD*, 2016.
33. M. T. Do, S.-e. Yoon, B. Hooi, and K. Shin. Structural patterns and generative models of real-world hypergraphs. In *KDD*, 2020.
34. M. Faloutsos, P. Faloutsos, and C. Faloutsos. On power-law relationships of the internet topology. *ACM SIGCOMM computer communication review*, 29(4):251–262, 1999.
35. S. R. Gallagher and D. S. Goldberg. Clustering coefficients in protein interaction hypernetworks. In *BCB*, 2013.
36. P. Gupta, V. Satuluri, A. Grewal, S. Gurumurthy, V. Zhabiyuk, Q. Li, and J. Lin. Real-time twitter recommendation: Online motif detection in large dynamic graphs. *VLDB*, 7(13):1379–1380, 2014.
37. G. Han and H. Sethu. Waddling random walk: Fast and accurate mining of motif statistics in large graphs. In *ICDM*, 2016.
38. W. Hoeffding. Probability inequalities for sums of bounded random variables. *The collected works of Wassily Hoeffding*, pages 409–426, 1994.
39. P. W. Holland and S. Leinhardt. A method for detecting structure in sociometric data. In *Social Networks*, pages 411–432. Elsevier, 1977.
40. S. Hu, X. Wu, and T. H. Chan. Maintaining densest subsets efficiently in evolving hypergraphs. In *CIKM*, 2017.
41. X. Hu, Y. Tao, and C.-W. Chung. Massive graph triangulation. In *SIGMOD*, 2013.
42. X. Hu, Y. Tao, and C.-W. Chung. I/o-efficient algorithms on triangle listing and counting. *TODS*, 39(4):1–30, 2014.
43. Y. Huang, Q. Liu, S. Zhang, and D. N. Metaxas. Image retrieval via probabilistic hypergraph ranking. In *CVPR*, 2010.
44. H. Hwang, S. Lee, C. Park, and K. Shin. Ahp: Learning to negative sample for hyperedge prediction. In *SIGIR*, 2022.
45. T. Hwang, Z. Tian, R. Kuangy, and J.-P. Kocher. Learning on weighted hypergraphs to integrate protein interactions and gene expressions for cancer outcome prediction. In *ICDM*, 2008.
46. U. Jeong, K. Ding, L. Cheng, R. Guo, K. Shu, and H. Liu. Nothing stands alone: Relational fake news detection with hypergraph neural networks. In *Big Data*, 2022.
47. M. Jha, C. Seshadhri, and A. Pinar. A space efficient streaming algorithm for triangle counting using the birthday paradox. In *KDD*, 2013.
48. J. Jiang, Y. Wei, Y. Feng, J. Cao, and Y. Gao. Dynamic hypergraph neural networks. In *IJCAI*, 2019.
49. U. Kang, C. E. Tsourakakis, A. P. Appel, C. Faloutsos, and J. Leskovec. Radius plots for mining tera-byte scale graphs: Algorithms, patterns, and observations. In *SDM*, 2010.
50. G. Karypis, R. Aggarwal, V. Kumar, and S. Shekhar. Multilevel hypergraph partitioning: applications in vlsi domain. *TVLSI*, 7(1):69–79, 1999.

51. G. Karypis and V. Kumar. Multilevel k-way hypergraph partitioning. *VLSI design*, 11(3):285–300, 2000.
52. H. Kim, J. Ko, F. Bu, and K. Shin. Characterization of simplicial complexes by counting simplexes beyond four nodes. In *WWW*, 2023.
53. J. Kim, W.-S. Han, S. Lee, K. Park, and H. Yu. Opt: a new framework for overlapped and parallel triangulation in large-scale graphs. In *SIGMOD*, 2014.
54. S. Kim, M. Choe, J. Yoo, and K. Shin. Reciprocity in directed hypergraphs: Measures, findings, and generators. In *ICDM*, 2022.
55. B. Klimt and Y. Yang. The enron corpus: A new dataset for email classification research. In *ECML PKDD*, 2004.
56. J. Ko, Y. Kook, and K. Shin. Growth patterns and models of real-world hypergraphs. *KAIS*, 64(11):2883–2920, 2022.
57. S. Ko and W.-S. Han. Turbograp++ a scalable and fast graph analytics system. In *SIGMOD*, 2018.
58. M. Latapy, C. Magnien, and N. Del Vecchio. Basic notions for the analysis of large two-mode networks. *Social networks*, 30(1):31–48, 2008.
59. D. Lee and K. Shin. I’m me, we’re us, and i’m us: Tri-directional contrastive learning on hypergraphs. In *AAAI*, 2023.
60. G. Lee, M. Choe, and K. Shin. How do hyperedges overlap in real-world hypergraphs?—patterns, measures, and generators. In *WWW*, 2021.
61. G. Lee, M. Choe, and K. Shin. Hashwalk: Hash and random walk based anomaly detection in hyperedge streams. In *IJCAI*, 2022.
62. G. Lee, J. Ko, and K. Shin. Hypergraph motifs: concepts, algorithms, and discoveries. *PVLDB*, 13(12):2256–2269, 2020.
63. G. Lee and K. Shin. Thyme+: Temporal hypergraph motifs and fast algorithms for exact counting. In *ICDM*, 2021.
64. G. Lee and K. Shin. Temporal hypergraph motifs. *KAIS*, 65(4):1549–1586, 2023.
65. J. B. Lee, R. A. Rossi, X. Kong, S. Kim, E. Koh, and A. Rao. Graph convolutional networks with motif-based attention. In *CIKM*, 2019.
66. J. Leskovec, J. Kleinberg, and C. Faloutsos. Graphs over time: densification laws, shrinking diameters and possible explanations. In *KDD*, 2005.
67. J. Leskovec and R. Sosič. Snap: A general-purpose network analysis and graph-mining library. *TIST*, 8(1):1, 2016.
68. D. Li, Z. Xu, S. Li, and X. Sun. Link prediction in social networks based on hypergraph. In *WWW*, 2013.
69. L. Li and T. Li. News recommendation via hypergraph learning: encapsulation of user behavior and news content. In *WSDM*, 2013.
70. M. Li, Y. Zhang, X. Li, L. Cai, and B. Yin. Multi-view hypergraph neural networks for student academic performance prediction. *Engineering Applications of Artificial Intelligence*, 114:105174, 2022.
71. P.-Z. Li, L. Huang, C.-D. Wang, and J.-H. Lai. Edmot: An edge enhancement approach for motif-aware community detection. In *KDD*, 2019.
72. Y. Li, H. Chen, X. Sun, Z. Sun, L. Li, L. Cui, P. S. Yu, and G. Xu. Hyperbolic hypergraphs for sequential recommendation. In *CIKM*, 2021.
73. Z. Liu, X. Xie, and L. Chen. Context-aware academic collaborator recommendation. In *KDD*, 2018.
74. H.-W. Ma, B. Kumar, U. Ditges, F. Gunzer, J. Buer, and A.-P. Zeng. An extended transcriptional regulatory network of *escherichia coli* and analysis of its hierarchical structure and network motifs. *Nucleic acids research*, 32(22):6643–6649, 2004.
75. R. Mastrandrea, J. Fournet, and A. Barrat. Contact patterns in a high school: a comparison between data collected using wearable sensors, contact diaries and friendship surveys. *PLoS one*, 10(9), 2015.
76. R. Matsuno and A. Gionis. Improved mixing time for k-subgraph sampling. In *SDM*, 2020.
77. T. Mikolov, I. Sutskever, K. Chen, G. S. Corrado, and J. Dean. Distributed representations of words and phrases and their compositionality. In *NIPS*, 2013.
78. R. Milo, S. Itzkovitz, N. Kashtan, R. Levitt, S. Shen-Orr, I. Ayzenshtat, M. Sheffer, and U. Alon. Superfamilies of evolved and designed networks. *Science*, 303(5663):1538–1542, 2004.
79. R. Milo, S. Shen-Orr, S. Itzkovitz, N. Kashtan, D. Chklovskii, and U. Alon. Network motifs: simple building blocks of complex networks. *Science*, 298(5594):824–827, 2002.
80. D. A. Nguyen, C. H. Nguyen, P. Petschner, and H. Mamitsuka. Sparse: a sparse hypergraph neural network for learning multiple types of latent combinations to accurately predict drug–drug interactions. *Bioinformatics*, 38:i333–i341, 2022.
81. C. C. Noble and D. J. Cook. Graph-based anomaly detection. In *KDD*, 2003.
82. M. Ouyang, M. Toulouse, K. Thulasiraman, F. Glover, and J. S. Deogun. Multilevel cooperative search for the circuit/hypergraph partitioning problem. *TCAD*, 21(6):685–693, 2002.
83. R. Pagh and C. E. Tsourakakis. Colorful triangle counting and a mapreduce implementation. *Information Processing Letters*, 112(7):277–281, 2012.
84. C. R. Palmer, P. B. Gibbons, and C. Faloutsos. Anf: A fast and scalable tool for data mining in massive graphs. In *KDD*, 2002.
85. A. Paranjape, A. R. Benson, and J. Leskovec. Motifs in temporal networks. In *WSDM*, 2017.
86. F. Pedregosa, G. Varoquaux, A. Gramfort, V. Michel, B. Thirion, O. Grisel, M. Blondel, P. Prettenhofer, R. Weiss, V. Dubourg, J. Vanderplas, A. Passos, D. Cournapeau, M. Brucher, M. Perrot, and E. Duchesnay. Scikit-learn: Machine learning in Python. *JMLR*, 12:2825–2830, 2011.
87. A. Pinar, C. Seshadhri, and V. Vishal. Escape: Efficiently counting all 5-vertex subgraphs. In *WWW*, 2017.
88. G. Preti, G. De Francisci Morales, and F. Bonchi. Fresco: Mining frequent patterns in simplicial complexes. In *WWW*, 2022.
89. R. A. Rossi, N. K. Ahmed, A. Carranza, D. Arbour, A. Rao, S. Kim, and E. Koh. Heterogeneous network motifs. *arXiv preprint arXiv:1901.10026*, 2019.
90. R. A. Rossi, N. K. Ahmed, and E. Koh. Higher-order network representation learning. In *WWW Companion*, 2018.
91. T. K. Saha and M. Al Hasan. Finding network motifs using mcmc sampling. In *Complex Networks VI*, pages 13–24. Springer, 2015.
92. S.-V. Sanei-Mehri, A. E. Sariyuce, and S. Tirthapura. Butterfly counting in bipartite networks. In *KDD*, 2018.
93. A. Sankar, X. Zhang, and K. C.-C. Chang. Motif-based convolutional neural network on graphs. *arXiv preprint arXiv:1711.05697*, 2017.
94. S. S. Shen-Orr, R. Milo, S. Mangan, and U. Alon. Network motifs in the transcriptional regulation network of *escherichia coli*. *Nature genetics*, 31(1):64–68, 2002.

95. K. Shin. Wrs: Waiting room sampling for accurate triangle counting in real graph streams. In *ICDM*, 2017.
96. K. Shin, S. Oh, J. Kim, B. Hooi, and C. Faloutsos. Fast, accurate and provable triangle counting in fully dynamic graph streams. *TKDD*, 14(2):1–39, 2020.
97. A. Sinha, Z. Shen, Y. Song, H. Ma, D. Eide, B.-J. Hsu, and K. Wang. An overview of microsoft academic service (mas) and applications. In *WWW*, 2015.
98. N. Sloane. *The On-Line Encyclopedia of Integer Sequences*.
99. J. Stehlé, N. Voirin, A. Barrat, C. Cattuto, L. Isella, J.-F. Pinton, M. Quaggiotto, W. Van den Broeck, C. Régis, B. Lina, et al. High-resolution measurements of face-to-face contact patterns in a primary school. *PLoS one*, 6(8), 2011.
100. L. Sun, S. Ji, and J. Ye. Hypergraph spectral learning for multi-label classification. In *KDD*, 2008.
101. Y. Sun, D. Zhu, H. Du, and Z. Tian. Motifs-based recommender system via hypergraph convolution and contrastive learning. *Neurocomputing*, 512:323–338, 2022.
102. C. E. Tsourakakis, U. Kang, G. L. Miller, and C. Faloutsos. Doulion: counting triangles in massive graphs with a coin. In *KDD*, 2009.
103. C. E. Tsourakakis, J. Pachocki, and M. Mitzenmacher. Scalable motif-aware graph clustering. In *WWW*, 2017.
104. P. Wang, P. Jia, Y. Qi, Y. Sun, J. Tao, and X. Guan. Rept: A streaming algorithm of approximating global and local triangle counts in parallel. In *ICDE*, 2019.
105. P. Wang, J. C. Lui, B. Ribeiro, D. Towsley, J. Zhao, and X. Guan. Efficiently estimating motif statistics of large networks. *TKDD*, 9(2):1–27, 2014.
106. P. Wang, Y. Qi, Y. Sun, X. Zhang, J. Tao, and X. Guan. Approximately counting triangles in large graph streams including edge duplicates with a fixed memory usage. *PVLDB*, 11(2):162–175, 2017.
107. D. J. Watts and S. H. Strogatz. Collective dynamics of ‘small-world’ networks. *Nature*, 393(6684):440, 1998.
108. X. Wu, Q. Chen, W. Li, Y. Xiao, and B. Hu. Adahgnn: Adaptive hypergraph neural networks for multi-label image classification. In *MM*, 2020.
109. D. Yang, B. Qu, J. Yang, and P. Cudre-Mauroux. Revisiting user mobility and social relationships in lbsns: A hypergraph embedding approach. In *WWW*, 2019.
110. E. Yeger-Lotem, S. Sattath, N. Kashtan, S. Itzkovitz, R. Milo, R. Y. Pinter, U. Alon, and H. Margalit. Network motifs in integrated cellular networks of transcription–regulation and protein–protein interaction. *Proceedings of the National Academy of Sciences*, 101(16):5934–5939, 2004.
111. H. Yin, A. R. Benson, J. Leskovec, and D. F. Gleich. Local higher-order graph clustering. In *KDD*, 2017.
112. S.-e. Yoon, H. Song, K. Shin, and Y. Yi. How much and when do we need higher-order information in hypergraphs? a case study on hyperedge prediction. In *WWW*, 2020.
113. J. Yu, D. Tao, and M. Wang. Adaptive hypergraph learning and its application in image classification. *TIP*, 21(7):3262–3272, 2012.
114. Y. Yu, Z. Lu, J. Liu, G. Zhao, and J.-r. Wen. Rum: Network representation learning using motifs. In *ICDE*, 2019.
115. Z. Yu and H. Gao. Molecular representation learning via heterogeneous motif graph neural networks. In *ICML*, 2022.
116. X. Yuan, N. Zhou, S. Yu, H. Huang, Z. Chen, and F. Xia. Higher-order structure based anomaly detection on attributed networks. In *Big Data*, 2021.
117. M. Zhang, Z. Cui, S. Jiang, and Y. Chen. Beyond link prediction: Predicting hyperlinks in adjacency space. In *AAAI*, 2018.
118. X. Zhang, L. Xu, and Z. Xu. Influence maximization based on network motifs in mobile social networks. *IEEE Transactions on Network Science and Engineering*, 9(4):2353–2363, 2022.
119. H. Zhao, X. Xu, Y. Song, D. L. Lee, Z. Chen, and H. Gao. Ranking users in social networks with higher-order structures. In *AAAI*, 2018.
120. H. Zhao, Y. Zhou, Y. Song, and D. L. Lee. Motif enhanced recommendation over heterogeneous information network. In *CIKM*, 2019.
121. D. Zhou, J. Huang, and B. Schölkopf. Learning with hypergraphs: Clustering, classification, and embedding. In *NIPS*, 2007.

A Proof of Theorem 2

We let $X_{ij}[t]$ be a random variable indicating whether the i -th sampled hyperedge (in line 3 of Algorithm 4) is included in the j -th instance of h-motif t or not. That is, $X_{ij}[t] = 1$ if the hyperedge is included in the instance, and $X_{ij}[t] = 0$ otherwise. We let $\bar{m}[t]$ be the number of times that h-motif t 's instances are counted while processing s sampled hyperedges. That is,

$$\bar{m}[t] := \sum_{i=1}^s \sum_{j=1}^{M[t]} X_{ij}[t]. \quad (9)$$

Then, by lines 8-9 of Algorithm 4,

$$\bar{M}[t] = \bar{m}[t] \cdot \frac{|E|}{3s}. \quad (10)$$

Proof of the Bias of $\bar{M}[t]$ (Eq. (4)): Since each h-motif instance contains three hyperedges, the probability that each i -th sampled hyperedge is contained in each j -th instance of h-motif t is

$$P[X_{ij}[t] = 1] = \mathbb{E}[X_{ij}[t]] = \frac{3}{|E|}. \quad (11)$$

From linearity of expectation,

$$\mathbb{E}[\bar{m}[t]] = \sum_{i=1}^s \sum_{j=1}^{M[t]} \mathbb{E}[X_{ij}[t]] = \sum_{i=1}^s \sum_{j=1}^{M[t]} \frac{3}{|E|} = \frac{3s \cdot M[t]}{|E|}.$$

Then, by Eq. (10), $\mathbb{E}[\bar{M}[t]] = \frac{|E|}{3s} \cdot \mathbb{E}[\bar{m}[t]] = M[t]$. \square

Proof of the Variance of $\bar{M}[t]$ (Eq. (5)): From Eq. (11) and $X_{ij}[t] = X_{ij}[t]^2$, the variance of $X_{ij}[t]$ is

$$\text{Var}[X_{ij}[t]] = \mathbb{E}[X_{ij}[t]^2] - \mathbb{E}[X_{ij}[t]]^2 = \frac{3}{|E|} - \frac{9}{|E|^2}. \quad (12)$$

Consider the covariance between $X_{ij}[t]$ and $X_{i'j'}[t]$. If $i = i'$, then from Eq. (11),

$$\begin{aligned} \text{Cov}(X_{ij}[t], X_{i'j'}[t]) &= \mathbb{E}[X_{ij}[t] \cdot X_{i'j'}[t]] - \mathbb{E}[X_{ij}[t]]\mathbb{E}[X_{i'j'}[t]] \\ &= P[X_{ij}[t] = 1, X_{i'j'}[t] = 1] - \mathbb{E}[X_{ij}[t]]\mathbb{E}[X_{i'j'}[t]] \\ &= P[X_{ij}[t] = 1] \cdot P[X_{i'j'}[t] = 1 | X_{ij}[t] = 1] \\ &\quad - \mathbb{E}[X_{ij}[t]]\mathbb{E}[X_{i'j'}[t]] \\ &= \frac{3}{|E|} \cdot \frac{l_{jj'}}{3} - \frac{9}{|E|^2} = \frac{l_{jj'}}{|E|} - \frac{9}{|E|^2}, \end{aligned} \quad (13)$$

where $l_{jj'}$ is the number of hyperedges that the j -th and j' -th instances share. However, since hyperedges are sampled independently (specifically, uniformly at random with replacement), if $i \neq i'$, then $\text{Cov}(X_{ij}[t], X_{i'j'}[t]) = 0$. This observation, Eq. (9), Eq. (12), and Eq. (13) imply

$$\begin{aligned} \text{Var}[\hat{m}[t]] &= \text{Var}\left[\sum_{i=1}^s \sum_{j=1}^{M[t]} X_{ij}[t]\right] \\ &= \sum_{i=1}^s \sum_{j=1}^{M[t]} \text{Var}[X_{ij}[t]] + \sum_{i=1}^s \sum_{j \neq j'}^{M[t]} \text{Cov}(X_{ij}[t], X_{i'j'}[t]) \\ &= s \cdot M[t] \cdot \left(\frac{3}{|E|} - \frac{9}{|E|^2}\right) + s \sum_{l=0}^2 p_l[t] \left(\frac{l}{|E|} - \frac{9}{|E|^2}\right), \end{aligned}$$

where $p_l[t]$ is the number of pairs of h-motif t 's instances sharing l hyperedges. This and Eq. (10) imply Eq. (5). \square

B Proof of Theorem 4

Let $\tau := M[t] \cdot \epsilon$ and $X_{ij}[t]$ be a random variable indicating whether the i -th sampled hyperedge (in line 3 of Algorithm 4) is included in the j -th instance of h-motif t or not. Also, let $\tilde{X}_i[t] = \frac{|E|}{3s} \sum_{j=1}^{M[t]} X_{ij}[t]$ (where the sum indicates the number of instances of h-motif t that contains i -th sampled hyperedge) so that $\bar{M}[t] = \sum_{i=1}^s \tilde{X}_i[t]$. Note that $0 \leq \tilde{X}_i[t] \leq \frac{|E| d_{\max}[t]^2}{3s}$ holds for every i . Since $\tilde{X}_1[t], \tilde{X}_2[t], \dots, \tilde{X}_s[t]$ are independent random variables and $\mathbb{E}[\bar{M}[t]] = M[t]$ (Theorem 2), we can apply Hoeffding's inequality (Lemma 3):

$$\begin{aligned} \Pr[|\bar{M}[t] - M[t]| \geq M[t] \cdot \epsilon] &\leq 2 \exp\left(-\frac{2\epsilon^2 M[t]^2}{s \cdot (d_{\max}[t]^2 |E|/3s)^2}\right) \\ &\leq 2 \exp\left(-\frac{18s\epsilon^2 M[t]^2}{|E|^2 d_{\max}[t]^4}\right) \leq \delta, \end{aligned}$$

which implies the condition for the sample size. \square

C Proof of Theorem 5

A random variable $Y_{ij}[t]$ denotes whether the i -th sampled hyperedge (in line 3 of Algorithm 5) is included in the j -th instance of h-motif t . That is, $Y_{ij}[t] = 1$ if the sampled hyperedge is included in the instance, and $Y_{ij}[t] = 0$ otherwise. We let $\hat{m}[t]$ be the number of times that h-motif t 's instances are counted while processing r sampled hyperedges. That is,

$$\hat{m}[t] := \sum_{i=1}^r \sum_{j=1}^{M[t]} Y_{ij}[t] \quad (14)$$

We use $w[t]$ to denote the number of hyperedges included in each instance of h-motif t . That is,

$$w[t] := \begin{cases} 2 & \text{if h-motif } t \text{ is open,} \\ 3 & \text{if h-motif } t \text{ is closed.} \end{cases} \quad (15)$$

Then, by lines 6-10 of Algorithm 5,

$$\hat{M}[t] = \hat{m}[t] \cdot \frac{1}{w[t]} \cdot \frac{|\Delta|}{r}. \quad (16)$$

Proof of the Bias of $\hat{M}[t]$ (Eq. (6)): Since each instance of h-motif t contains $w[t]$ hyperedges, the probability that each i -th sampled hyperedge is contained in each j -th instance of h-motif t is

$$P[Y_{ij}[t] = 1] = \mathbb{E}[Y_{ij}[t]] = \frac{w[t]}{|\Delta|}. \quad (17)$$

From linearity of expectation,

$$\mathbb{E}[\hat{m}[t]] = \sum_{i=1}^r \sum_{j=1}^{M[t]} \mathbb{E}[Y_{ij}[t]] = \sum_{i=1}^r \sum_{j=1}^{M[t]} \frac{w[t]}{|\Delta|} = \frac{w[t] \cdot r \cdot M[t]}{|\Delta|}.$$

Then, by Eq. (16), $\mathbb{E}[\hat{M}[t]] = \mathbb{E}[\hat{m}[t]] \cdot \frac{1}{w[t]} \cdot \frac{|\Delta|}{r} = M[t]$. \square

Proof of the Variance of $\hat{M}[t]$ (Eq. (7) and Eq. (8)):

From Eq. (17) and $Y_{ij}[t] = Y_{ij}[t]^2$, the variance of each random variable $Y_{ij}[t]$ is

$$\text{Var}[Y_{ij}[t]] = \mathbb{E}[Y_{ij}[t]^2] - \mathbb{E}[Y_{ij}[t]]^2 = \frac{w[t]}{|\Delta|} - \frac{w[t]^2}{|\Delta|^2}. \quad (18)$$

Consider the covariance between $Y_{ij}[t]$ and $Y_{i'j'}[t]$. If $i = i'$, then from Eq. (17),

$$\begin{aligned} \text{Cov}(Y_{ij}[t], Y_{i'j'}[t]) &= \mathbb{E}[Y_{ij}[t] \cdot Y_{i'j'}[t]] - \mathbb{E}[Y_{ij}[t]]\mathbb{E}[Y_{i'j'}[t]] \\ &= P[Y_{ij}[t] = 1, Y_{i'j'}[t] = 1] - \mathbb{E}[Y_{ij}[t]]\mathbb{E}[Y_{i'j'}[t]] \\ &= P[Y_{ij}[t] = 1] \cdot P[Y_{i'j'}[t] = 1 | Y_{ij}[t] = 1] - \mathbb{E}[Y_{ij}[t]]\mathbb{E}[Y_{i'j'}[t]] \\ &= \frac{w[t]}{|\Delta|} \cdot \frac{n_{jj'}}{w[t]} - \frac{w[t]^2}{|\Delta|^2} = \frac{n_{jj'}}{|\Delta|} - \frac{w[t]^2}{|\Delta|^2}, \end{aligned} \quad (19)$$

where $n_{jj'}$ is the number of hyperedges that the j -th and j' -th instances share. However, since hyperedges are sampled independently (specifically, uniformly at random with replacement), if $i \neq i'$, then $\text{Cov}(Y_{ij}[t], Y_{i'j'}[t]) = 0$. This observation, Eq. (14), Eq. (18), and Eq. (19) imply

$$\begin{aligned} \text{Var}[\hat{m}[t]] &= \text{Var}\left[\sum_{i=1}^r \sum_{j=1}^{M[t]} Y_{ij}[t]\right] \\ &= \sum_{i=1}^r \sum_{j=1}^{M[t]} \text{Var}[Y_{ij}[t]] + \sum_{i=1}^r \sum_{j \neq j'}^{M[t]} \text{Cov}(Y_{ij}[t], Y_{i'j'}[t]) \\ &= r \cdot M[t] \cdot \left(\frac{w[t]}{|\Delta|} - \frac{w[t]^2}{|\Delta|^2}\right) + r \sum_{n=0}^1 q_n[t] \cdot \left(\frac{n}{|\Delta|} - \frac{w[t]^2}{|\Delta|^2}\right), \end{aligned}$$

where $q_n[t]$ is the number of pairs of h-motif t 's instances that share n hyperedges. This and Eq. (16) imply Eq. (7) and Eq. (8). \square

D Proof of Theorem 7

Let $\tau := M[t] \cdot \epsilon$ and $Y_{ij}[t]$ denotes whether the i -th sampled hyperedge (in line 3 of Algorithm 5) is included in the j -th instance of h-motif t . Also, let $\tilde{Y}_i[t] = \frac{|\Delta|}{w[t]s} \sum_{j=1}^{M[t]} Y_{ij}[t]$ with $w[t]$ defined in Eq. (15), where the sum indicates the number of instances of h-motif t that contains the i -th sampled hyperedge, so that $\bar{M}[t] = \sum_{i=1}^r \tilde{Y}_i[t]$. Then, $0 \leq \tilde{Y}_i[t] \leq \frac{|\Delta| d_{\max}[t]}{w[t]r}$ holds for every i . Since $\tilde{Y}_1[t], \tilde{Y}_2[t], \dots, \tilde{Y}_r[t]$

are independent random variables and $\mathbb{E}[\hat{M}[t]] = M[t]$ (in Theorem 5), we can apply Hoeffding's inequality:

$$\begin{aligned} & \Pr \left[|\hat{M}[t] - M[t]| \geq M[t] \cdot \epsilon \right] \\ & \leq 2 \exp \left(- \frac{2\epsilon^2 M[t]^2}{r \cdot (d_{\max}[t]|A|/w[t]r)^2} \right) \\ & \leq 2 \exp \left(- \frac{2 \cdot w[t]^2 r \epsilon^2 M[t]^2}{|A|^2 d_{\max}[t]^2} \right) \leq \delta, \end{aligned}$$

which implies the condition for the sample size. \square

E Correlation between Global Structural Properties and H-motifs

We investigate the correlation between global structural properties and the hypergraph motifs (h-motifs). We consider eight global properties, categorized into five as follows.

- **Size:** We consider (1) the number of nodes and (2) the number of hyperedges.
- **Average degree:** The degree of a node is defined as the number of hyperedges that contain the node. The degree of a hyperedge is defined as the number of nodes that the hyperedge contains. We consider (3) the average degree of all nodes and (4) the average degree of all hyperedges.
- **Clustering coefficients:** In [35, 58], the clustering coefficient of two nodes $u \neq v$ is defined as:

$$CC(u, v) = \frac{|E_u \cap E_v|}{|E_u \cup E_v|},$$

where E_u is the set of hyperedges that contain the node u . Then, the average clustering coefficient of each node is defined as the mean of the clustering coefficients of it and each of its neighbors, i.e.,

$$CC(u) = \frac{\sum_{v \in N_u} CC(u, v)}{|N_u|},$$

where N_u is the set of neighbors of node u (i.e., $\{v \in V : E_u \cap E_v \neq \emptyset\}$). Similarly, we can define the clustering coefficients of hyperedge pairs and those of hyperedges. We consider (5) the mean of the clustering coefficients of all nodes and (6) the mean of the clustering coefficients of all hyperedges.

- **Effective diameter:** The diameter of a graph is defined as the maximum length of the shortest paths in the graph. Similarly, we define (7) the diameter of a hypergraph as the maximum length of the shortest hyperpaths in the hypergraph. In hypergraphs, a hyperpath between two nodes v_1 and v_k is a sequence of distinct nodes and hyperedges $v_1, e_1, v_2, e_2, \dots, e_{k-1}, v_k$ where there $v_i \in e_i$ and $v_{i+1} \in e_i$ for $1 \leq i < k$ [121]. The length of a hyperpath is the number of intermediate hyperedges contained in the hyperpath. In hypergraphs that have disconnected components, the diameter is not computable. Thus, we compute effective diameter [84], which is the 90th percentile of the distribution of shortest-path lengths. We use `GetAnfEffDiam` function provided by [67].
- **Total number of h-motifs:** We consider (8) the total number of hypergraph motifs computed using `MoCHy`.

The statistics of the global properties of hypergraphs are provided in Table 6. We compute the Pearson correlation coefficients between each h-motif's CP value and eight different

Algorithm 6: Chung-Lu Model [7]

Input : bipartite graph G' : $G' = (V \cup E, E')$
Output: randomized bipartite graph $\tilde{G} = (V \cup E, \tilde{E})$

- 1 $\{d_i^V\}_{i=1}^{|V|} \leftarrow$ degrees of nodes in V
- 2 $\{d_j^E\}_{j=1}^{|E|} \leftarrow$ degrees of nodes in E
- 3 $\tilde{E} \leftarrow$ an empty multiset
- 4 **for** $k = 1, \dots, |E'|$ **do**
- 5 $v_i \leftarrow$ sample from V with probability \propto degree
- 6 $e_j \leftarrow$ sample from E with probability \propto degree
- 7 add (v_i, e_j) to \tilde{E}
- 8 **return** $\tilde{G} = (\tilde{V}, \tilde{E})$

Algorithm 7: Transformation from Incidence

Graphs to Hypergraphs

Input : incidence graph $\tilde{G} = (V \cup E, \tilde{E})$
Output: hypergraph $\hat{G} = (V, \hat{E})$

- 1 **for each** $\tilde{e}_j \in \tilde{E}$ **do**
- 2 $\hat{e}_j \leftarrow \emptyset$
- 3 **for each** $(v_i, e_j) \in \tilde{E}$ **do**
- 4 $\hat{e}_j \leftarrow \hat{e}_j \cup \{v_i\}$
- 5 $\hat{E} \leftarrow \emptyset$
- 6 **for each** $e_j \in E$ **do**
- 7 **if** $\hat{e}_j \neq \emptyset$ **then**
- 8 $\hat{E} \leftarrow \hat{E} \cup \{\hat{e}_j\}$
- 9 **return** $\hat{G} = (V, \hat{E})$

global properties. As seen in Table 7, different h-motifs show different correlations with each global property. For example, h-motif 13 shows the lowest correlation with the node size (-0.558), the node-based clustering coefficient (-0.650), the hyperedge-based clustering coefficient (-0.499), and the effective diameter (-0.620), but the highest correlation with the average node degree (0.523) and the average hyperedge degree (0.522). In addition, some global properties are strongly correlated with h-motifs, while some are weakly correlated. For example, there are many h-motifs highly correlated with the node size, the node-based clustering coefficient, and the effective diameter, while most of the h-motifs have near-zero correlations with the average hyperedge degree and the hyperedge-based clustering coefficient.

F Randomized Hypergraphs

To create randomized hypergraphs, we extend the Chung-Lu model [7], which is a configuration model designed to generate random bipartite graphs, to hypergraphs. Algorithm 6 provides the pseudocode for the Chung-Lu model, where V and E represent two sets of nodes in both the input and output bipartite graphs. Note that the output bipartite graph \tilde{G} allows parallel edges (i.e. \tilde{E} is a multiset). The Chung-Lu model preserves the degrees of nodes in expectation, i.e., the following equalities hold:

$$\mathbb{E}[\tilde{d}_i^V] = d_i^V, \quad \mathbb{E}[\tilde{d}_j^E] = d_j^E, \quad (20)$$

Table 6: Global structural properties of real-world hypergraphs.

Dataset	Size		Average Degree		Clustering Coeff.		Effective Diameter	# of H-motifs
	Node	Hyperedge	Node	Hyperedge	Node	Hyperedge		
coauth-DBLP	1,924,991	2,466,792	4.013	3.132	0.296	0.225	6.590	26.3B
coauth-geology	1,256,385	1,203,895	3.015	3.146	0.382	0.208	6.809	6B
coauth-history	1,014,734	895,439	1.354	1.535	0.575	0.331	12.946	83.2M
contact-primary	242	12,704	126.9	2.418	0.011	0.270	1.888	617M
contact-high	327	7,818	55.6	2.326	0.018	0.286	2.564	69.7M
email-Enron	143	1,512	31.8	3.009	0.064	0.249	2.583	9.6M
email-EU	998	25,027	85.9	3.425	0.030	0.207	2.836	7B
tags-ubuntu	3,029	147,222	164.8	3.391	0.007	0.182	2.262	4.3T
tags-math	1,629	170,476	364.1	3.479	0.005	0.180	2.189	9.2T
threads-ubuntu	125,602	166,999	2.538	1.908	0.160	0.301	4.657	11.4B
threads-math	176,445	595,749	8.261	2.446	0.033	0.250	3.662	2.2T

Table 7: Correlation between global structural properties and characteristic profiles (CPs). Strong positive or negative correlations (≥ 0.5) are colored as **red** (positive) or **blue** (negative).

h-motif	Size		Average Degree		Clustering Coeff.		Effective Diameter	# of H-motifs
	Node	Hyperedge	Node	Hyperedge	Node	Hyperedge		
1	+0.787	+0.648	-0.497	+0.003	+0.751	+0.115	+0.626	-0.530
2	-0.169	-0.110	-0.023	-0.645	-0.027	+0.479	+0.099	+0.101
3	+0.710	+0.587	-0.492	+0.065	+0.718	+0.067	+0.633	-0.501
4	+0.901	+0.783	-0.480	-0.071	+0.891	+0.122	+0.806	-0.410
5	+0.469	+0.315	-0.506	-0.126	+0.498	+0.316	+0.406	-0.730
6	+0.877	+0.762	-0.311	-0.161	+0.872	+0.151	+0.801	-0.249
7	+0.229	+0.071	-0.436	-0.188	+0.313	+0.394	+0.215	-0.744
8	+0.388	+0.237	-0.561	-0.154	+0.447	+0.359	+0.361	-0.772
9	+0.138	-0.023	-0.266	-0.081	+0.229	+0.293	+0.124	-0.606
10	+0.444	+0.288	-0.584	-0.178	+0.537	+0.363	+0.447	-0.733
11	+0.123	-0.041	+0.023	+0.098	+0.200	+0.077	+0.087	-0.329
12	+0.611	+0.540	-0.246	-0.096	+0.676	+0.050	+0.643	-0.061
13	-0.558	-0.485	+0.523	+0.552	-0.650	-0.499	-0.620	+0.413
14	-0.490	-0.567	+0.232	+0.156	-0.351	-0.010	-0.417	-0.064
15	+0.166	+0.042	-0.148	+0.080	+0.299	+0.045	+0.224	-0.224
16	+0.481	+0.464	-0.184	+0.028	+0.531	-0.110	+0.532	+0.106
17	+0.754	+0.608	-0.501	-0.127	+0.828	+0.231	+0.741	-0.481
18	+0.442	+0.298	-0.444	+0.031	+0.551	+0.149	+0.473	-0.532
19	+0.623	+0.471	-0.507	-0.089	+0.677	+0.251	+0.584	-0.596
20	+0.628	+0.473	-0.483	-0.001	+0.724	+0.136	+0.633	-0.514
21	+0.089	-0.047	-0.315	-0.136	+0.141	+0.346	+0.074	-0.676
22	+0.554	+0.522	-0.157	-0.299	+0.724	+0.127	+0.763	+0.154
23	+0.332	+0.181	-0.434	-0.130	+0.365	+0.334	+0.273	-0.722
24	+0.428	+0.275	-0.492	-0.147	+0.459	+0.341	+0.368	-0.737
25	+0.747	+0.593	-0.508	-0.151	+0.758	+0.269	+0.666	-0.610
26	+0.883	+0.812	-0.330	-0.203	+0.877	+0.118	+0.830	-0.129

where d_i^V and d_j^E denote the degrees of nodes $v_i \in V$ and $e_j \in E$ in the input graph; and \hat{d}_i^V and \hat{d}_j^E denote the degrees (weighted by edge multiplicity) of nodes $v_i \in V$ and $e_j \in E$ in the output graph \hat{G} , respectively. Moreover, it can be shown that the obtained random graph is a uniform sample. The Chung-Lu model is widely used due to efficiency because configuration models that preserve node degrees exactly exist are slower in generating a uniform sample.

In order to create a hypergraph randomized from the input hypergraph $G = (V, E)$, we first apply this model to its incidence graph G' to obtain a random bipartite graph \tilde{G} , and then we transform \tilde{G} into a random hypergraph \hat{G} , as described in Algorithm 7. Note that the multiplicity of edges in \tilde{E} does not affect the output hypergraph since each hyper-

edge \hat{e}_j in line 4 is a set, instead of a multiset. If G' does not have parallel edges (although they are allowed), Eq. (20) implies the following equalities:

$$\mathbb{E}[\hat{d}_i] = d_i, \quad \mathbb{E}[|\hat{e}_j|] = |e_j|, \quad (21)$$

where d_i and $|e_j|$ denote the degree of $v_i \in V$ and the size of $e_j \in E$ in the input hypergraph G ; and \hat{d}_i and $|\hat{e}_j|$ denote those in the random hypergraph \hat{G} . That is, both the node degree distribution and the hyperedge size distribution of G are preserved in expectation in \hat{G} . While these properties do not hold theoretically when G' has parallel edges, empirically both distributions are preserved accurately for real-world hypergraphs, as shown in Figure 17. We present additional basic statistics for the generated hypergraphs in Table 8.

Table 8: Statistics of generated random hypergraphs. Isolated nodes are ignored. The average values of 5 random hypergraphs are reported.

Dataset	$ V $	$ E $
coauth-DBLP	1,483,582	2,221,017
coauth-geology	927,693	1,042,749
coauth-history	685,637	634,385
contact-primary	242	11,416
contact-high	327	6,954
email-Enron	142	1,365
email-EU	964	22,764
tags-ubuntu	2,974	139,170
tags-math	1,606	162,260
threads-ubuntu	88,225	135,076
threads-math	134,722	522,149

G Extensions beyond Three Hyperedges

The concept of h-motifs can be generalized to k hyperedges. Defining h-motifs describing the connectivity pattern of k connected hyperedges requires the following conditions:

- **No symmetric patterns:** Each connectivity pattern should be described by exactly one h-motif.
- **No disconnected hyperedges:** All k hyperedges should be connected.
- **No duplicated hyperedges:** All k hyperedges should be distinct.

Given a set $\{e_{s_1}, e_{s_2}, \dots, e_{s_k}\}$ of k connected hyperedges, a node can be included in 1 (e.g., $e_{s_1} \setminus e_{s_2} \setminus \dots \setminus e_{s_k}$) to k ($e_{s_1} \cap e_{s_2} \cap \dots \cap e_{s_k}$) hyperedges at the same time. Thus, its connectivity pattern can be described by the emptiness of $2^k - 1$ sets, which can be expressed as a binary vector of size $2^k - 1$. Therefore, there can be $2^{2^k - 1}$ h-motifs, while only a subset of them remains once we exclude those violating any of the three conditions above. As a result, the number of remaining h-motifs is

$$2^{2^k - 1} - |P_1^{(k)} \cup P_2^{(k)} \cup P_3^{(k)}|, \quad (22)$$

where $P_1^{(k)}$, $P_2^{(k)}$, and $P_3^{(k)}$ represent the sets of (1) the k -hyperedge patterns that are symmetric, (2) those that cannot be obtained from connected hyperedges, and (3) those that cannot be obtained from distinct hyperedges, respectively. For $P_1^{(k)}$, among the binary representations that imply the same pattern, all but the lexicographically smallest one are removed. That is, $P_1^{(k)}$ represents a set of patterns that are *not* lexicographically smallest among those representing the same pattern.

H-motifs with Two Hyperedges: Given a pair of two connected hyperedges $\{e_i, e_j\}$, its connectivity can be described by the emptiness of three sets: $e_i - e_j$, $e_j - e_i$, and $e_i \cap e_j$. Once we remove the pattern that has duplicated hyperedges ($e_i - e_j = \emptyset$, $e_j - e_i = \emptyset$, and $e_i \cap e_j \neq \emptyset$), 3 patterns remain: (1) $e_i - e_j = \emptyset$, $e_j - e_i \neq \emptyset$, and $e_i \cap e_j \neq \emptyset$, (2) $e_i - e_j \neq \emptyset$, $e_j - e_i = \emptyset$, and $e_i \cap e_j \neq \emptyset$, and (3) $e_i - e_j \neq \emptyset$, $e_j - e_i \neq \emptyset$, and $e_i \cap e_j \neq \emptyset$. Since (1) and (2) are symmetric, we remove one of them, then 2 patterns remain.

H-motifs with Four Hyperedges: Given a set $\{e_i, e_j, e_k, e_l\}$ of four hyperedges, its connectivity pattern can be described

by the emptiness of 15 sets, which makes the total of 32,768 patterns. Once we remove symmetric patterns and leave the unique ones, 1,992 patterns remain. Among these, 80 patterns cannot be obtained from connected hyperedges, 73 patterns cannot be obtained from distinct hyperedges, and there are 14 patterns that are common between the two sets. Removing these leaves 1,853 h-motifs with four hyperedges.

H-motifs with k Hyperedges: From (22), we can notice that the number of connectivity patterns of k -hyperedge h-motifs rapidly increases with k . If $k = 5$, there exists a total of 2,147,483,648 ($= 2^{31}$) patterns, while 18,656,322 remain once we filter those that violate any one of the three conditions. The statistics of the number of h-motifs for $k = 2$ to 6 are shown in Table 9. In case of $k = 2$ to 5-hyperedge h-motifs, the number of connectivity patterns is counted via enumeration. For a larger k , we use *OEIS* [98] to obtain the numbers. The sequence of the numbers of patterns after removing symmetric (redundant) ones ($2^{2^k - 1} - |P_1^{(k)}|$) can be found at [1], which is explained as the sequence of *number of P -equivalence classes of switching functions of k or fewer variables, divided by 2*¹². Since we can infer from Table 9 that the number of h-motif patterns is tightly upper-bounded by the remainder of the first filtering, this sequence gives us a good reference for the actual number of h-motifs ($2^{2^k - 1} - |P_1^{(k)} \cup P_2^{(k)} \cup P_3^{(k)}|$). The sequence increases rapidly, and if $k = 10$, there exist 2.48^{301} patterns. We also note that [2] describes the sequence after the second filtering, $2^{2^k - 1} - |P_1^{(k)} \cup P_2^{(k)}|$, which is the *number of non-isomorphic connected set-systems covering k vertices*. Note that there are known formulas for both sequences [1, 2].

H Number of k H-motifs

The number of kh -motifs for any $k > 1$ can be calculated by subdividing each h-motif into multiple kh -motifs. For example, in h-motif 1 in Figure 3, depending on the cardinality of the the seven considered sets, there are $(k - 1)$ possibilities for the red region,¹³ and $\binom{k-1}{2} + k - 1 = \binom{k}{2}$ possibilities for the two symmetric green regions.¹⁴ Therefore, $(k - 1) \times \binom{k}{2} = \frac{k(k-1)^2}{2}$ kh -motifs are subdivided from h-motif 1. By applying the same process to each h-motif and summing up the results, we obtain the following formula:

$$X(k) = \frac{k(k-1)(k^5 + k^4 + 4k^3 + k^2 - 4k + 2)}{6} \quad (23)$$

where $X(k)$ is the number of kh -motifs for each $k \geq 2$. Note that the number of h-motifs is $X(2) = 26$, and the number of 3h-motifs is $X(3) = 431$.

I Details of On-the-Fly MoChy

In this section, we provide detailed explanations of the on-the-fly version of MoChy, which counts the instances of h-motifs

¹² It is also commented that the sequence is equivalent to the number of non-isomorphic fillings of a Venn diagram of k sets.

¹³ A colored region cannot be empty, and thus there are $k - 1$ possible states.

¹⁴ There are $\binom{k-1}{2}$ possibilities when they have different states and $k - 1$ (symmetric) possibilities when they have the same state.

Table 9: The number of h-motifs with $k = 2$ to 6 hyperedges. For $k = 2$ to 5-hyperedge h-motifs, the number of cases are counted via enumeration. For $k = 6$, the number of cases is inferred.

Conditions	2 Hyperedges	3 Hyperedges	4 Hyperedges	5 Hyperedges	6 Hyperedges
2^{2^k-1}	8	128	32,768	2,147,483,648	9,223,372,036,854,775,808
$2^{2^k-1} - P_1^{(k)} $	6	40	1,992	18,666,624	12,813,206,169,137,152
$2^{2^k-1} - P_1^{(k)} \cup P_2^{(k)} $	3	30	1,912	18,662,590	12,813,206,131,799,685
$2^{2^k-1} - P_1^{(k)} \cup P_2^{(k)} \cup P_3^{(k)} $	2	26	1,853	18,656,322	?
Actual Count	2	26	1,853	18,656,322	?

without line-graph construction in the preprocessing step (see Section 4.4). We present two versions of on-the-fly algorithms for MoCHy-A⁺: **On-the-fly MoCHy-A⁺ (Basic)** and **On-the-fly MoCHy-A⁺ (Adv.)**. The pseudocodes for these algorithms are provided in Algorithms 8 and 9, respectively. Unlike the basic version of MoCHy-A⁺, the line graph is not given as an input. Instead, the budget b of memoization is given. To this end, we use three additional data structures:

- Q : a priority queue that prioritizes high-degree hyperedges. The index of an hyperedge is stored as a key, and its degree is used as the corresponding priority. It is initialized to \emptyset .
- A : a map that memoizes the neighbors of a subset of hyperedges. It is initialized to \emptyset . The maximum capacity of A is given as the budget b .
- cap : a variable that records the remaining capacity of A . This variable is initialized to b .

On-the-fly MoCHy-A⁺ (Basic) (Algorithm 8): For each hyperedge e_i in each sampled hyperwedge $\wedge_{ij} \in \wedge$, Algorithm 8 first checks whether its neighbors are memoized in the map A (line 9). If the neighbors are not memoized, it checks the remaining capacity cap and memoizes the neighbors of e_i in A if the remaining capacity allows (i.e., if $d_i \leq cap$). Otherwise, it removes the neighbors of a hyperedge with the lowest priority from A . Specifically, since we prioritize hyperedges with high degree in \bar{G} , a hyperedge with the lowest degree is dequeued from Q (line 11), and its neighbors are evicted from A (line 14). Evicting these neighbors increases the remaining capacity cap of A (line 13). This is repeated until the remaining capacity cap becomes large enough to memoize e_i 's neighbors (i.e., $cap \geq d_i$). Then, the neighbors of e_i are retrieved by calling the `getNeighbors` function and memoized (line 15), followed by the reduction of the remaining capacity cap .

On-the-fly MoCHy-A⁺ (Adv.) (Algorithm 9): We additionally develop **On-the-fly MoCHy-A⁺ (Adv.)**, an advanced on-the-fly version of MoCHy-A⁺ in Algorithm 9. In **On-the-fly MoCHy-A⁺ (Basic)**, when the same hyperedge is processed again after its neighbors are evicted from the line graph, it requires the reconstruction of its neighbors, thereby increasing the computational overhead. **On-the-fly MoCHy-A⁺ (Adv.)** is designed to mitigate this by taking the processing order of hyperwedges into account, aiming to reduce unnecessary reconstruction. The high-level idea behind **On-the-fly MoCHy-A⁺ (Adv.)** is to consecutively process hyperwedges consisting of the same hyperedges, thereby increasing the chance of utilizing memoized neighbors before they are evicted. **On-the-fly MoCHy-A⁺ (Adv.)** first collects r hyperwedges (lines 7-8). For each hyperedge, we define its *key hyperedge* as one of the two hyperedges forming the hyperwedge whose degree in \bar{G} (or

index in the case of a tie) is greater than that of the other hyperedge. Then, it groups the collected hyperwedges based on their respective key hyperedge (line 9-12). After that, the hyperwedges are processed group by group (line 14) in descending order of the degree in \bar{G} (or index in the case of a tie) of key hyperedges (line 13), thereby increasing the chance of utilizing memoized neighbors before they are evicted. The processing method for each hyperwedge remains the same as that of **On-the-fly MoCHy-A⁺ (Basic)**. After processing each group, the neighbors of its key hyperedge are evicted from the line graph (lines 28-30) permanently, as all hyperwedges containing it have been processed.

J Hyperedge Prediction

In this section, we provide detailed information about the hyperedge prediction task in Section 6.5 and additional experimental results.

Settings: To generate training and test sets, we first extract hyperedges whose sizes are at least 3 from each domain. In the test set, we remove hyperedges that contain out-of-sample nodes (i.e., nodes that are not contained in the training set). In both training and test sets, a fake hyperedge is generated from each real hyperedge to balance the numbers of real and fake hyperedges.

Negative Hyperedge Sampling: For each positive hyperedge e , we first generate a random probability α ($\frac{1}{3} \leq \alpha \leq 1$ ¹⁵). Then, we replace $\alpha \cdot |e|$ among the nodes with randomly selected nodes. Instead of sampling negative nodes from V uniformly at random, we sample based on the noisy distribution, as in [77], where the probability of each node v_i being selected is:

$$P(v_i) = \frac{|E_{v_i}|^{\frac{3}{4}}}{\sum_{j=1}^{|V|} |E_{v_j}|^{\frac{3}{4}}}.$$

For each generated negative hyperedge e' , we ensure that the size is the same as the positive one (i.e., no duplicated nodes in the hyperedge satisfying $|e| = |e'|$) and it is negative (i.e., e' does not exist in both training and test sets of positive hyperedges).

Results with More Classifiers: We evaluate the performance of the four considered feature sets in hyperedge prediction using four additional classifiers: Logistic Regression, Decision Tree, Random Forest, and MLP, in addition to XGBoost. We use the implementation of all classifiers provided

¹⁵ α is at least $\frac{1}{3}$ since the minimum size of sampled hyperedges is 3.

Algorithm 8: On-the-fly MoCHy-A⁺ (Basic): A Basic On-the-Fly Version of MoCHy-A⁺ without Line Graph Construction

Input : (1) input hypergraph: $G = (V, E)$
(2) number of samples: r
(3) budget size: b

Output: estimated count of each h-motif t 's instances: $\hat{M}[t]$

```

1  $\{d_1, \dots, d_{|E|}\} \leftarrow$  hyperedge degrees in  $\bar{G}$  (# of adjacent hyperedges)
2  $\hat{M} \leftarrow$  map whose default value is 0
3  $Q \leftarrow$  a priority queue whose default value is  $\emptyset$ 
4  $A \leftarrow$  a map whose default value is  $\emptyset$ 
5  $cap \leftarrow$  the remaining capacity of  $A$ . Its default value is  $b$ 
6 for  $n \leftarrow 1 \dots r$  do
7    $\wedge_{ij} \leftarrow$  a uniformly random hyperwedge
8   for each index  $l \in \{i, j\}$  do
9     if  $A[e_l] = \emptyset$  then
10       while  $cap < d_l$  do
11          $m \leftarrow Q.pop()$ 
12         if  $m \notin \{i, j\}$  then
13            $cap \leftarrow cap + d_m$ 
14            $A[e_m] \leftarrow \emptyset$ 
15          $A[e_l] \leftarrow \text{getNeighbors}(e_l, G)$ 
16          $cap \leftarrow cap - d_l$ 
17          $Q.push(l, d_l)$ 
18   for each index  $l \in \{i, j\}$  do
19     if  $A[e_l] \neq \emptyset$  and  $l \notin Q$  then
20        $Q.push(l, d_l)$ 
21   for each hyperedge  $e_k \in (A[e_i] \cup A[e_j] \setminus \{e_i, e_j\})$  do
22      $\hat{M}[h(\{e_i, e_j, e_k\})] += 1$ 
23 for each h-motif  $t$  do
24   if  $17 \leq t \leq 22$  then ▷ open h-motifs
25      $\hat{M}[t] \leftarrow \hat{M}[t] \cdot \frac{|\Delta|}{2r}$ 
26   else ▷ closed h-motifs
27      $\hat{M}[t] \leftarrow \hat{M}[t] \cdot \frac{|\Delta|}{3r}$ 
28 return  $\hat{M}$ 

29 Subroutine  $\text{getNeighbors}(e, G)$ 
30    $\hat{N}_e \leftarrow$  a map whose default value is 0
31   for each node  $v \in e$  do
32     for each hyperedge  $e' \in E_v \setminus \{e\}$  do
33        $\hat{N}_e[e'] \leftarrow \hat{N}_e[e'] + 1$ 
34   return  $\hat{N}_e$ 

```

by scikit-learn [86] with default hyperparameters. In Table 10, we report the accuracy (ACC) and the area under the ROC curve (AUC) of each classifier on each dataset. The results indicate that XGBoost, which we use in the main paper, yields higher average ACC and AUC than the other classifiers for all feature sets except for HP7, where XGBoost yields the highest average ACC but the second-highest average AUC.

K Node Classification

In this section, we provide detailed information about the node classification task in Section 6.5 and additional experimental results.

Settings: We randomly sample 100 nodes from each of the 11 real-world hypergraphs, ensuring that the corresponding radial ego-networks contain between 10 and 13,500 hyperedges. Note that the tags-math-sx dataset has the largest radial ego-networks, with a mean of around 13,500 hyperedges. We split the selected 1,100 nodes into a training set (80%) and a test

Algorithm 9: On-the-fly MoCHy-A⁺ (Adv.): An Advanced On-the-Fly Version of MoCHy-A⁺ without Line Graph Construction

Input : (1) input hypergraph: $G = (V, E)$
(2) number of samples: r
(3) budget size: b

Output: estimated count of each h-motif t 's instances: $\hat{M}[t]$

```

1  $\{d_1, \dots, d_{|E|}\} \leftarrow$  hyperedge degrees in  $\bar{G}$  (# of adjacent hyperedges)
2  $\hat{M} \leftarrow$  map whose default value is 0
3  $Q \leftarrow$  a priority queue whose default value is  $\emptyset$ 
4  $A \leftarrow$  a map whose default value is  $\emptyset$ 
5  $cap \leftarrow$  the remaining capacity of  $A$ . Its default value is  $b$ 
6  $W \leftarrow$  a map whose default value is  $\emptyset$ 
7 for  $n \leftarrow 1 \dots r$  do
8    $\wedge_{ij} \leftarrow$  a uniformly random hyperwedge
9   if  $d_i > d_j$  or ( $d_i = d_j$  and  $i > j$ ) then
10      $W[e_i] \leftarrow W[e_i] \cup \{\wedge_{ij}\}$ 
11   else
12      $W[e_j] \leftarrow W[e_j] \cup \{\wedge_{ij}\}$ 
13  $K \leftarrow$  sort the keys (i.e., hyperedges) of  $W$  in descending order of  $(d_i, i)$  of each key  $e_i$ 
14 for each hyperedge  $e_i \in K$  do
15   for each hyperwedge  $\wedge_{ij} \in W[e_i]$  do
16     for each index  $l \in \{i, j\}$  do
17       if  $A[e_l] = \emptyset$  then
18         while  $cap < d_l$  do
19            $m \leftarrow Q.pop()$ 
20           if  $m \notin \{i, j\}$  then
21              $cap \leftarrow cap + d_m$ 
22              $A[e_m] \leftarrow \emptyset$ 
23            $A[e_l] \leftarrow \text{getNeighbors}(e_l, G)$  ▷ Algorithm 8
24            $cap \leftarrow cap - d_l$ 
25            $Q.push(l, d_l)$ 
26       for each hyperedge  $e_k \in (A[e_i] \cup A[e_j] \setminus \{e_i, e_j\})$  do
27          $\hat{M}[h(\{e_i, e_j, e_k\})] += 1$ 
28      $Q.remove(i)$ 
29      $cap \leftarrow cap + d_i$ 
30      $A[e_i] \leftarrow \emptyset$ 
31 for each h-motif  $t$  do
32   if  $17 \leq t \leq 22$  then ▷ open h-motifs
33      $\hat{M}[t] \leftarrow \hat{M}[t] \cdot \frac{|\wedge|}{2r}$ 
34   else ▷ closed h-motifs
35      $\hat{M}[t] \leftarrow \hat{M}[t] \cdot \frac{|\wedge|}{3r}$ 
36 return  $\hat{M}$ 

```

set (20%) while ensuring that each label has an equal number of nodes in both sets.

Additional Experimental Results: We evaluate the performance of the four considered feature sets in node classification using all combinations of three ego-network types (spec., star, radial, and contracted) and five classifiers (spec., Logistic Regression, Decision Tree, Random Forest, MLP, and XGBoost). We use the implementation of all classifiers provided by scikit-learn [86] with default hyperparameters. In

Table 11, we report the accuracy (ACC) and the average area under the ROC curve (AVG AUC) for each combination. It should be noticed that the combination of radial ego-networks and XGBoost, which we use in the main paper, performs well for all feature sets. Specifically, the combination yields higher ACC and AVG AUC than the other combinations for NP26 and TNP. Additionally, for NP7, the combination yields the highest ACC but the second highest AVG AUC. For BASELINE, the combination yields the highest AVG AUC but the second highest ACC.

Table 10: Accuracy (ACC) and area under the ROC curve (AUC) for hyperedge prediction using five different classifiers for each dataset. D1 to D7 refer to the coauth-DBLP, coauth-MAG-Geology, coauth-MAG-History, contact-primary-school, contact-high-school, email-Enron, and email-Eu datasets in order. For each dataset, the best and second-best results are in **bold** and underlined, respectively.

(a) HP26									
	Classifier	D1	D2	D3	D4	D5	D6	D7	AVG
ACC*	Logistic Regression	0.764 ± 0.000	0.743 ± 0.000	0.654 ± 0.000	0.770 ± 0.000	0.895 ± 0.000	0.815 ± 0.000	0.904 ± 0.000	0.792 ± 0.000
	Decision Tree	0.729 ± 0.000	0.705 ± 0.001	<u>0.689 ± 0.005</u>	0.749 ± 0.003	0.886 ± 0.002	0.769 ± 0.013	0.881 ± 0.001	0.773 ± 0.004
	Random Forest	0.774 ± 0.002	0.740 ± 0.004	0.633 ± 0.010	0.765 ± 0.002	0.879 ± 0.003	0.704 ± 0.005	0.876 ± 0.003	0.767 ± 0.004
	MLP	0.804 ± 0.002	0.786 ± 0.003	0.678 ± 0.007	0.773 ± 0.009	<u>0.906 ± 0.012</u>	<u>0.812 ± 0.011</u>	0.915 ± 0.004	<u>0.811 ± 0.007</u>
	XGBoost	<u>0.801 ± 0.000</u>	<u>0.782 ± 0.000</u>	0.696 ± 0.000	<u>0.772 ± 0.000</u>	0.907 ± 0.000	0.815 ± 0.000	<u>0.911 ± 0.000</u>	0.812 ± 0.000
AUC†	Logistic Regression	0.843 ± 0.000	0.827 ± 0.000	0.688 ± 0.000	<u>0.892 ± 0.000</u>	<u>0.971 ± 0.000</u>	0.928 ± 0.000	0.969 ± 0.000	0.874 ± 0.000
	Decision Tree	0.730 ± 0.000	0.707 ± 0.001	0.698 ± 0.007	0.749 ± 0.003	0.886 ± 0.002	0.769 ± 0.013	0.881 ± 0.001	0.774 ± 0.003
	Random Forest	<u>0.862 ± 0.002</u>	0.826 ± 0.003	0.679 ± 0.006	0.885 ± 0.001	0.966 ± 0.001	0.897 ± 0.004	0.946 ± 0.001	0.866 ± 0.004
	MLP	0.886 ± 0.002	0.867 ± 0.002	<u>0.781 ± 0.008</u>	0.893 ± 0.000	0.973 ± 0.001	0.917 ± 0.006	0.973 ± 0.001	<u>0.899 ± 0.007</u>
	XGBoost	0.886 ± 0.000	<u>0.865 ± 0.000</u>	0.811 ± 0.000	0.879 ± 0.000	0.968 ± 0.000	<u>0.922 ± 0.000</u>	<u>0.972 ± 0.000</u>	0.900 ± 0.000

* accuracy, † area under the ROC curve.

(b) HP7									
	Classifier	D1	D2	D3	D4	D5	D6	D7	AVG
ACC	Logistic Regression	0.713 ± 0.000	0.698 ± 0.000	0.605 ± 0.000	0.764 ± 0.000	0.859 ± 0.000	0.676 ± 0.000	0.858 ± 0.000	0.739 ± 0.000
	Decision Tree	0.657 ± 0.000	0.629 ± 0.001	0.645 ± 0.003	0.751 ± 0.002	0.847 ± 0.008	0.699 ± 0.005	0.845 ± 0.002	0.725 ± 0.003
	Random Forest	0.736 ± 0.000	0.704 ± 0.003	0.592 ± 0.006	0.777 ± 0.002	0.826 ± 0.008	0.639 ± 0.005	0.785 ± 0.004	0.723 ± 0.004
	MLP	<u>0.742 ± 0.005</u>	0.723 ± 0.005	<u>0.654 ± 0.006</u>	0.767 ± 0.006	0.873 ± 0.011	<u>0.722 ± 0.008</u>	<u>0.876 ± 0.007</u>	<u>0.765 ± 0.007</u>
	XGBoost	0.744 ± 0.000	<u>0.722 ± 0.000</u>	0.683 ± 0.000	<u>0.769 ± 0.000</u>	<u>0.860 ± 0.000</u>	0.725 ± 0.000	0.878 ± 0.000	0.769 ± 0.000
AUC	Logistic Regression	0.775 ± 0.000	0.770 ± 0.000	0.612 ± 0.000	<u>0.879 ± 0.000</u>	<u>0.955 ± 0.000</u>	0.804 ± 0.000	0.939 ± 0.000	0.819 ± 0.000
	Decision Tree	0.657 ± 0.000	0.629 ± 0.001	0.631 ± 0.006	0.743 ± 0.002	0.847 ± 0.008	0.711 ± 0.006	0.830 ± 0.003	0.721 ± 0.004
	Random Forest	0.776 ± 0.001	0.755 ± 0.003	0.630 ± 0.003	0.880 ± 0.000	0.938 ± 0.001	0.737 ± 0.003	0.882 ± 0.002	0.800 ± 0.002
	MLP	0.820 ± 0.002	0.799 ± 0.002	<u>0.731 ± 0.006</u>	0.880 ± 0.002	0.960 ± 0.001	0.831 ± 0.004	0.955 ± 0.000	0.854 ± 0.002
	XGBoost	0.820 ± 0.000	<u>0.798 ± 0.000</u>	0.761 ± 0.000	0.868 ± 0.000	0.949 ± 0.000	<u>0.816 ± 0.000</u>	<u>0.954 ± 0.000</u>	<u>0.852 ± 0.000</u>

(c) THP									
	Classifier	D1	D2	D3	D4	D5	D6	D7	AVG
ACC	Logistic Regression	0.803 ± 0.000	0.786 ± 0.000	0.693 ± 0.000	<u>0.770 ± 0.000</u>	0.895 ± 0.000	<u>0.815 ± 0.000</u>	<u>0.915 ± 0.000</u>	0.811 ± 0.000
	Decision Tree	0.772 ± 0.000	0.738 ± 0.001	<u>0.695 ± 0.005</u>	0.755 ± 0.003	0.872 ± 0.005	0.806 ± 0.011	0.887 ± 0.002	0.789 ± 0.004
	Random Forest	0.776 ± 0.003	0.740 ± 0.003	0.597 ± 0.011	0.768 ± 0.003	0.860 ± 0.007	0.712 ± 0.016	0.870 ± 0.002	0.760 ± 0.006
	MLP	<u>0.824 ± 0.004</u>	0.805 ± 0.003	<u>0.695 ± 0.010</u>	0.767 ± 0.009	0.906 ± 0.016	0.807 ± 0.006	0.911 ± 0.006	<u>0.816 ± 0.008</u>
	XGBoost	0.836 ± 0.000	0.819 ± 0.000	0.716 ± 0.000	0.779 ± 0.000	<u>0.904 ± 0.000</u>	0.827 ± 0.000	0.920 ± 0.000	0.829 ± 0.000
AUC	Logistic Regression	0.870 ± 0.000	0.853 ± 0.000	0.705 ± 0.000	0.891 ± 0.000	<u>0.969 ± 0.000</u>	<u>0.907 ± 0.000</u>	<u>0.975 ± 0.000</u>	0.881 ± 0.000
	Decision Tree	0.772 ± 0.000	0.738 ± 0.001	0.717 ± 0.006	0.755 ± 0.003	0.872 ± 0.005	0.806 ± 0.011	0.887 ± 0.002	0.792 ± 0.004
	Random Forest	0.858 ± 0.004	0.830 ± 0.003	0.632 ± 0.008	0.885 ± 0.001	0.962 ± 0.001	0.899 ± 0.005	0.956 ± 0.001	0.860 ± 0.003
	MLP	<u>0.898 ± 0.003</u>	<u>0.876 ± 0.006</u>	<u>0.769 ± 0.011</u>	0.882 ± 0.003	0.971 ± 0.001	0.895 ± 0.002	0.971 ± 0.003	<u>0.895 ± 0.004</u>
	XGBoost	0.909 ± 0.000	0.892 ± 0.000	0.820 ± 0.000	<u>0.886 ± 0.000</u>	0.967 ± 0.000	0.921 ± 0.000	0.977 ± 0.000	0.910 ± 0.000

(d) BASELINE									
	Classifier	D1	D2	D3	D4	D5	D6	D7	AVG
ACC	Logistic Regression	0.640 ± 0.000	0.659 ± 0.000	0.670 ± 0.000	0.539 ± 0.000	0.532 ± 0.000	0.517 ± 0.000	0.607 ± 0.000	0.595 ± 0.000
	Decision Tree	0.613 ± 0.000	0.627 ± 0.001	0.612 ± 0.002	<u>0.588 ± 0.003</u>	<u>0.580 ± 0.005</u>	0.566 ± 0.025	<u>0.655 ± 0.002</u>	0.606 ± 0.005
	Random Forest	0.646 ± 0.001	0.678 ± 0.002	0.699 ± 0.000	0.557 ± 0.002	0.527 ± 0.002	<u>0.614 ± 0.037</u>	0.612 ± 0.003	<u>0.619 ± 0.007</u>
	MLP	0.646 ± 0.001	0.653 ± 0.006	0.663 ± 0.005	0.537 ± 0.012	0.537 ± 0.008	0.562 ± 0.007	0.574 ± 0.032	0.596 ± 0.010
	XGBoost	0.646 ± 0.000	<u>0.661 ± 0.000</u>	0.608 ± 0.000	0.603 ± 0.000	0.585 ± 0.000	0.633 ± 0.000	0.702 ± 0.000	0.634 ± 0.000
AUC	Logistic Regression	0.696 ± 0.000	0.712 ± 0.000	0.800 ± 0.000	0.555 ± 0.000	0.561 ± 0.000	0.574 ± 0.000	0.650 ± 0.000	0.650 ± 0.000
	Decision Tree	0.617 ± 0.000	0.628 ± 0.001	0.613 ± 0.002	<u>0.588 ± 0.003</u>	<u>0.580 ± 0.005</u>	0.566 ± 0.025	0.655 ± 0.002	0.607 ± 0.005
	Random Forest	0.699 ± 0.001	0.742 ± 0.001	0.656 ± 0.009	0.580 ± 0.001	0.563 ± 0.002	0.706 ± 0.010	<u>0.667 ± 0.002</u>	0.659 ± 0.004
	MLP	<u>0.702 ± 0.002</u>	0.727 ± 0.003	<u>0.770 ± 0.007</u>	0.569 ± 0.008	0.569 ± 0.002	0.635 ± 0.015	0.663 ± 0.011	<u>0.662 ± 0.007</u>
	XGBoost	0.707 ± 0.000	<u>0.741 ± 0.000</u>	0.732 ± 0.000	0.647 ± 0.000	0.641 ± 0.000	<u>0.701 ± 0.000</u>	0.781 ± 0.000	0.707 ± 0.000

L Details and Variants of 3H-motifs

In this section, we explore potential variations of 3h-motifs and assess their performance through experiments. We aim to show that the proposed 3h-motifs strike a balance between simplicity and strong characterization power, making them an effective tool for analyzing hypergraph structures. Visual representations of all 431 3h-motifs are provided in Figure 18. We consider the following variants in which the two states of each non-empty set are defined differently:

- **Absolute - Abs(θ)**: The states of each non-empty set are defined based on its cardinality c as (1) $0 < c \leq \theta$ and

(2) $c > \theta$, where $\theta = 1$. Note that 3h-motifs are equivalent to Abs(1).

- **Motif Ratio - MR(p)**: The states of each non-empty set are defined based on its cardinality c and the total number of unique nodes n in the considered instance as (1) $0 < \frac{c}{n} \leq p$ and (2) $\frac{c}{n} > p$, where $0 < p < 1$.
- **Hyperedge Ratio - HR(p, σ)**: The states of each non-empty set are defined based on its cardinality c and the hyperedges S containing the set as (1) $0 < \sigma(\frac{c}{|e|})_{e \in S} \leq p$ and (2) $\sigma(\frac{c}{|e|})_{e \in S} > p$, where $0 < p < 1$ and $\sigma(\cdot)$ is

Table 11: Accuracy (ACC) and average area under the ROC curve (AVG AUC) for node classification using three types of ego-networks and five classifiers. For each feature set, the best and second-best results are in **bold** and underlined, respectively.

(a) NP26					(b) NP7				
	Classifier	Star	Radial	Contracted		Classifier	Star	Radial	Contracted
ACC	Logistic Regression	0.327 ± 0.000	0.200 ± 0.000	0.236 ± 0.000	ACC	Logistic Regression	0.309 ± 0.000	0.223 ± 0.000	0.241 ± 0.000
	Decision Tree	0.475 ± 0.013	0.654 ± 0.009	0.540 ± 0.009		Decision Tree	0.469 ± 0.011	0.490 ± 0.009	<u>0.526 ± 0.013</u>
	Random Forest	0.488 ± 0.010	0.570 ± 0.015	0.496 ± 0.013		Random Forest	0.400 ± 0.015	0.501 ± 0.011	0.425 ± 0.008
	MLP	0.383 ± 0.057	0.569 ± 0.035	0.474 ± 0.086		MLP	0.342 ± 0.028	0.440 ± 0.017	0.368 ± 0.079
	XGBoost	0.555 ± 0.000	0.682 ± 0.000	<u>0.618 ± 0.000</u>		XGBoost	0.523 ± 0.000	0.545 ± 0.000	0.482 ± 0.000
AVG AUC	Logistic Regression	0.827 ± 0.000	0.765 ± 0.000	0.727 ± 0.000	AVG AUC	Logistic Regression	0.835 ± 0.000	0.716 ± 0.000	0.731 ± 0.000
	Decision Tree	0.726 ± 0.007	0.810 ± 0.005	0.747 ± 0.005		Decision Tree	0.720 ± 0.006	0.744 ± 0.005	0.760 ± 0.007
	Random Forest	0.890 ± 0.001	0.912 ± 0.002	0.909 ± 0.002		Random Forest	0.856 ± 0.001	0.873 ± 0.003	0.880 ± 0.002
	MLP	0.768 ± 0.034	0.836 ± 0.023	0.778 ± 0.056		MLP	0.734 ± 0.024	0.749 ± 0.012	0.699 ± 0.051
	XGBoost	0.919 ± 0.000	0.952 ± 0.000	<u>0.942 ± 0.000</u>		XGBoost	0.895 ± 0.000	<u>0.901 ± 0.000</u>	0.910 ± 0.000
(c) TNP					(d) BASELINE				
	Classifier	Star	Radial	Contracted		Classifier	Star	Radial	Contracted
ACC	Logistic Regression	0.432 ± 0.000	0.318 ± 0.000	0.268 ± 0.000	ACC	Logistic Regression	0.309 ± 0.000	0.505 ± 0.000	0.418 ± 0.000
	Decision Tree	0.585 ± 0.016	0.647 ± 0.011	0.593 ± 0.013		Decision Tree	0.549 ± 0.013	0.649 ± 0.013	0.590 ± 0.015
	Random Forest	0.515 ± 0.014	0.598 ± 0.014	0.542 ± 0.028		Random Forest	0.597 ± 0.016	0.581 ± 0.012	0.538 ± 0.011
	MLP	0.502 ± 0.026	0.627 ± 0.038	0.480 ± 0.040		MLP	0.530 ± 0.034	0.542 ± 0.045	0.476 ± 0.061
	XGBoost	0.650 ± 0.000	0.723 ± 0.000	<u>0.673 ± 0.000</u>		XGBoost	0.550 ± 0.000	<u>0.659 ± 0.000</u>	0.668 ± 0.000
AVG AUC	Logistic Regression	0.876 ± 0.000	0.838 ± 0.000	0.784 ± 0.000	AVG AUC	Logistic Regression	0.848 ± 0.000	0.904 ± 0.000	0.871 ± 0.000
	Decision Tree	0.772 ± 0.009	0.806 ± 0.006	0.776 ± 0.007		Decision Tree	0.762 ± 0.007	0.807 ± 0.007	0.774 ± 0.008
	Random Forest	0.915 ± 0.003	0.936 ± 0.002	0.933 ± 0.001		Random Forest	0.920 ± 0.002	0.922 ± 0.001	0.930 ± 0.001
	MLP	0.842 ± 0.012	0.875 ± 0.021	0.787 ± 0.025		MLP	0.910 ± 0.007	0.922 ± 0.016	0.898 ± 0.026
	XGBoost	0.946 ± 0.000	0.967 ± 0.000	<u>0.956 ± 0.000</u>		XGBoost	0.922 ± 0.000	0.951 ± 0.000	<u>0.950 ± 0.000</u>

Table 12: Comparison of 3h-motifs and its variants. For $MR(p)$, $HR(p, \text{mean})$, $HR(p, \text{max})$, and $HR(p, \text{min})$, the min, average, and max performances over $p = \{0.1, 0.2, \dots, 0.9\}$ are reported. For each task, the best and second-best results are in **bold** and underlined, respectively. Surprisingly, despite the simplicity of 3h-motifs, using it consistently outperforms or achieves similar results compared to other variants across all tasks, providing evidence of its effectiveness.

	Hypergraph Clustering			Hyperedge Prediction (coauth-DBLP)						Node Classification					
	NMI score			ACC			AUC			ACC			AVG AUC		
	min	mean	max	min	mean	max	min	mean	max	min	mean	max	min	mean	max
3H-motifs (i.e., Abs(1))	1.000			0.836			<u>0.909</u>			0.723			0.967		
Abs(2)	1.000			<u>0.830</u>			0.908			0.673			0.955		
$MR(p)$	0.824	0.932	1.000	0.802	0.814	0.829	0.886	0.895	0.902	0.677	0.690	0.700	0.951	0.956	0.961
$HR(p, \text{mean})$	0.877	<u>0.965</u>	1.000	0.804	0.819	0.829	0.887	0.899	0.910	0.664	0.681	0.695	0.952	0.955	0.960
$HR(p, \text{max})$	0.877	0.934	1.000	0.805	0.820	<u>0.830</u>	0.890	0.900	0.910	0.682	0.695	<u>0.709</u>	0.951	0.957	<u>0.963</u>
$HR(p, \text{min})$	0.877	0.934	1.000	0.805	0.818	0.826	0.890	0.898	0.907	0.673	0.694	0.723	0.954	0.957	0.962

the *mean*, *max*, or *min* function.

We conduct experiments to compare the effectiveness of 3H-motifs (i.e., Abs(1)), Abs(2), $MR(p)$, $HR(p, \text{mean})$, $HR(p, \text{max})$, $HR(p, \text{min})$ for $p = \{0.1, 0.2, \dots, 0.9\}$. We evaluate the variants through hypergraph clustering, hyperedge prediction, and node classification using the same experimental settings described in Sections 6.4 and 6.5. For hyperedge prediction task is performed on the coauth-DBLP dataset.

Table 12 presents the results of comparing the performances. For $MR(p)$, $HR(p, \text{mean})$, $HR(p, \text{max})$, and $HR(p, \text{min})$, the table reports the min, average, and max performances over $p = \{0.1, 0.2, \dots, 0.9\}$. Remarkably, even though the definition of 3h-motifs is simplest, the use of 3h-motifs leads to the best performance in hypergraph clustering and node classification tasks. In hyperedge prediction, using 3h-

motifs achieves the highest ACC and the second-highest AUC. These results provide support for the effectiveness of 3h-motifs.

We further investigate a wider range of θ value (spec., from 1 to 15) in Abs(θ) to assess its impact on performance in the considered tasks. As shown in Figure 15, our empirical findings reveal that employing a threshold of 1 (i.e., utilizing 3h-motifs) consistently results in the highest performance across the tasks. Especially, as shown in Figure 15(d), with θ fixed at 1, the hyperedge prediction performance remains very close to that achieved with the optimal θ value for each dataset. In Appendix M, we provide additional analysis regarding the effectiveness of employing $\theta = 1$.

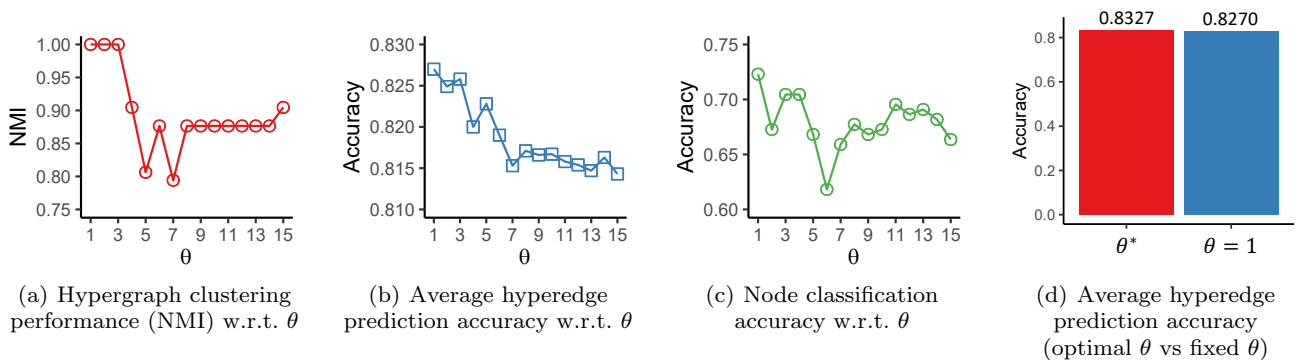


Fig. 15: 3H-motifs (i.e., Abs(1)) consistently demonstrates superior performance in all three applications compared to Abs(θ) with other θ values. In (b), we report the hyperedge prediction accuracy averaged over all datasets. In (d), θ^* (red bar) represents the average hyperedge prediction accuracy achieved with the optimal θ value for each dataset, while $\theta = 1$ (blue bar) represents the average hyperedge prediction accuracy with θ fixed at 1. Remarkably, even with θ fixed at 1, the performance remains very close to the highest accuracy attainable.

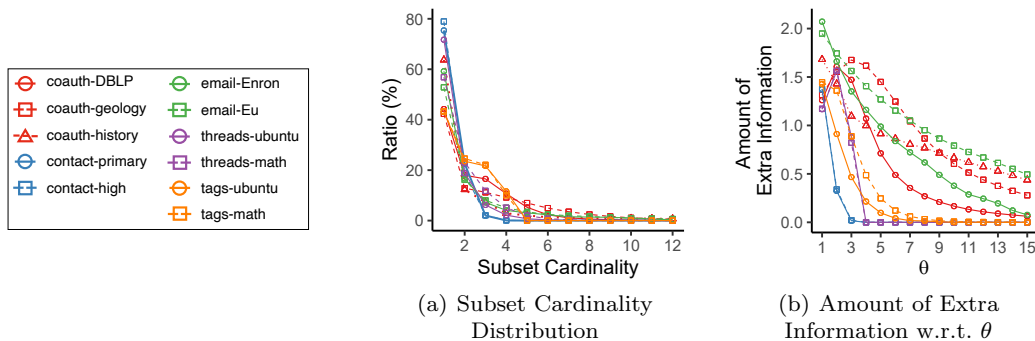


Fig. 16: (a) The cardinalities of subsets, upon which both h-motifs and 3h-motifs are defined, exhibit a strong bias toward the value 1 in all datasets. (b) The amount of extra information gained with 3h-motifs over h-motifs is maximized when utilizing the cardinality threshold $\theta = 1$, as employed by 3h-motifs, in 7 out of 11 hypergraphs.

M Data Analysis Regarding the Effectiveness of 3H-motifs

In this section, we present data analyses for gaining insights into the effectiveness of 3h-motifs, which is demonstrated by comprehensive experiments in Appendix L. Recall that 3h-motifs employs a threshold value of $\theta = 1$ to categorize the states of the seven subsets into three distinct groups based on their cardinalities. Our analyses below demonstrate why choosing $\theta = 1$ is a suitable decision.

Subset Cardinality Distribution: We first investigate the cardinalities of the seven subsets, based on which h-motifs and 3h-motifs are defined, in the 11 real-world hypergraphs. As shown in Figure 16(a), in all considered real-world hypergraphs, the count of subsets with each cardinality diminishes considerably as the cardinality increases. This observation suggests that when employing a threshold value θ greater than 1, only a very small fraction of subsets falls into the state $> \theta$, which is a new state introduced in 3h-motifs but not present in h-motifs. Intuitively, this limited utilization of this new state leads to a reduction in the amount of additional information provided by 3h-motifs in comparison to h-motifs.

Amount of Extra Information: To numerically validate our intuition above, we measure the amount of extra information in 3h-motifs over h-motifs using the *conditional entropy* as follows:

$$H(3\text{h-motif}|\text{h-motif}) = - \sum_{i=1}^{26} \frac{N_i}{N_{tot}} \sum_{j \in K_i} \frac{n_j}{N_i} \ln \frac{n_j}{N_i}, \quad (24)$$

where N_{tot} is the count of all h-motif instances, N_i is the count of the instances of h-motif i , K_i is the set of the indices of 3h-motifs that can share instances with h-motif i (e.g. $K_1 = \{1, \dots, 6\}$, as shown in Figure 5), and n_j is the count of the instances of 3h-motif j . If we treat the h-motif and 3h-motif corresponding to each instance as random variables, the conditional entropy measures the amount of information needed to describe the corresponding 3h-motif given the corresponding h-motif. If the instances of each h-motif are uniformly distributed among the corresponding 3h-motifs, we can achieve the maximum amount of additional information, which is $\sum_{i=1}^{26} \frac{N_i}{N_{tot}} \ln |K_i|$. Conversely, if the instance counts of h-motif i are highly skewed toward one of the corresponding 3h-motifs, the extra information would approach zero, indicating a minimum. In Figure 16(b), we report the amount of extra information in each real-world hypergraph

while varying θ from 1 to 15. In all datasets, the most significant additional information is obtained with a small θ , with 7 out of 11 hypergraphs yielding the highest amount at $\theta = 1$. This potentially explains the superior performance observed in machine tasks when $\theta = 1$ (see Figure 15).

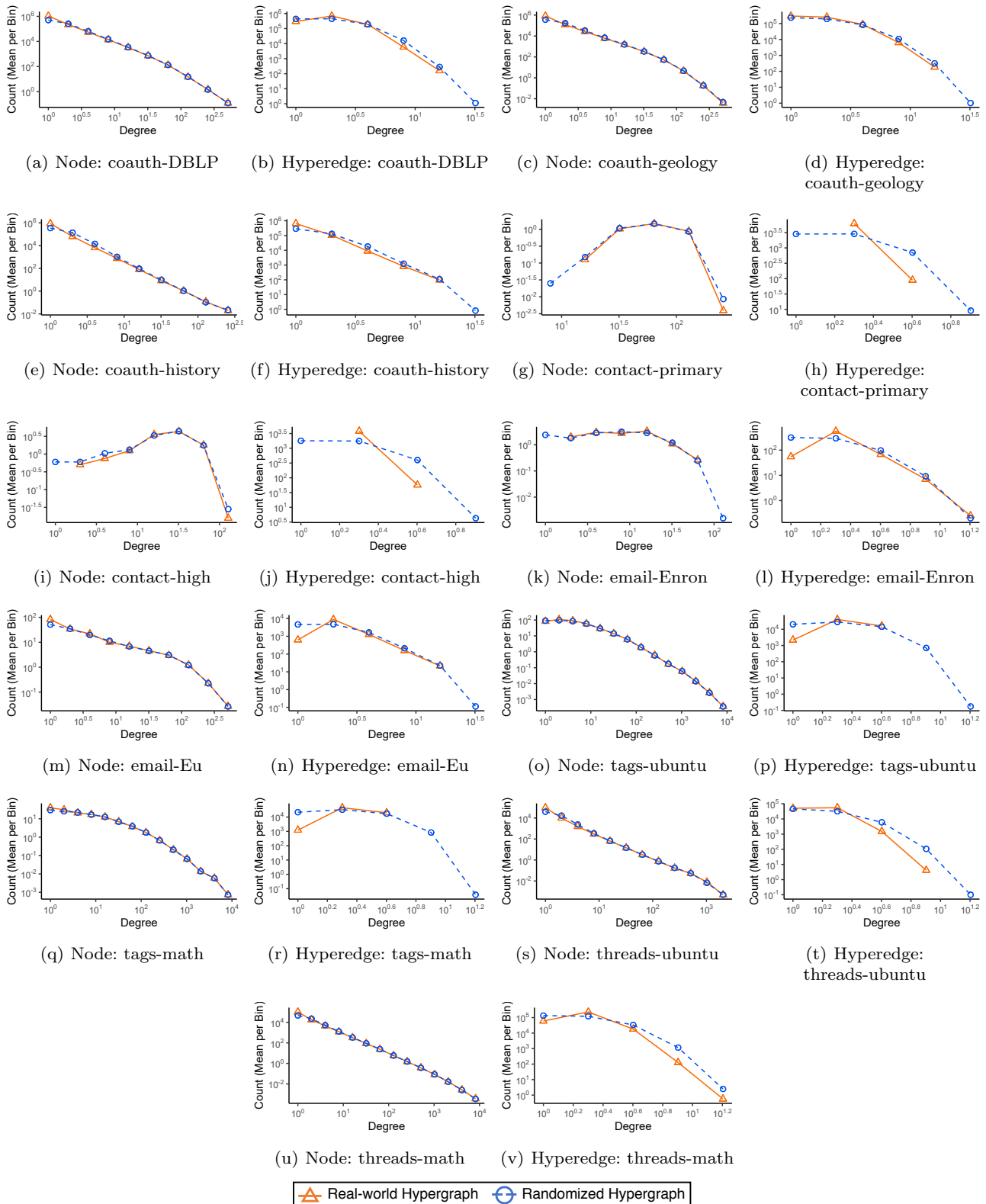


Fig. 17: Degree distributions of nodes and size distributions of hyperedges in real-world hypergraphs and the corresponding random hypergraphs.

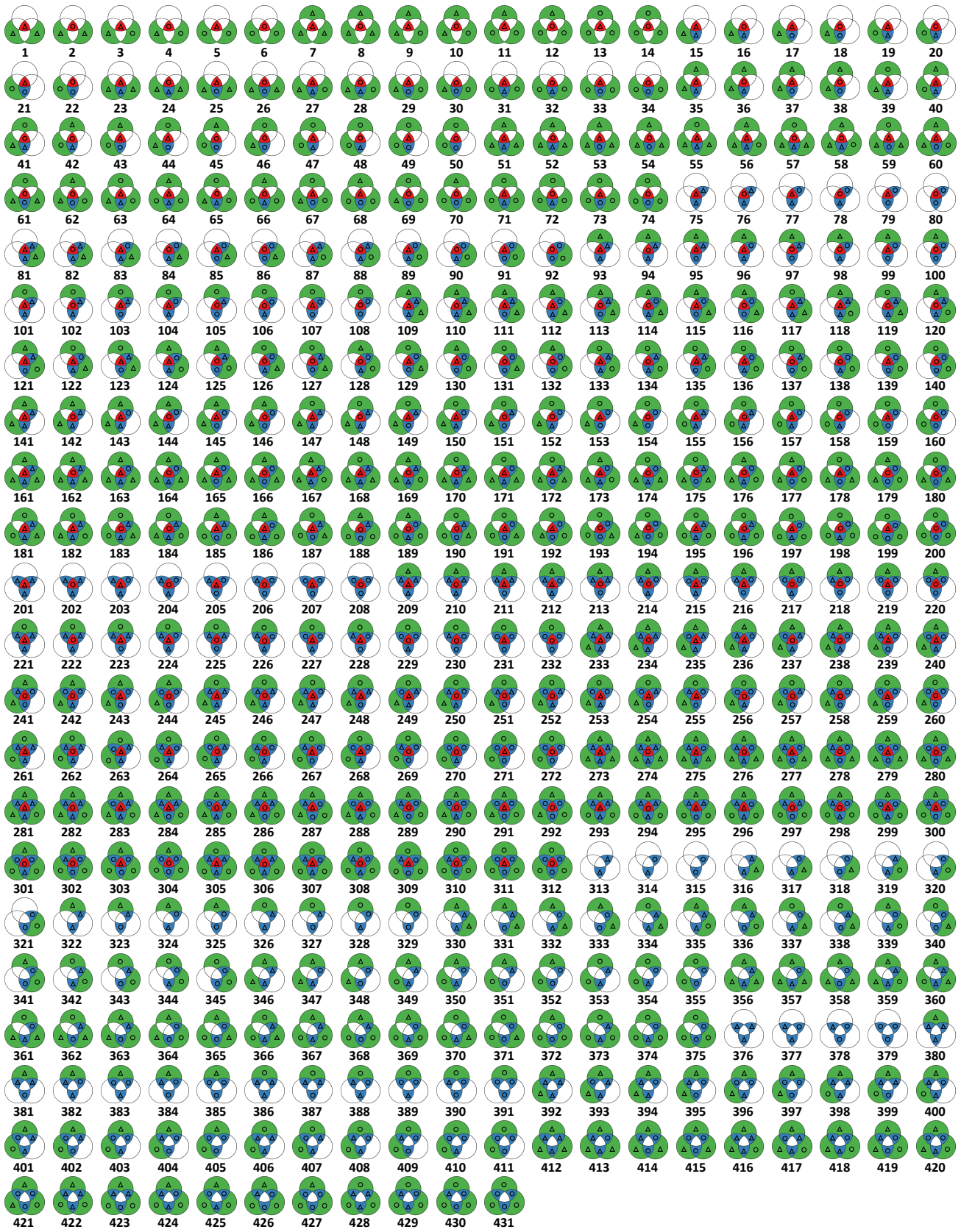


Fig. 18: The 431 3H-motifs studied in this work. In each Venn diagram, uncolored regions are empty without containing any nodes. Colored regions with a triangle contain more than 0 and at most θ nodes, while colored regions with a circle contain more than θ nodes.